Universitetet i Stavanger

FACULTY OF SCIENCE AND TECHNOLOGY

MASTER'S THESIS

Study programme/specialization: **MSc in Marine and Offshore Technology/ Marine and Subsea Technology**	The spring semester, 2022 Open / ~~Confidential~~
Author: **Usman Nawaz Ahmad**	Usman Nawaz (Writers' signature)
Course coordinator: **Professor Yihan Xing** Supervisor: **Professor Yihan Xing, University of Stavanger**	
Title of master's thesis: **The Baseline Design of The UiS Subsea Glider for Cargo and Liquid Carbon Dioxide Transportation**	
Credits (ECTS): 30	
Keywords: PID LQR AUV Subsea Technology USFG Submarine CCS	Number of pages: 68 + appendix: 102 Stavanger, 15th June, 2022

Abstract

This dissertation presents the baseline design of the UiS subsea-freight glider (USFG) for cargo and liquid carbon dioxide transportation. The USFG is a cutting-edge autonomous vessel developed to be an alternative to active transportation technologies and satisfy the demands of small-scale fields for CO_2 transportation. Usually, these smaller fields fail to economically justify the costs of large tanker or cargo ships or underwater pipelines on the seabed, as the transport volume is nominal compared to larger fields. The USFG can travel underwater at an operational depth of 200 meters, allowing the glider to carry freight operations without considering ideal weather windows. The length of the USFG is 5.50 meters, along with a beam of 50.25 meters, which allows the vessel to carry 518 m^3 of CO_2 while serving the storage needs of the carbon capture and storage (CCS) ventures on the Norwegian continental shelf. It can maneuver itself underwater by monitoring the flow between the ballast tanks. During the entire mission of the USFG, from capturing to injection locations, it follows a pre-laid route while experiencing transient loads from the ocean current. An analytical model for analysing equilibrium glide paths of the USFG is presented. The model is developed using Simscape Multibody in MATLAB/Simulink to study the volatile dynamics of the glider. Subsequently, the gliding paths of USFG in the vertical plane are analyzed along with the observability and controllability of the steady equilibrium glides. Along with the control gliding design of the USFG, the mechanical design is also presented in this work. The maneuvering model of the USFG is presented along with two operational case studies: the equilibrium glide and the -38° dive. The extreme motion along the surge direction affects the range of the glider (vital for battery design) and the dynamic controller parameters concerning maneuverability. Finally, the averaged conditional exceedance rate (ACER) is employed to scrutinize the extreme motion (surge direction) of the USFG while gliding to a defined depth. This analysis is done when the glider is exposed to an average current velocity of 0.5 m/s and 1.0 m/s. The presented ACER method efficiently uses the available data points and accurately predicts the extreme surge responses precisely and accurately.

To Aiman, my Mother, and my Brothers.

Acknowledgments

This thesis concludes my master's studies at the University of Stavanger's Marine and Offshore Technology program, Department of Mechanical and Structural Engineering and Materials Science. I want to thank everyone who has assisted and supported me during this thesis project.

First and foremost, I would like to thank Professor Yihan Xing for giving me the chance to work under his supervision during my master's studies at the University of Stavanger. I consider this opportunity to work with him a great privilege. I also thank him for all his work advising my research and his extensive help editing the research articles. Moreover, I would like to sincerely thank him for his kindness, encouragement, vast knowledge, and inspiring guidance and for providing me with the prospect to develop my interest and career in Subsea Technology, particularly Underwater Vehicles.

I would also like to thank the PhD candidate Yucong Ma at my department and Shuaishuai Wang from the Norwegian University of Science and Technology, whose collaboration, comments and discussions have helped my research. Finally, I appreciate the University of Stavanger Department of Mechanical and Structural Engineering and Materials Science for providing all the resources necessary to complete the presented work.

Most of all, I wish to show appreciation to my wife, Aiman Usman - I simply could not have done this without you; special thanks for her endless love, support, care, advice and inspiration. Furthermore, I owe my deepest gratitude to my mother, Shenaz Begum, and brothers, Adeem Hassan Khan and Bilal Nawaz Ahmed, for providing me with the most excellent education possible and their unwavering support throughout my studies and life, and for their kind wishes. Finally, I would also thank my friends, particularly Nouman Bin Asif; I am thankful for their support and help throughout the process.

Publications

The following four papers were written during the time of the thesis. These papers are annexed in the same format they were submitted or published to the respective conferences and journals.

Paper A Ahmad, U., & Xing, Y. (2021). A 2D model for the study of equilibrium glide paths of UiS Subsea Freight-Glider. IOP Conference Series: Materials Science and Engineering.

Paper B Ahmad, U., & Xing, Y. (2022). *UIS Subsea Freight Glider: controller design and analysis* International Conference on Offshore Mechanics and Arctic Engineering, Hamburg, Germany.

Paper C Ahmad, U. N., Xing, Y., & Ma, Y. (2022). UiS Subsea-Freight Glider: A Large Buoyancy Driven Autonomous Cargo Glider. *Journal of Offshore Mechanics and Arctic Engineering*. (Under review)

Paper D Ahmad, U. N., Xing, Y., & Wang, S. (2022). Determination of extreme responses of USFG's equilibrium glide path hovering in ocean current. *Ocean Engineering*. (Under review)

Table of Contents

List of Figures

List of Tables

Acronyms

MT	Million Tons
GHGs	Greenhouse Gases
CCS	Carbon Capture And Storage
USFG	Uis Subsea-Freight Glider
DWT	Deadweight Tonnage
SST	Subsea Shuttle Tanker
AUVs	Autonomous Underwater Vehicles
LNG	Liquefied Natural Gas
G	Center of Gravity
B	Center Of Buoyancy
PID	Proportional-Integral-Derivative
LQR	Linear Quadratic Regulator
OPEX	Operational Expenditure
AWGNs	Additive White Gaussian Noises
SISO	Single Input Single Output
SIMO	Single Input And Multiple Output
GPS	Global Positioning System
ASME BPVC	American Society Of Mechanical Engineers Boilers And Pressure Vessel Code
ACPS	Active Pressure Compensating System
BF	Ballast Fraction
ACER	Averaged Conditional Exceedance Rate
CI	Confidence Interval
GEV	Generalized Extreme Value
MPC	Model Predictive Control

Symbols

x_{cg}, y_{cg}, z_{cg}	Coordinates of the center of gravity
x_{cb}, y_{cb}, z_{cb}	Coordinates of the center of buoyancy
O_{bb}, X_{bb}, Y_{bb}, Z_{bb}	Coordinates of the body frame
O_{EB}, X_{EB}, Y_{EB}, Z_{EB}	Coordinates of the local axis system
m_o	Mass of the USFG
X_e	Added mass in the surge
Z_e	Damping force in heave
Q_e	Pitching moment
u	Velocity in surge
q	Velocity in pitch
w	Velocity in heave
$\dot{u}$	Acceleration in surge
$\dot{q}$	Acceleration in pitch
$\dot{w}$	Acceleration in heave
I_{zz}	Moment of inertia
D_f	Drag force
L_f	Lift force
M_T	Rotational torque
D_c	Drag coefficient
L_c	Lift coefficient
C_M	Damping moment coefficient
δ	Density of seawater
V_s	Submerged volume
S	Net maneuvering velocity of the USFG
α	Angle of attack
H_D	Hydrofoil's drag force
H_L	Hydrofoil's lift force
M_H	Hydrofoil's external moment
D_{ch}	Volumetric drag coefficient for hydrofoil
L_{ch}	Volumetric lift coefficient for hydrofoil
C_{Mh}	Volumetric damping moment coefficient for hydrofoil
U_c	Current velocity
φ_c	Flow angle of ocean current
$\nu_{1,2}$	Time constants of the Gauss-Markov process
$\lambda_{1,2}$	Additive white gaussian noises
u_{wc}	The velocity of the incoming flow of water in the horizontal direction
w_{wc}	The velocity of the incoming flow of water in the vertical direction
u_{USFG}	USFG's net velocity magnitude in the surge
w_{USFG}	USFG's net velocity magnitude in heave

ξ	Glide path angle
T_i	Integral time
T_d	Derivative time
K_p	Proportional gain
K_i	Integral gain
K_d	Derivative gain
$e(t)$	Steady-state error
$x_{1,2}$	State vectors of the system
$y_{1,2}$	Output vectors of the system
$u_{1,2}$	Input vectors of the system
K	Input matrix
J	State matrix
L	Output matrix
G	Gain matrix
N	State cost matrix
M	Actuator cost matrix
S_r	Required velocity
ξ_r	Required glide path angle
θ	Pitch angle
x	Displacement in surge
z	Displacement in heave
z'	The perpendicular distance from the desired path
x'	The horizontal distance from the desired path
S_r	Required velocity
S	USFG's net velocity
M_b	Variable mass for main ballast tanks
M_s	Variable mass for secondary ballast tanks
$\dot{\theta}$	Pitch rate
M	Metacenter of the USFG

Chapter 1 - Introduction and Background

1.1 Motivation and Background

The higher percentage of CO_2 in the earth's atmosphere is one of the main contributors to drastic climate change and global warming. Global CO_2 emissions have incessantly increased from the outset of the twenty-first century. CO_2 emissions at the start of 1990 were 12,165 million tons (MT) compared to 38,016 MT in 2019. This significant surge of around 70 percent was reported by the Emissions Database for Global Atmospheric Research (Crippa et al., 2020). Combustion of fossil fuels and massive-scale deforestation is responsible for this rise in CO_2 concentrations. The outlook for CO_2 concentrations suggests a reduction by 2030; otherwise, the earth would suffer irreversible losses. The most vulnerable ecosystem of the globe would be in a bind (Allen et al., 2019; Intergovernmental Panel on Climate Change, 2018; IPCC, 2018).

Global warming has become one of the critical themes of the Paris Agreement (Nations, 2015), which targets global warming below 1.5°C with a 2°C limit. By 2030, the emissions of Greenhouse Gases (GHGs), comprising carbon dioxide, are directed to be cut down by at least 55 percent compared to the levels of the year 1990 as per the agreement. Carbon capture and storage (CCS) technology plays a significant role in reaching this target. CCS can reduce power and energy generation emissions by capturing and transferring carbon emissions. These emissions can then be stored at storage sites, i.e., subsea wells. It is currently possible to store and collect CO_2 emissions in large amounts (Carbon Capture and Storage Association [CCSA], 2020). Therefore, any tactic that increases total CCS storage volume is vital to minimalize the increasing trend in the earth's mean temperature rise.

Most oil and gas produced offshore is transported to land-based facilities via pipelines (Fullenbaum et al., 2013). Since World War II, when the United Kingdom first installed and used subsea pipe laying technology, the technology has significantly developed (Palmer & King, 2008). However, the use of this technology has been limited by several technical and economic factors. The installation costs are the primary disadvantage. The costs of pipelines can be significantly high for remote fields, especially as the length of the pipe increases. Apart from that, deep-water activities such as pipeline inspection are also challenging and expensive.

Pipeline maintenance is costly financially because it involves complete or partial shutdowns, which are not possible on marginal oil and gas fields.

In the meantime, tanker ships, explicitly shuttle tankers, are often utilized (Vestereng, 2019). With fewer steps-outs in the operations of subsea pipelines, they provide an attractive solution for large offshore projects with higher revenue (WILSON, 2008). Furthermore, shuttle tankers provide enhanced flexibility in various situations, i.e., increased demand, as they can swiftly be deployed to the desired location. As for accidents or unforeseen events, it is advantageous to use tankers instead of conventional pipelines, as an auxiliary ship can be sent quickly. Unfortunately, though, large tanker operations are weather restricted and dependent. Dynamic loads highly influence them in harsh weather situations from the environment, such as wind and wave loads. Therefore, the UiS subsea-freight glider (USFG) was introduced to tackle these potential problems.

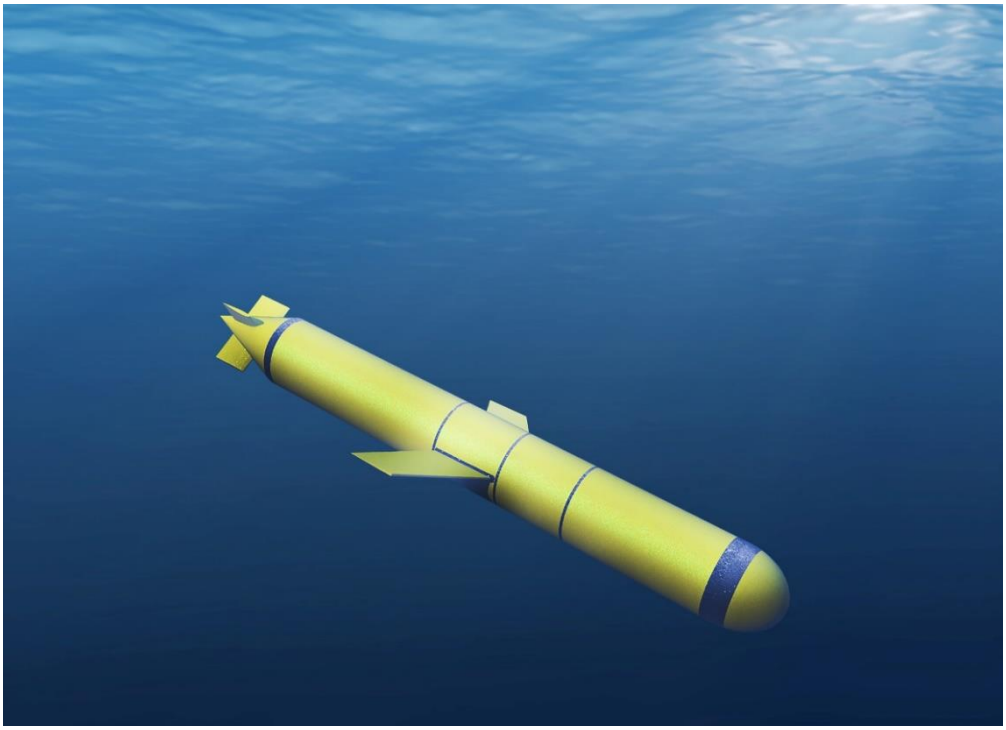

Figure 1.1 Illustration of the UiS subsea-freight glider.

The UiS subsea-freight glider (USFG), shown in **Figure 1.1**, is a 531-deadweight tonnage (DWT) autonomous subsea vessel designed to transport CO_2 and other forms of payloads. The glider can travel underwater as it utilizes the characteristics of submarines. At the same time, it inherits the perpetual availability and economic traits of the marine tanker ships. The USFG is proposed as a lucrative substitute for contemporary CO_2 conveyance methods. The cost for

each ton of CO_2 transported is anticipated to be comparable, if not better, than the subsea shuttle tanker (SST) (Xing, Santoso, et al., 2021). In addition, the USFG enables marginal underwater storage sites to be commercially feasible, as laying underwater pipelines is not a cost-effective solution for such sites.

The Norwegian continental shaft CCS projects, including Sleipner, Utgards, and Snøhvit fields (Norwegian Petroleum Directorate [NPD], 2020), are the primary targets for the baseline design of the USFG. It must be noted that the initial design target for the USFG is technically feasible for these CCS ventures, but the USFG can be easily configured to operate in any part of the globe. The main objective of these CCS projects is to reduce the CO_2 footprint induced by the hydrocarbon production projects. This is accomplished by capturing the carbon dioxide and driving it into the subsea petroleum reservoir. **Figure 1.2** shows the location of these sites along with their rated storage capacity. In addition to these projects, the Northern Lights project (Equinor, 2022) is in work by Equinor, as they aim to transport CO_2 produced by onshore industries and inject it into the Utsira formation (Troll field). In this thesis, CO_2 is the primary cargo for transportation, but the USFG can be designed to diversify by carrying crude oil products, electricity (stored in batteries), and subsea tools.

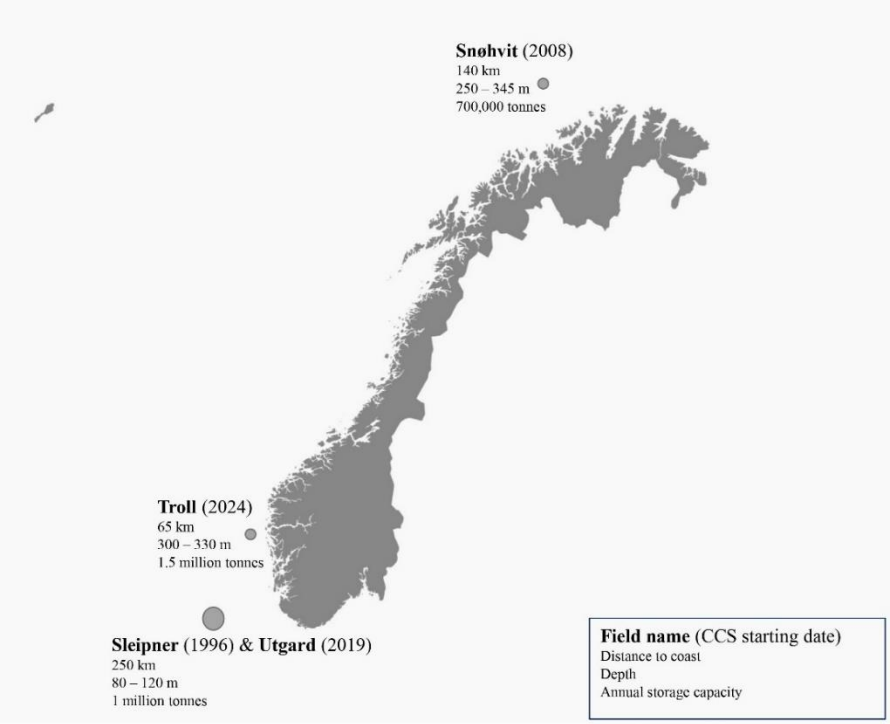

Figure 1.2 Norwegian sector storage sites for the CCS projects (Ma et al., 2021).

The significant size of the USFG induces some technical issues that involve further research and development. For example, the following problems require consideration: (A) an autonomous actuating mechanism with a robust control system capable of handling variations in the operating conditions, and (B) a design method to reduce the overall weight of the vessel and increase the freight capacity.

1.2 Objectives of the Thesis

This dissertation will cover the critical considerations relating to the baseline design of the USFG followed by well-defined design specifications, which will remove all the knowledge barriers as previously defined. Conferring to the background and introduction mentioned earlier, the theme of this thesis is divided into subsequent parts:

1. Modeling the dynamics of the USFG to analyze the control system for ballasting and flight path. The aim is to develop a dynamic model to cater to buoyancy and hydrodynamic forces to investigate the equilibrium glides and their applications for USFG, which involves the sawtooth gliding path in a 2D plane.

2. Development of the mechanical design of the USFG to study this innovative concept and establish its technical and operational limits (if they exist). The aim is to maximize the cargo-carrying ability.

3. Analyze and predict the extreme motion (surge direction) of the USFG during gliding in the ocean current.

1.3 Outline

This dissertation comprises 7 chapters. Following the introduction in **Chapter 1**, the literature study of the USFG is presented. The characteristics, mission requirements, and specifications, general arrangement of the USFG are highlighted in **Chapter 2**. The mathematical model of the USFG is given in **Chapter 3**. Here, the axis system is defined before the Simulink implementation of the vessel, and various modules of the model are also presented extensively in this chapter. **Chapter 4** contains the dynamic responses of the USFG during gliding, and these simulations define the controller characteristics and present an assessment study. **Chapter 5** presents the mechanical design to access the technical and functional limits of the USFG**.** The extreme responses of the vessel in surge motion are evaluated and analyzed in

Chapter 6. Lastly, **Chapter 7** reviews the entire work completed in this dissertation while extending recommendations for future work. Additionally, **Appendix A** illustrates the method to evaluate the hydrofoil area given in **Chapter 5**. The manuscripts, approved and submitted, that form the basis of this work are attached in **Appendix B**.

1.4 Previous Work

Underwater gliders are now considered an innovative group of Autonomous Underwater Vehicles (AUVs). They maneuver in the ocean environment with an internal actuating mechanism by varying their buoyancy utilizing the tails and wings. Previously, gliders have been employed for several practical applications, predominantly aquatic life monitoring, oceanographic surveys, and data collection. In 1989, an autonomous system capable of monitoring and collecting ocean data was presented (Stommel, 1989). The observation system comprised "1000 neutrally buoyant floats called Slocums" these floats navigated through the ocean by regulating the mass of ballast water while maneuvering with their hydrodynamic wings. The system was named Slocum; it originated from the name Joshua Slocum; the first sailor to sail around the world. The initial glider concept presented by Henrey Stommel has progressed from marginal scanning floats to innovative AUVs in just a few years. Examples include Glider AUV (DOF Subsea, 2018) from Skandi explorer gliders and Manta Ray AUV (EvoLogics, 2017). Nevertheless, due to their limited applications in amassing ocean data, these AUVs are not practical for subsea freight transportation as they have a restricted loading potential.

First examples of underwater cargo transportation date back to the 1970s, two submarines with a load capacity ranging from 20,000 to 420,000 DWT (Jacobsen, 1971; Taylor & Montgomery, 1977) were proposed to transport crude oil in the northernmost region of the earth (the Arctic or polar region). Subsequently, in 1983, two significantly-sized subsea tankers were presented (Jacobsen et al., 1983). The primary purpose of these vessels was to transport liquefied natural gas (LNG), transporting an enormous mass of 727,400 and 660,000 DWT. Theseus, a cable laying vessel with autonomous capabilities, was established in the early 1990s by LSE Ltd. due to the Spinnaker program (Griffiths, 2002). Moreover, recent development in underwater technologies saw a boost as an autonomous underwater tanker (Ellingsen et al., 2020; Equinor Energy AS, 2019) was proposed to carry CO_2, hydrogen, and hydrocarbons. Also, an efficient underwater glider was proposed (Ellingsen et al., 2020) for large-capacity payload. In response

to the prior work, an ultra-efficient freight-carrying glider with less than 10 kW power consumption was presented (Xing, 2021). It must be noted that the research above only referred to concept studies and did not provide any technical information or details.

Chapter 2 - The UiS Subsea-Freight Glider (USFG)

This chapter highlights the literature study of the UiS subsea-freight glider (USFG). The USFG is designed to transport 518 m^3 of CO_2, with a characteristic length of 50.25 meters and a beam that measures 5.50 meters. The USFG is a 531-DWT vessel that can travel at a gliding speed of 1 m/s (2 knots); this is limited to conserve power. In addition, the cruising range is controlled to 216 nautical miles (400 kilometers) to limit the battery size. This chapter contains characteristics, mission requirements and specifications, and the general arrangement of the USFG.

2.1 Characteristics

The concept of the USFG is innovative and unique due to its actuating mechanism, as it maneuvers in the ocean by varying the buoyancy force (responsible for generating thrust) by utilizing its large hydrofoils. This mechanism consumes less power than the current technologies, i.e., propellers. The essential design features of the USFG are summarized in **Table 2.1**. **Figure 2.1** illustrates the equilibrium glide path; this sawtooth or sinusoid path is the route taken by the glider, and it is laid out in advance for each mission (Bahlman et al., 2012).

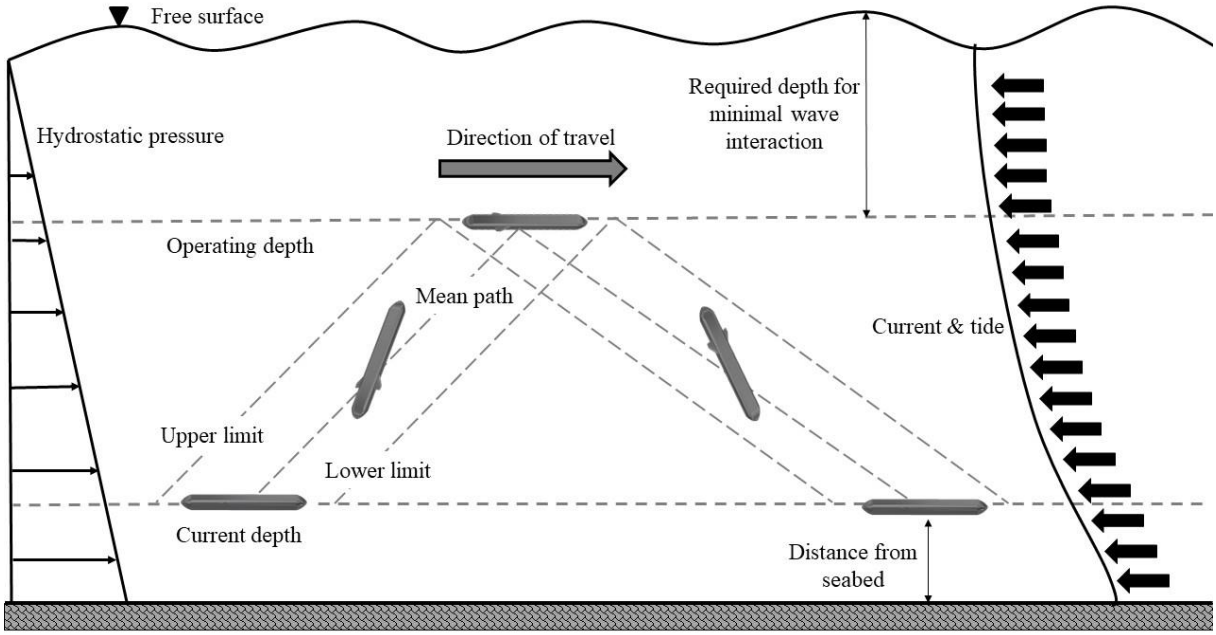

Figure 2.1 USFG subjected to environmental loads during equilibrium glides.

Table 2.1 Characteristics of the USFG.

Parameter	Value	Unit
Length	50.25	[m]
Operating depth	200	[m]
Center of gravity (G) $[x_{cg}, y_{cg}, z_{cg}]$	[-0.78, 0.00, 0.40]	[m]
Weight	1379	[tons]
CO_2 cargo capacity	518	[m^3]
Beam	5.50	[m]
Range	400	[km]
Wing area	5	[m^2]
Center of buoyancy (B) $[x_{cb}, y_{cb}, z_{cb}]$	[-1.48, 0.00, 0.00]	[m]

Ballasting system

The USFG navigates by operating its ballast tanks. This entire process is demonstrated in **Figure 2.1**. Firstly, the vessel's negative pitch angle (bow heading down) is obtained by pumping the ballast water out of the tanks. Next, a positive net buoyancy force is generated as the glider becomes lightweight. Doing this enables the USFG to climb to the desired depth with an angle of attack. Furthermore, the velocity difference between incoming flow and USFG generates a lift force, allowing the vessel to move toward its destination. Correspondingly, ballast water is pumped into the vessel, which increases the overall weight, a positive pitch angle (bow heading up), and a negative net buoyancy force is produced; this aids the USFG in descending to its original operating depth while moving forward. This to-and-fro movement of the glider is responsible for generating the drag and lift forces as it propels by employing its hydrodynamic wings. This sinusoidal process is repeated throughout the entire journey of the glider, and it consumes less energy as this process only utilizes pumps for varying ballast, contrary to internal actuating masses for other gliders.

A large number of gliders maneuver underwater by varying the overall ballast volume, which alters the net buoyancy force acting on the submerged glider. Simultaneously, motion in the pitch and roll directions are controlled through internal mass actuators. This implementation is not practicable or feasible for significantly-sized freight gliders, such as the USFG, as the size of the hydraulic network increases drastically with an increase in tonnage capacity. Underwater glider dynamics demand a robust yet agile system that can respond to variations in the operating conditions and the environment. Response times are reduced for roll and pitch motion as the USFG employs a combination of ballast tanks and hydrofoils to obtain the required angles, as depicted in **Figure 2.2**.

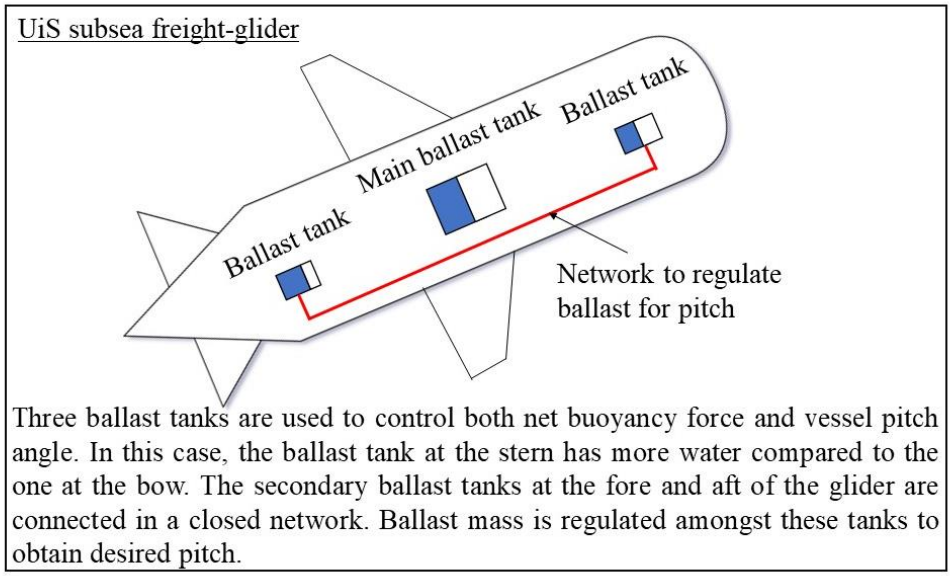

Figure 2.2 Ballasting system for USFG.

The actuating mechanism aboard the USFG is accompanied by two separate proportional-integral-derivative (PID) and linear quadratic regulator (LQR) controllers (Ahmad & Xing, 2021, 2022). These controllers are responsible for controlling the ballast to regulate pitch and heave motion. As shown in Figure 2.2, the main ballast tank adjusts the motion of the USFG in the heave direction, allowing it to ascend and descend when required. The two ancillary ballast tanks, connected in a closed system, control the pitch motion.

Application area

As shown in **Figure 2.3**, the USFG plays an integral part in the logistic network of the marine CCS. The USFG is responsible for delivering CO_2 (captured and stored by onshore facilities) to the subsea wells capable of acting as storage sites. The USFG can transport cargo autonomously, and suitable weather windows do not limit its operations compared to conventional tankers, which are not deployed in extreme sea states. The USFG aims to decrease the global carbon footprint and can contribute to it in several ways. With a significant increase in population each year, the energy need is also rising. As a result, the carbon content in the earth's atmosphere is predicted to increase two times by 2100, contrary to the concentrations in 1960 (Taylor, 2010). The emissions for all the conveyance operations concerning the USFG are zero, as the vessel utilizes electrical power stored in battery cells to power the pumps and all the auxiliaries onboard.

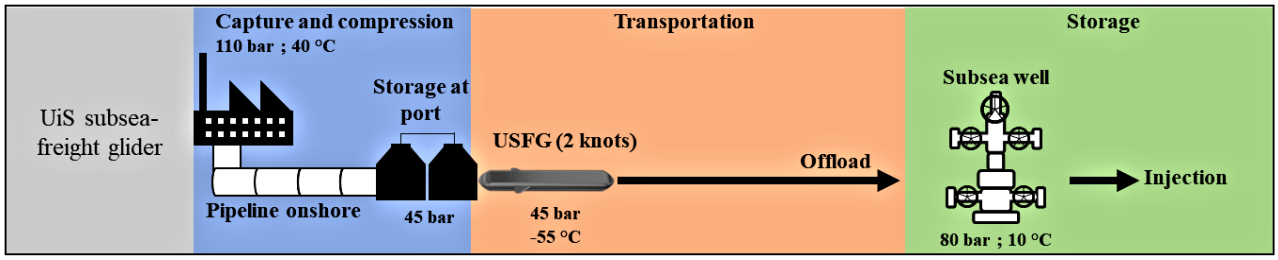

Figure 2.3 Marine CCS process utilizing USFG.

The ultra-efficient propulsion system of the USFG can lessen the overall emissions of the shipping industry, as maritime transportation activities produce nearly 3.3 percent of the hydrocarbon-bearing CO_2 emissions (Papanikolaou, 2014). In addition, modern technologies enable us to capture and process CO_2 from the air. Therefore, the imminent requirements of the CCS (Carbon Capture and Storage Association [CCSA], 2020) can be met by utilizing the USFG and small offshore fields to haul and store CO_2, respectively.

2.2 Mission Requirements and Specifications

The primary input of the entire design process is marked by the mission requirements and the specifications of USFG. USFG's baseline parameters for the design process are shown in **Table 2.2**.

Table 2.2 Design parameters of the USFG.

Character	Value	Unit
Functional depth	200	[m]
Determined range	400	[km]
Operating speed	2	[knots]
Cargo pressure	35 - 55	[bar]
Freight temperature	0 - 20	[°C]
Current velocity	0.5 – 1.0	[m/s]
Collapse depth	400	[m]

Freight capacity

The USFG can be scaled up or down depending upon the demands and applications of the various CCS markets around the globe. It can haul 531-tons of cargo (CO_2, subsea equipment, and crude oil) for every 400 km trip. Instead of deploying a large tanker vessel with significant capacity, numerous USFGs can be employed to carry an equivalent volume of CO_2 daily. This

solution can lead to significant financial advantages: the operational expenditures (OPEX) for smaller capacity vessels are lesser than for larger carriers.

Environmental conditions

The underwater environment defines the operating temperatures of the USFG, and the temperatures vary from 0 to 20 °C. As a reference, the North Sea (0 – 10 °E, 60 – 70 °N) has temperature fluctuations between 2 °C and 12 °C (National Centers for Environmental Information [NCEI]). Furthermore, the regular current speeds monitored in the North sea are around 0.2 m/s. Therefore, to accurately represent the typical current velocities of the Norwegian coast and the North Atlantic region, the current speed for this analysis is limited to 0.5 and 1.0 m/s (Ersdal, 2001; Mariano et al., 1995; Sætre, 2007).

Range of nominal operating depth

A safety depth of 40 meters is distinctly defined to avoid collision or accident with ships or floating constructions on the free surface. This depth also minimizes the effect of waves on the USFG, rendering its operations independent of weather conditions. The safety depth is also depicted in **Figure 2.1**. At the same time, situations responsible for losing control of the vessel define the nominal diving depth, as the retrievable depth is considered while defining it. Therefore, while transporting CO_2, the nominal depth of the USFG is defined to be 200 meters.

Consequently, the operating depth ranges from 40 to 200 meters. Moreover, the test diving and collapse depths are 1.25 and 2.00 times the operating depth between 250 and 400 meters. Therefore, all the depths agree with Table 1 in DNV-RU-NAVAL-Pt4CH1 (DNV-GL, 2018). **Figure 2.4** illustrates various depths of the USFG along with the depths of the CCS sites in the Norwegian sector.

Transportation range

The USFG is designed for a range of 400 km and to complete a one-sided mission to Sleipner and Utgard offshore fields. Additionally, a round trip is feasible for storage sites at Snøhvit and Troll. For the latter case, the USFG is planned to be charged while docking at the offshore facilities of Utsira High (Ivar Aasen, Edvard Grieg, and the Gina Krog fields). These facilities are powered from the land-based grid with the aid of the Johan Sverdrup field.

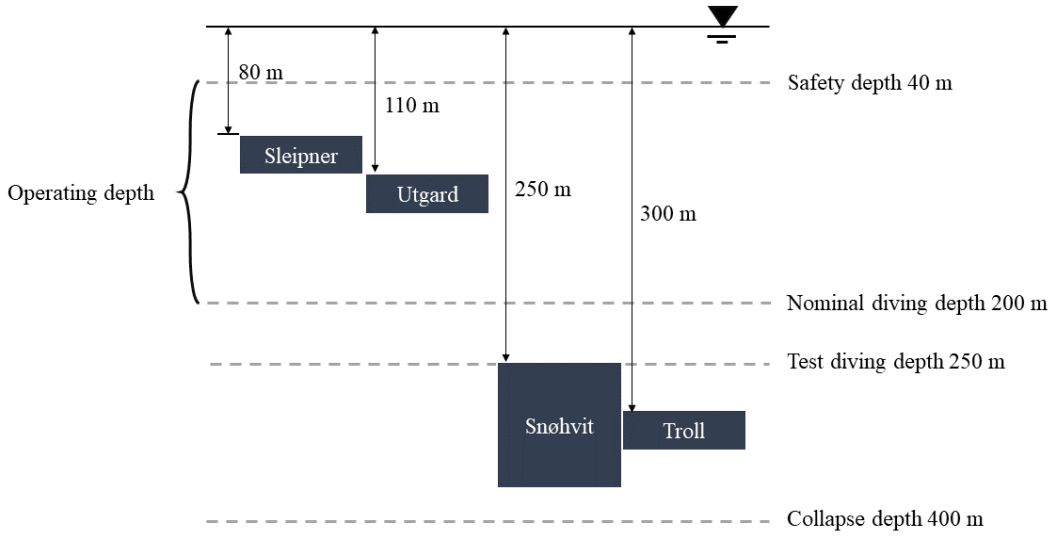

Figure 2.4 CCS site depth with USFG depth definitions.

2.3 General Arrangement

The general arrangement of the USFG shows the location of all the mechanical elements of the USFG. As shown in **Figure 2.5**, the general arrangement is separated into two parts: the internal tanks and compartments of the external hull.

The external hull of the USFG is designed to depict a torpedo-shaped geometry; this minimizes the effects of resistive drag forces. It contains a conical-shaped aft, a hemispherical designed bow, and a cylindrical mid-body, while steel is the preferred material for the external hull of the USFG. The aft and bow sections occupy approximately 23 percent of the total steel weight. A dual-hull/shell design is applied for the cylindrical body to avoid designing the mid-body for failure under collapse pressure. As a result, the mid-body's external hull is independent of differential loading (loads from hydrostatic pressure). The pressure hulls (buoyancy tubes and cargo tanks) are provided with enhanced reinforcement using bulkheads. These four bulkheads are also employed to isolate the mid-body (flooded section of the USFG) from the freely-flooded compartments. As a result, the cargo tanks and the buoyancy tubes, as shown in **Figure 2.5**, are compact pressure hulls that can resist burst and collapse pressures.

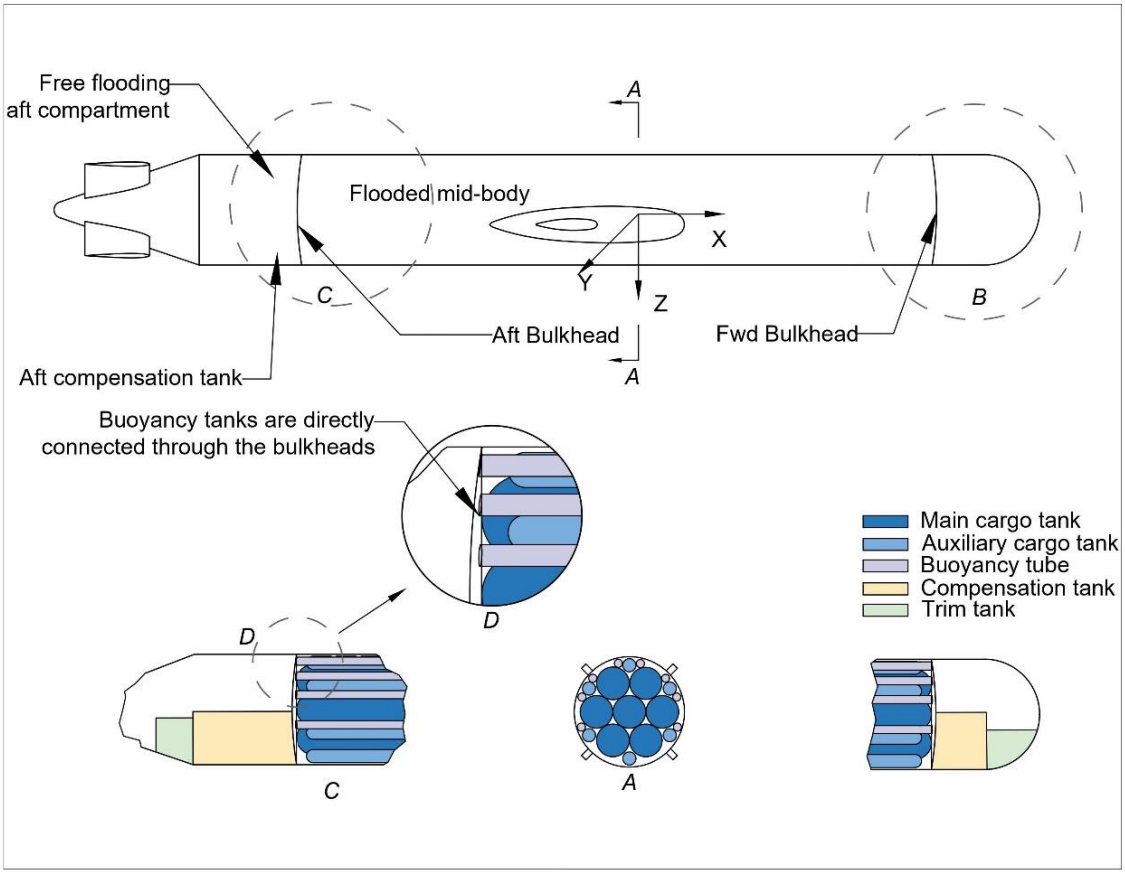

Figure 2.5 USFG's general arrangement.

The external shell or hull aboard the USFG incorporates three distinct components: (1) a free-flooding section positioned at the fore of the USFG comprises sonar, radio, fore compensation tank, a control terminal, sensors, fore trim tank, and pumps for offloading CO_2; (2) a central mid-body compartment (flooded) which carries cargo and buoyancy tanks along with piping equipment, and has the largest capacity amongst all the compartments on the USFG; (3) a free-flooded compartment situated at USFG's stern, this section encloses all humidity-sensitive equipment namely, battery, motor, rudder control mechanism, aft and trim compensation tanks, and gearbox. In addition, the USFG has five kinds of internal pressure vessels, including trim tanks, main cargo tanks, buoyancy tubes, compensation tanks, and auxiliary cargo tanks.

- *Trim tanks:* The baseline design of the USFG contains two trim tanks located at different locations. One is positioned in the cone (stern of the vessel), and the other is located in the fore hemisphere. The objective of these tanks is to assist the USFG in attaining a neutral equilibrium state longitudinally. This is accomplished by carefully

adjusting and placing the center-of-gravity (G) of the vessel under the center-of-buoyancy (B). A closed network of pipes and connections enables the trim tanks to regulate the ballast. Furthermore, the tanks are created to endure the internal pressure from the water, since they are located in a flooded compartment (mid-body). As a consequence, these tanks are independent of the external pressure variations due to changes in depth.

- *Main and supplementary cargo tank:* The tanks organized in a rotational symmetry are cargo tanks, as shown in Figure 2.5. These consist of seven primary and six auxiliary or secondary cargo tanks. The cargo tanks are designed to have hemispherical heads along with cylindrical shells.

- *Buoyancy tubes:* Eight buoyancy tubes aboard the USFG can resist collapse pressures. The length of these tubes is identical to that of the cargo tanks as they are placed in the upper section of the vessel (bulkheads hold these tubes). The buoyancy tubes are utilized to render the USFG neutrally buoyant.

- *Compensation tanks:* The two compensation tanks provide enhanced stability to the USFG while experiencing different hydrostatic loading scenarios (Ref. **Chapter 5**). These tanks work by changing the moment (trim) and the vessel's weight to attain neutral buoyancy. In addition, trim tanks and cargo and compensation tanks are designed to resist high burst pressures.

Chapter 3 - The Glider Control Model

This chapter concerns designing the dynamics of the USFG to evaluate a robust and stable control system for operation. The objective is to create a mathematical model of the USFG capable of capturing the effects of external forces, namely, hydrodynamic and buoyancy forces. The targeted studies are the equilibrium glides of the USFG (Ref. **Figure 2.1**) and its applications. The USFG must follow a pre-defined route to optimize gliding efficiency while enhancing its range during the entire mission. When designing an autonomous underwater vessel, its ability to navigate appropriately is vital. At the same time, the energy onboard the USFG can likely be conserved by keeping the defined path, as the aim is not to surpass the one-fourth portion of the defined energy budget (Langebrake, 2003). In this context, the USFG is programmed to avoid detours or deviations while following the route. For autonomous vessels, position tracking is only done in the early phases of the mission (Griffiths, 2002).

Simulink (Simscape Multibody toolbox) is employed to develop the planar multibody model of the USFG. This model involves designing the USFG with the aid of blocks or modules. These blocks are simulated in MATLAB, enabling the glider's dynamics to be captured and expressed ultimately. The proposed model can be applied to a wide range of USFG sizes and an extensive variety of underwater gliders, contrasting to USFG explicit.

3.1 USFG's Axis System

To define and study the system dynamics of the USFG, earth and a body-bounded frame are specified. The USFG's center of gravity (G) is accurately situated at the body-bounded frame (O_{bb}, X_{bb}, Y_{bb}, Z_{bb}). The local coordinate system (O_{EB}, X_{EB}, Y_{EB}, Z_{EB}) includes north, east, and down directions. The USFG must remain stable or upright throughout the mission as it moves in this saw-tooth pattern. Therefore, the buoyancy center (B) settles above the G. The axis system, USFG's motion, and direction are illustrated in **Figure 3.1**.

3.2 Simulink Application

The mathematical model of the UiS subsea freight-glider has been designed and implemented in MATLAB Simscape Multibody, also referred to as SimMechanics.

Figure 3.2 and **Figure 3.3** depict the control loop and the mathematical model utilized for the glider system.

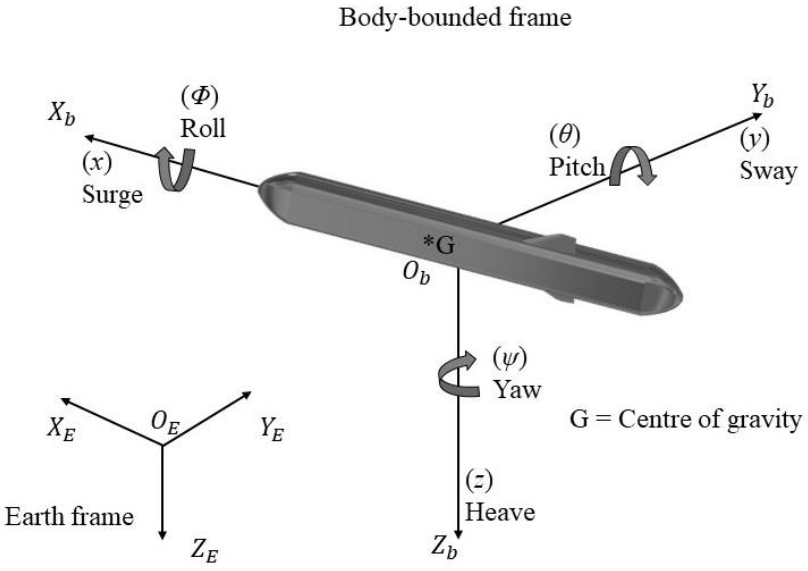

Figure 3.1 Axis system for the control model.

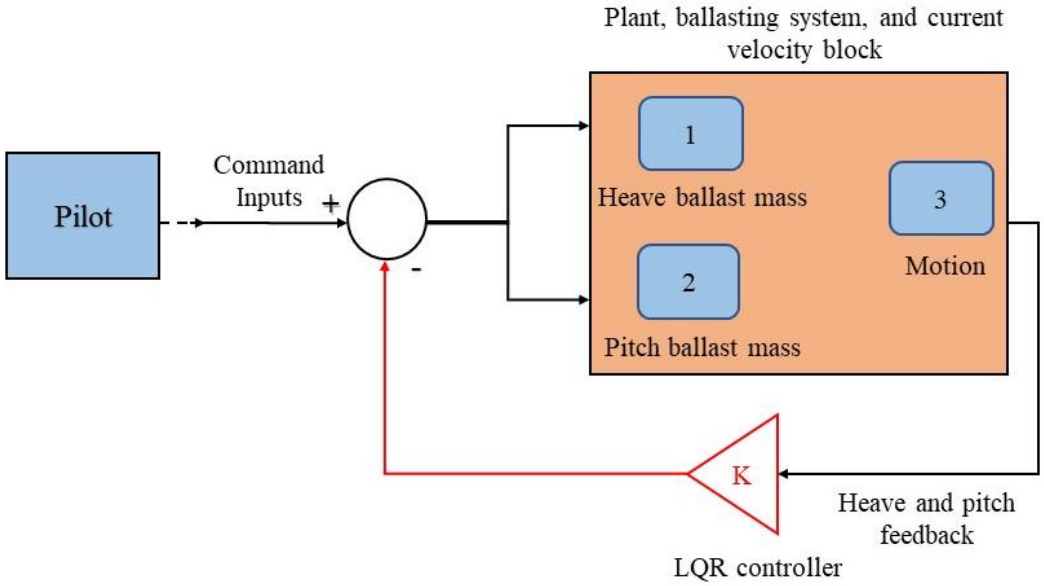

Figure 3.2 Control loop for the mathematical model.

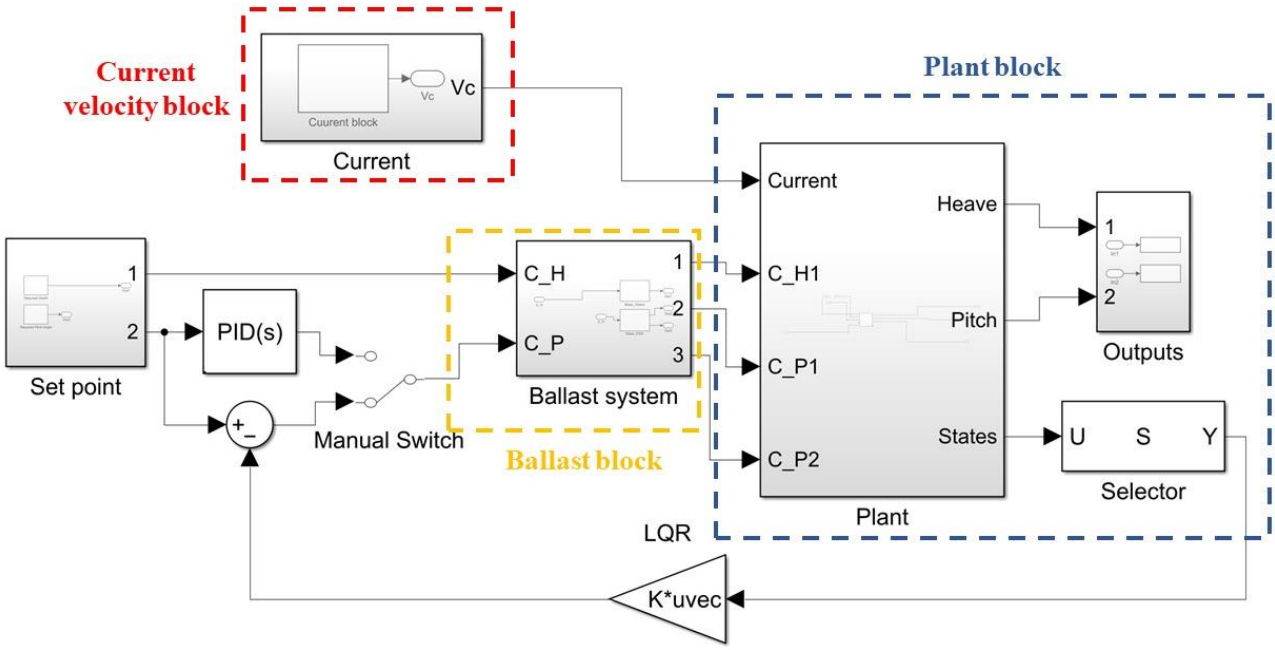

Figure 3.3 Simulink design - ballast, current velocity, and plant block.

USFG is designed as a multibody system; this is done to analyze the dynamic response of the vessel itself with the actuating mechanism. All the sub-systems of the USFG are presented as the main modules, which are explained subsequently:

- *Plant module/block:* in the Simulink environment, this block is utilized to characterize the USFG. This module implements all the equations of motion for the USFG, especially the equilibrium glides and their applications. This is achieved by studying the effects of hydrodynamic derivatives, body, and hydrofoils' lift and drag forces along with the hydrostatics of the USFG.

- *Ballast system module/block:* This block is responsible for representing the actuating mechanism aboard the USFG. The function of this module is to govern the ballast mass among various tanks. This block provides the actuation that enables the glider to maneuver in the heave direction. The hydrofoils also aid the motion along the heave direction (responsible for generating the lift and drag forces). Likewise, this block allows the glider to pitch backward (bow heading up) and the other way around. Additionally, a rate-limiter is also employed that restricts the volumetric flow rate of the ballast among the tanks. Similarly, a saturation unit controls the amount of ballast between the tanks.

- *Current block*: this block is added to simulate USFG's responses to the oceanic current loads. Stochastic currents of 0.5 and 1.0 m/s are generated to be analyzed in this thesis.

- *Control system block:* represented as LQR in **Figure 3.3**, this module embodies the control system of the USFG. Moreover, this encompasses the PID and LQR controllers used for various studies in **Chapter 4**.

3.2.1 Plant Module/Block

As shown in **Figure 3.3**, the plant module is briefly described in this subsection. A rigid planar structural member characterises the USFG during multibody modeling. This body has three degrees of freedom or is allowed to move in three directions ($x, z, and\ \theta$). The motion is characterized by the surge, heave, and pitch described in **Figure 3.1**. The following equations are solved and implemented in this block:

$$M(\dot{u} + wq - xq^2 + z\dot{q}) = \sum X_e$$ $$M(\dot{w} + uq - zq^2 + x\dot{q}) = \sum Z_e$$ $$I_{zz}\dot{q} + M\lfloor z(\dot{u} + wq) - x(\dot{w} - uq)\rfloor = \sum Q_e$$	**Equation 3.1**

M represents the mass of the USFG, X_e, and Z_e are added mass and damping forces in surge the and heave direction, and Q_e, is the peripheral pitching moment. Velocities are given by u (surge direction), q (pitch direction), and w (heave direction). Likewise, $\dot{u}$, $\dot{q}$, and $\dot{w}$ gives acceleration in the corresponding directions, whereas I_{zz} represent the moment of inertia of the USFG during the pitching motion. Additionally, the external forces acting on the USFG are shown as a total (sum) on the right side of the equations (**Equation 3.1**), while the inertial terms are presented on the other side.

This module also calculates the external forces acting on the body (**Equation 3.2**), namely, drag (D_f) and lift (L_f), along with the rotational torque (M_T). D_c and L_c (**Equation 3.3**) are the drag and lift coefficients, accordingly, whereas C_M is the coefficient for damping moment,

whose value is defined as 1000. δ is the seawater density, V_s is the overall submerged volume of the USFG, and S is the net maneuvering velocity of the USFG.

$D_f = \frac{1}{2} \times D_c \times \delta \times V_s \times S^2$ $L_f = \frac{1}{2} \times L_c \times \delta \times V_s \times S^2$ $M_T = -\frac{1}{2} \times C_M \times \delta \times V_s \times q^2$	**Equation 3.2**

$D_c = 0.4\alpha^2 + \alpha + 0.1$ $L_c = 5\alpha^2 + 10\alpha$	**Equation 3.3**

The volumetric constants (**Equation 3.3**) are a function of the angle of attack (α) or the approach angle of the incoming flow of ocean currents. Furthermore, these coefficients are built on the presented model (Graver, 2005), as the proposed glider design in this dissertation is similar to that of USFG's outer hull.

Likewise, the drag and lift forces produced by the large hydrodynamic wings of the USFG are also modeled and utilized in this sub-system. The reference wing area for the hydrofoils is determined in **Appendix A - Calculation of Reference Wing Area**, which is also combined within this module (Ahmad et al., 2022). The NACA 4412 airfoil (Airfoil Tools, 2022) design is applied as a reference to capture and model the kinetics of the hydrofoils. Further, the volumetric coefficients are modified in this case (**Equation 3.4**). H_D and H_L are the drag and lift forces induced by the wings, and M_H is the moment. The improved equations for hydrofoil design are:

$H_D = \frac{1}{2} \times D_{ch} \times \delta \times V_s \times S^2$ $H_L = \frac{1}{2} \times L_{ch} \times \delta \times V_s \times S^2$	**Equation 3.4**

$$M_H = -\frac{1}{2} \times C_{Mh} \times \delta \times V_s \times q^2$$	

The revised volumetric coefficients (D_{ch}, L_{ch}, and C_{Mh}) for the hydrofoil design are also highlighted (**Equation 3.5**).

$$D_{ch} = Ae^{(B\alpha)} + Ce^{(D\alpha)}$$ $$A = 2 \times 10^{-3}; B = -0.2093; C = 2.5 \times 10^{-3}; D = 0.1892$$ $$L_{ch} = a\alpha^3 + b\alpha^2 + c\alpha + d$$ $$a = -10 \times 10^{-5}; b = -9 \times 10^{-4}; c = 0.114; d = 0.4942$$ $$C_{Mh} = q + w\cos(\alpha u) + r\sin(\alpha u) + t\cos(2\alpha u) + y\sin(2\alpha u)$$ $$q = -0.085; w = -0.026; r = 0.014; t = 0.0076; y = -0.0076$$ $$u = 0.1595$$	**Equation 3.5**

3.2.2 Ballast Module/Block

This block includes the actuating mechanism (ballast tanks), as it is utilized to analyze the kinematic responses of the USFG during gliding. No ancillary thrust sources (skegs, thrusters, and propellers) are designed or employed in the mathematical model, as the USFG generates thrust by a combination of hydrofoils and by varying the ballast mass in the tanks. The tank layout for the USFG is illustrated in **Figure 2.5**.

There are two types of ballast tanks onboard the USFG: compensation and trim. Both of these tanks contribute to the stability of the USFG, as they produce neutral floating and trim conditions. The compensation tanks (situated at the stern and bow) deliver the required trimming moment and ballast mass to the glider to provide neutral buoyancy. Additionally, two marginal trim tanks, located at the bow and stern, provide minor adjustments to the vessel's stability by ensuring the G of the glider always remains below the B. Doing this enables the

USFG to keep a neutral or zero trim state. Similarly, the buoyancy tanks aboard the USFG can improve the stability by expanding the ballasting capacity, contrary to ballast tanks which regulate the ballast mass.

3.2.3 Current Module/Block

The ocean current is simulated using the first-order Gauss-Markov process (Fossen, 2011). The velocity of the inflowing current U_c, along with flow angle φ_c is given:

$\dot{U}_c + \nu_1 U_c = \lambda_1$ $\dot{\varphi}_c + \nu_2 \varphi_c = \lambda_2$	**Equation 3.6**

The constants ν_1 and ν_2 (magnitude should be greater than zero) are employed to define the Gauss-Markov process with the aid of the time constants (Fossen, 2011). Additive White Gaussian Noise (AWGN) is represented by λ_1 and λ_2. Marginal values of ν_1 and ν_2 are applied in this study, i.e., 1, to yield a steady current profile. Also, a value of 10^{-1} is assigned to the noise power. Doing this ensures a fluctuating effect in the current speed and direction. The extreme ocean current velocity recorded at the NCS is 1 m/s (Ersdal, 2001), which is the design current speed for USFG.

The current velocities in surge along with heave directions, as highlighted in USFG's body frame (Ref. **Figure 3.1**), are provided as:

$u_{wc} = U_c \cos \varphi_c$ $w_{wc} = U_c \sin \varphi_c$	**Equation 3.7**

The velocity of the incoming flow of water in horizontal (x) and vertical (z) directions are represented by u_{wc} and w_{wc}, correspondingly. At the same time, the inflowing relative velocity encountered by the USFG in these directions is given:

$u = u_{USFG} - u_{wc}$ $w = w_{USFG} - w_{wc}$	**Equation 3.8**

The USFG's net velocity magnitude in surge and heave is shown by u_{USFG} and w_{USFG}.

3.2.4 Control System Module/Block

The scope of this thesis (for the mathematical model) is restricted to a two-dimensional problem for the USFG, i.e., only kinetic responses and kinematic motions in heave and pitch directions are recorded and analyzed. The motions along the other remaining degrees of freedom are not included in the domain of this work. The following assumptions are made to carry out this analysis:

- The USFG is assumed to be in a state of hydrodynamic equilibrium. The system, therefore, is uncoupled; no coupling can be detected for the hydrodynamic terms since all forces are directed at the glider's geometric center.

- It is understood that the USFG operates far off from the region where waves are predominant; wave loads are minimal.

As mentioned earlier, two popular controllers are employed, forming the entire control system of the USFG.

PID-type control

The Proportional-integral-derivative (PID) controllers have been extensively utilized in autonomous applications, especially underwater vehicles. For instance, Slocum, which maneuvers by using an internal actuating mass, employs PID-type control to regulate the motion of this mass (Webb et al., 2001).

The USFG's implementation aims to regulate the pitching motion in a closed feedback loop, which develops a single input single output (SISO) system. The PID controller varies the motion along the pitch direction using the glide path angle (ξ) as the feedback. As an example, if $P(s)$ is the transfer function of a control loop, so $P_c(s)$ (**Equation 3.9**) yields the PID controller.

$$P_c(s) = K_p\left(1 + \frac{1}{T_i s} + T_d s\right)$$	**Equation 3.9**

$$p(t) = K_p\, e(t) + K_i \int_{to}^{t} e(\tau) d\tau + K_d \dot{e}$$	

The integral and derivative times are represented by T_i and T_d, respectively, and the proportional gain is depicted by K_p. The control system's performance can be improved by carefully tuning these constraints. $p(t)$ characterizes $P_c(s)$ in the time domain. The integral and the derivative gains are defined by $K_i = K_p/T_i$ and $K_d = K_p T_d$, correspondingly. The steady-state error is denoted by $e(t)$, which shows the difference between the output response obtained from the system and the required response.

LQR-type control

Linear quadratic regulator (LQR) is also used in this analysis. Similar to the PID controller, it is designed to manage the USFG's kinematics in heave and pitch directions. Due to its robust and stable performance, LQR has already been applied to numerous autonomous marine vehicles. Earlier, it has been employed to administer the steering and depth control of underwater vessels (Bae et al., 2014; Burlacu et al., 2007). The LQR type controller adjusts the system's phase responses using a full state feedback strategy. This strategy entails feeding optimal and configurable controller gains into the system's control loop. Consequently, this enhances the overall responsiveness of the system. The state-space equations of the USFG are applied to deduce the gains. The equations for a single input and multiple output system (SIMO) are:

$$\frac{dx_{1,2}}{dt} = Jx_{1,2} + Ku_{1,2}$$ $$y_{1,2} = Lx_{1,2}$$	**Equation 3.10**

$x_{1,2}$ denotes the state vectors of the system, $y_{1,2}$ and $u_{1,2}$ are the output and input vectors, correspondingly. Whereas K represents the input matrix, J and L are shown as state and output matrices, respectively. L, K, and J matrices are evaluated in **4.1.1 System Linearization**.

For LQR-type control, the energy spent by the actuating mechanism is collated and balanced with the desired or ideal system performance. By doing this, optimum and robust controller gains are obtained. The control law is given by, $S = -Gx$; for this analysis, G signifies the

optimal gain matrix. The applied control law is designed to minimize the immense total of variations obtained from the principal quantities of the system, also recognized as the quadratic cost function:

$$C = \int_0^{\infty} \delta x^T N \delta x + \delta u^T M \delta u \, dt$$	**Equation 3.11**

The weights of the state and actuator cost are given by N and M matrices; the strategy is to fine-tune the weights of these matrices while monitoring the system output; the aim is to decrease the energy spent by the actuators. Also, necessary tuning for the LQR controller can be done by changing the weights of N and M matrices, as deduced from **4.2.2 Tuning of LQR Controller**.

3.3 Summary

An analytical model for analysing equilibrium glides and their applications for USFG is presented. The glider control model presents the two-dimensional mathematical model of the USFG. An axis system must be defined for the vessel before establishing its mathematical design. This chapter presents the coordinate system utilized while modeling the glider. Simulink, a graphical user-interface design environment founded on MATLAB, is used to capture the system dynamics using modules or sub-systems. The mathematical model consists of the plant, ballast, current, and control block; these blocks constitute the entire USFG. In this system, two different controllers regulate motion in the heave and pitch direction. A brief comparison of PID and LQR controllers is also presented. Additional model details can be found in the enclosed papers in **Appendix B – Appended Papers.**

Chapter 4 - Dynamic Responses of Controlled Glides

The USFG needs to have a durable, steady, and rigorous control system to attain improved range and optimal average velocities: this ensures an accurate navigation system that allows the USFG to glide more efficiently. In addition, a robust controller can cater to external uncertainties induced by the environmental instabilities, as it is designed on feedback the system provides. Doing this provides enhanced utility during the entire mission of the vessel.

This chapter highlights the characteristics of a control technique along with its application. This technique removes the need for re-tuning controllers if the operating conditions of the USFG are modified, as it is based on feedback from the model. An integrated observer can evaluate the kinematics of the USFG in a two-dimensional plane; this helps to deduce the dynamic states, namely, gliding velocities. The gliding paths of USFG, restricted to the vertical plane, are investigated along with the observability and controllability of the equilibrium glides. The glider's heave and pitch are controlled and monitored by two different controllers, PID and LQR, which are included in the control system. The final collation study assesses the critical characteristics of controllers for tuning and response prediction. This evaluation can likely aid in designing the ideal control for the essential applications of the USFG.

4.1 Controlled Gliding of the USFG

This section analyzes the two vital characteristics of a control system, controllability and observability. The USFG must be controlled and observed since these characteristics determine whether the states of the system can be controlled and measured by the actuators and sensors, respectively. The gliding path of a vessel can be described and examined by the required velocity (S_r), and the glide path angle (ξ_r). These parameters, along with lift force (L_f), pitch angle (θ), angle of attack (α), and drag force (D_f) are depicted in **Figure 4.1**. The glide angle and velocity of the USFG are:

$$\xi = \theta - \alpha$$ $$S = \sqrt{(u_{USFG})^2 + (w_{USFG})^2}$$	**Equation 4.1**

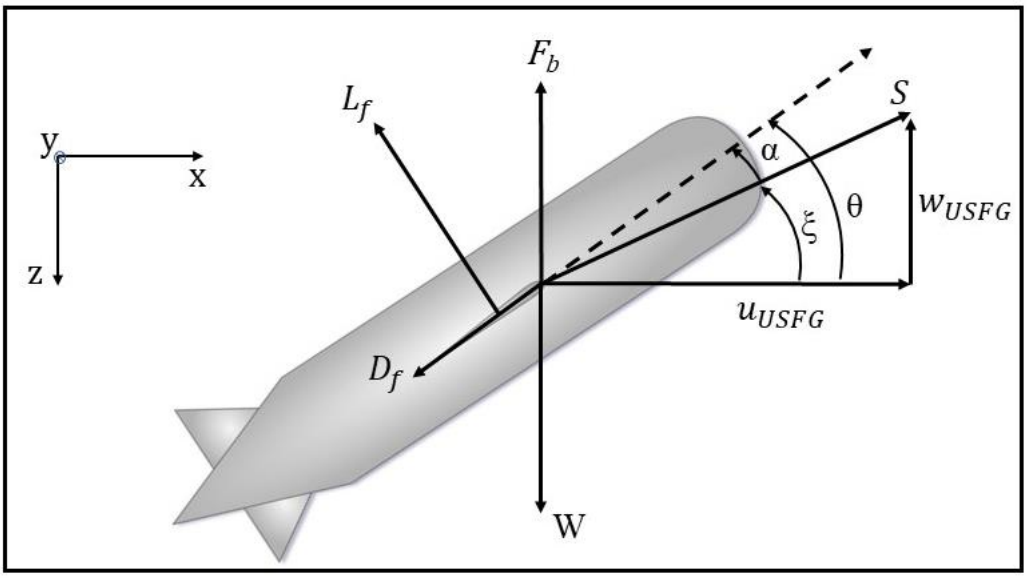

Figure 4.1 USFG's gliding parameters – side view of the glider.

Equation 4.2 gives the coordinates (x', z'), where z' is the perpendicular distance from the desired path, and x' converges with the probable path, as depicted in **Figure 4.2**.

$$\begin{bmatrix} x' \\ z' \end{bmatrix} = \begin{bmatrix} \cos \xi_r & -\sin \xi_r \\ \sin \xi_r & \cos \xi_r \end{bmatrix} \begin{bmatrix} x \\ z \end{bmatrix}$$	**Equation 4.2**

Two objectives are defined for enhanced understanding concerning the kinematics of the USFG:

- **T01** primary objective is to govern USFG's gliding motion characteristics, i.e., path and velocity. It must be noted that for this case, x and z are not measured.
- **T02** secondary task is designed such that the USFG must observe a straight route or line, illustrated in **Figure 4.2**. Here z' is the key variable, as the focus is to decrease it while obtaining $z' = 0$, without utilizing x'.

4.1.1 System Linearization

The mathematical model of the USFG, presented in **Chapter 3**, is linearized for two glide angles, 30° and 40°, as shown in **Table 4.1**. Linearization is done to deduce the state-space

equations of the system, as the resulting linear model cannot be utilized to extract the state model of the USFG.

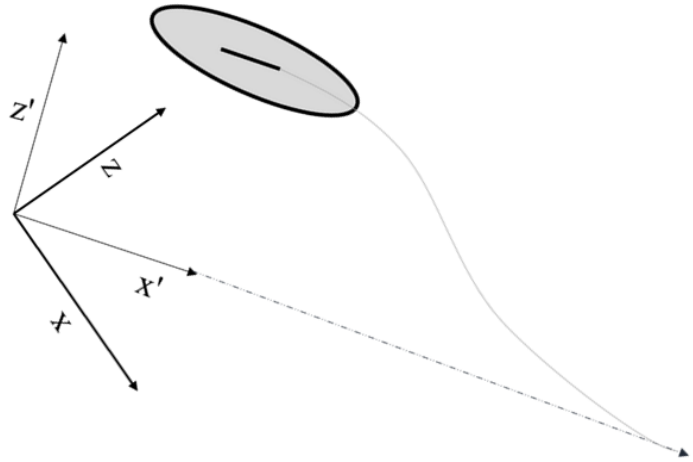

Figure 4.2 T02 depicted in 2D Plane.

Table 4.1 Glide paths for linearization.

Parameter	30° Downwards	30° Upwards	40° Downwards	40° Upwards
θ_r (deg)	-30.00	30.00	-40.00	40.00
α_r (deg)	4.65	-4.65	2.04	-2.04
ξ_r (deg)	-35.35	35.55	-42.04	42.04
S_r (m/s)	0.35	0.35	0.80	0.80

The model linearizer toolbox, an extension of Simulink, is employed to linearize the two-dimensional model at model operational points (MathWorks, 2022). At the same time, a Bode plot for the system can be generated after configuring the input/output functional points. Consequently, L, K, and J matrices can be deduced.

The extracted state-space model of the USFG, with linear characteristics, determines the design specifications of the control system, i.e., controllability and observability. It is possible to automate the design process for various gliding applications of the USFG by using linearization. The process can be automated by implementing the Routh criterion to various model parameters such as ballast mass, velocity, and glide angle. Doing this determines the stability of the USFG's gliding motion.

4.1.2 Controllability

This subsection examines the controllability of the steady gliding paths of the USFG since this also affects the stability. It is worth noting that this technique can be applied to any autonomous glider or vessel design, provided its mathematical model is obtainable.

The mathematical model of the USFG is controllable for all the applications of the glide path, including the simulated cases detailed in **Table 4.1**. Specifically, the rank condition relating to the controllability matrix is satisfied; the rank of matrix J is equal to the rank of the controllability matrix. This condition is valid for all the equilibrium glide path operating conditions. Furthermore, according to the linearization presented in the previous section, the condition of the state variable z' is examined; z' is observed in the linear equations. This implies that controllability is also applied to the variable z' of the system. Hence, current controller can be configured for the USFG that can achieve **T01** and **T02**.

4.1.3 Observability

Observability for the various glide conditions highlighted in **Table 4.1** is analyzed in this section. For **T01**, variable z' is not required for this application since only the USFG's velocity, and the direction of travel is controlled for each glide path. The dynamic model of the USFG is entirely observable, concerning M_{b} and M_{s} (variable mass for main ballast and secondary ballast tanks). That is because the rank of matrix K equals the rank of the observability matrix. For this scenario, detection of θ pitch angle, $\dot{\theta}$ pitch rate and the velocity components u_{USFG} and w_{USFG} are not required. Consequently, a mathematical observer can be designed which corresponds with M_{b} and M_{s} to approximate $\theta, u_{USFG}, w_{USFG}$ and $\dot{\theta}$ which are the unmeasured variables or states of the USFG. An observer has the added benefit of estimating the velocity components u_{USFG}, and w_{USFG} as θ pitch angle is commonly measured, as for $\dot{\theta}$ pitch rate is generally easy to measure using onboard instruments. The mathematical model of the USFG, if restricted to state variables θ, M_{s} and M_{b} is fully observable.

High precision and accuracy can be obtained in **T01** by employing a dynamic observer. By doing this, the observer approximates the variables or states of the vehicle, and the accuracy of the entire process may be significantly enhanced. Moreover, present-day measurement methods induce some simplifications to the system for measuring states, i.e., constant angle of

attack. For instance, Slocum utilizes velocity calculated from depth measurements, global positioning system (GPS) locations, and quantified pitch angles θ and implicit angle of attack to compute the horizontal motion throughout gliding (Graver, 2005). Similarly, for the Spray glider, the horizontal distance during the gliding is measured depending on constant attack angle, pitch, and heading (Sherman et al., 2001).

For **T02,** i.e., to control the glider's motion along a straight path, z' needs to be measured. From **Equation 4.2**, it is seen that z' is dependent on the horizontal state-space variable x (cannot be measured) and the depth coordinate z (measurable). The state-space variables M_{s} and M_{b} along with the estimation of z are not enough for observing x. To measure the trajectory of USFG $x(t)$, measurements at initial conditions are required, rendering x non-observable. Moreover, an observer cannot be designed to detect z', but the horizontal position or motion of the vehicle can be dead reckoned with the assistance of velocity approximations from the mathematical observer by using initial GPS measurements. In this way, an error $(z' - z'_{DR})$ can be inducted into the state variable z'.Finally, **T02** can then be completed by presenting the inferred z'_{DR} feedback into the control loop, enabling the USFG to glide along the commanded or required route. The dead-reckoned velocity in the horizontal direction, $\dot{x}_{DR}$ is given by:

$\dot{x}_{DR} = u_{USFG_e} \cos\theta + w_{USFG_e} \sin\theta$	**Equation 4.3**

x_{DR} can then be obtained by integrating **Equation 4.3,** which is then used to deduce z'_{DR}. The glide parameters, ξ_r, θ and z are defined by the glide path taken by the glider and can be measured without any difficulty. Whereas velocity estimates u_{USFG_e} and w_{USFG_e} can be acquired from the observer. The dead-reckoned parameter z'_{DR} is given by:

$z'_{DR} = sin\,\xi_r\, x_{DR} + cos\,\xi_r\, z$	**Equation 4.4**

For linearization to be operational and practical, the observed variables $u_{USFG_e}$and w_{USFG_e} will tend to close in on the actual state-space variables u_{USFG} and w_{USFG} when the glider is in-line or adequately close to the desired path. On the other hand, if there is an error, subsequently, the result will be $z' - z'_{DR} \neq 0$. Moreover, this error is dependent on state variables and is sensitive to external environmental disturbances.

4.2 Controller Assessment: PID Vs LQR

This section discusses the tuning and response characteristics of two controllers commonly used in marine vehicles, PID and LQR. Two different glides are designed to study the controller characteristics. The following glides are discussed in this section:

- The Equilibrium glide path
- The -38° glider dive

4.2.1 Tuning of PID Controller

The PID tuner app is utilized for tuning the PID-type controller. It is based on the system's transfer function, while it uses the linear model of the system. This method applies the basic tuning principles to obtain the desired system output (Åström et al., 2006). The bandwidth and phase margin of the system is varied to obtain the impulse or step responses. This variation is restricted to the frequency domain. Different combinations of the bandwidths and the phase margins provide the gains for the PID controller. The effects of phase margin and bandwidth on controller parameters such as settling time (time needed by the oscillating signal to gain 2 percent of the conclusive value), percentage overshoot (a steady-state error between the obtained and desired value), and rise time (time needed by the signal to move from 10 to 90 percent of its absolute value) are highlighted subsequently.

Effects of varying phase margin

Figure 4.3 illustrates a comparison of block and tuned response. The block response represents a phase margin of 50°, while the tuned response is evaluated at a 90° phase margin. The heave and pitch motions of the USFG are simulated and presented adjacently in this analysis. The transient behavior of the output response is enhanced with increasing phase margin values. This behavior induces robustness in the control system as the overshoot decreases considerably along with the PID gains. Therefore, the system fails to respond quickly to any changes in the operating conditions, as indicated by higher settling and rise times. At the same time, if the phase margin is decreased, contrary performance is detected.

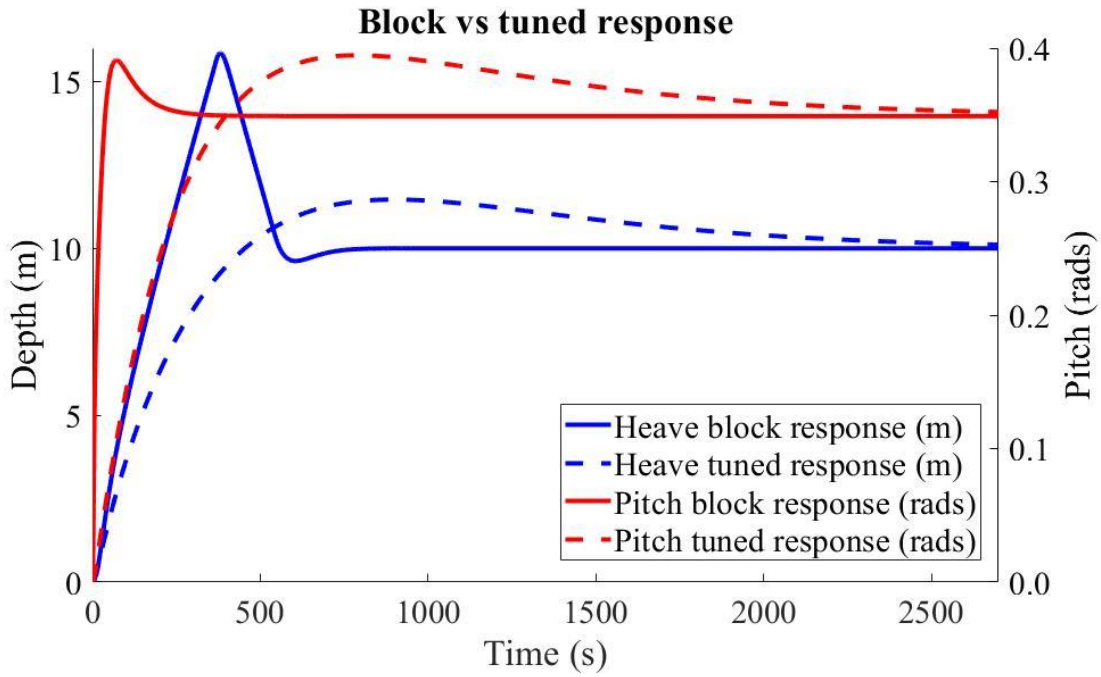

Figure 4.3 Variable phase margin response.

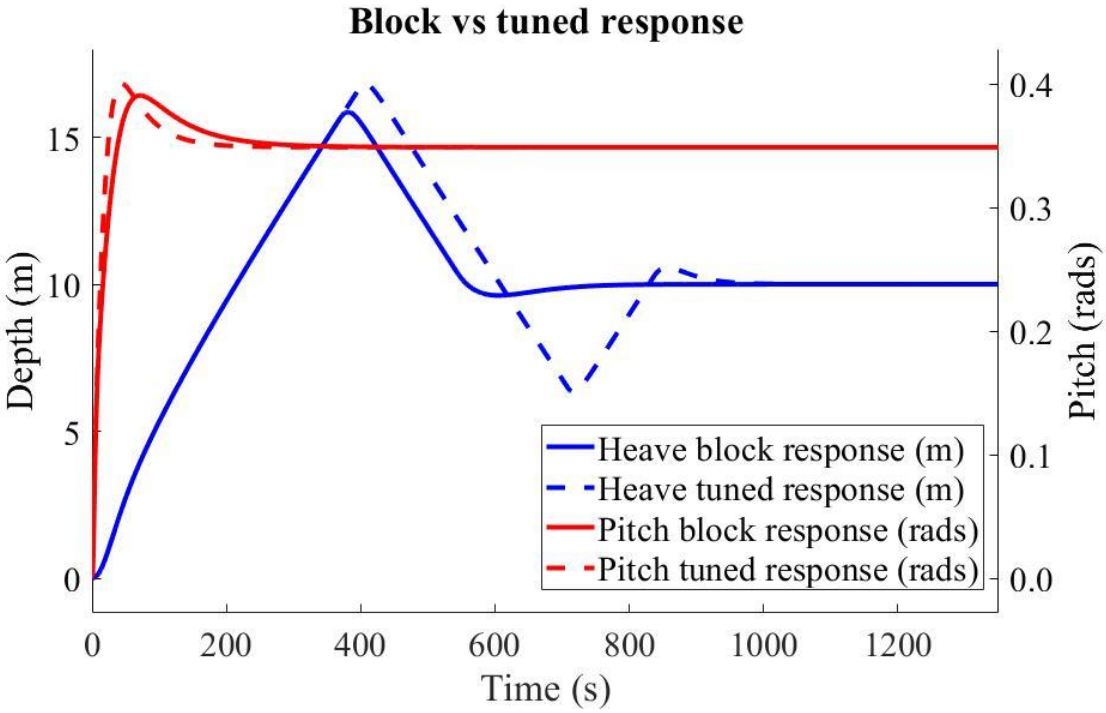

Figure 4.4 Variable bandwidth response.

Effects of changing bandwidth

Figure 4.4 shows the step plots of the bandwidth study. Two responses are simulated, block and tuned signals with a bandwidth of 0.20 and 0.35, respectively. It was observed that higher

values of bandwidth enable the control system to respond to changes efficiently, as indicated by the tuned response. Also, bandwidth is not always beneficial, and amplifying it beyond a specific value induces oscillations (shown in **Figure 4.4** as the tuned response of heave). Thus, the stability of the control system is compromised. The controller gains are observed to increase as response and rise times are reduced. As for the block response, lower PID gains yield a delayed response due to higher settling and rise times for the block response.

This study came to the following conclusions:

- With increased bandwidth, the rise time can be reduced. However, it stands unaffected by any variations in the phase margin.
- Bandwidth does not affect overshoot. From **Figure 4.4**, it is evident that the peaks of block and tuned responses are similar.
- This analysis suggests a bandwidth of 0.3 rad/s and a phase margin of 90°.

4.2.2 Tuning of LQR Controller

An LQR-type controller can be tuned after the system has been linearized. So linearization performed in section **4.1.1 System Linearization** will be utilized here. Based on the state matrices (J and K) obtained from linearization, LQR is tuned to obtain the desired response of the glider. Tuning is done by adjusting the values (penalties) of the N and M matrices (**Equation 4.5)**. A complete and holistic understanding of the kinematics of the USFG is essential to tuning the controller. These dynamics involve studying the system's response time for anticipated system performance. The penalty on the M matrix governs the actuator effort. As for the N matrix, it administers the error amongst the output variables/states.

$N = \begin{bmatrix} 0 \\ 0 \\ 0 \\ 10^3 \end{bmatrix}$ $M = [10^{-2}]$	**Equation 4.5**

The 10^3 for the 41-coefficient represents the acceleration in the pitch direction is corrected heavily, as the system is planned to attain a required pitching angle in the targeted study. The gain matrix is given:

$G = [-5.3 \times 10^{-10} \quad 2.4 \times 10^{-10} \quad 3.2 \times 10^{-10} \quad 2.6]$	**Equation 4.6**

4.2.3 The Equilibrium Glide Path

The sinusoidal path taken by the glider, as depicted in **Figure 2.1**, is analyzed in this subsection. The USFG takes this equilibrium path to expand its travel range since it may allow for a more efficient freight operation when it takes a planned route.

Ideal controller gains from the PID tuning study are selected here to be compared against the LQR implementation. In this analysis, the USFG is assigned an operating depth of 200 meters with a gliding angle of 38°. This scenario is simulated for both controllers (PID and LQR). The equilibrium glide paths against the required response are shown in **Figure 4.5**. The crux of this study is to observe how efficiently each controller enables the vessel to follow the intended path.

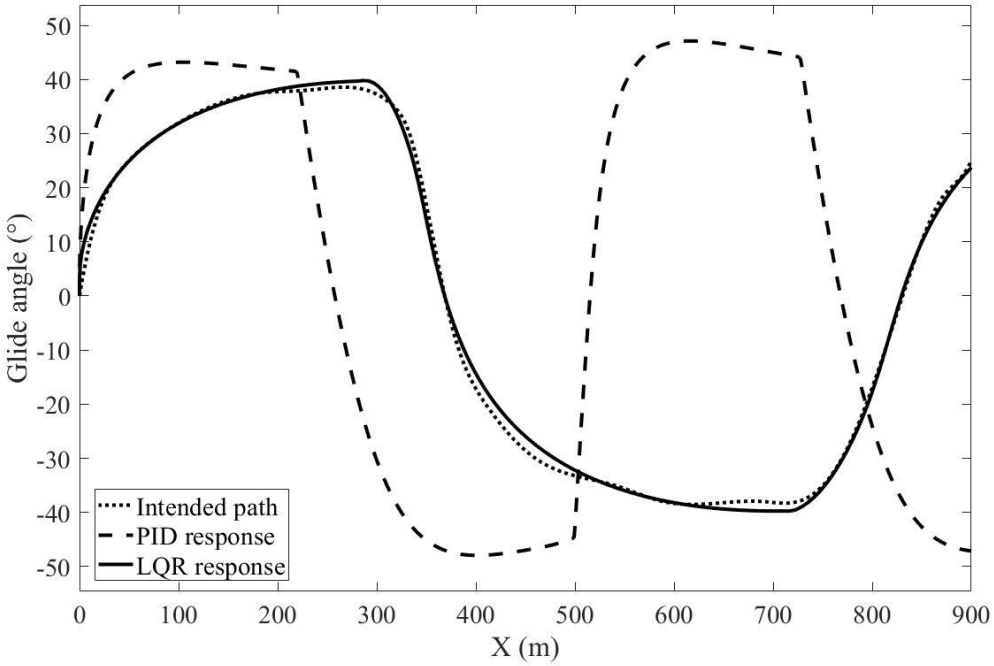

Figure 4.5 Equilibrium glide paths (PID vs LQR) in the vertical plane.

For PID, the glider quickly responds to changes, which can be seen in **Figure 4.5** as a rapid change in glide angle. This abrupt change leads to more glides/dives for a certain distance

traveled, resulting in higher power consumption. Significant overrun is also experienced when PID controls the equilibrium glides. Moreover, these PID gains do not have room for improvement, as added optimization leads to an undesired glider response.

On the other hand, for LQR, the system is stabilized for the said application. By consuming less actuator effort, LQR enables the glider to respond to variations in operating conditions effortlessly and effectively. In contrast, the PID error is 11 percent rather than 3 percent for LQR. For LQR, this error can be further reduced with enhanced tuning. The upper and lower bound deviations are also reduced because of a reduction in overrun.

4.2.4 The -38° Glider Dive

For this scenario, the controlled glide requires the USFG to obtain a pitch angle of -38° (Bow heading down). The amount of energy spent acquiring this glide angle is used as a benchmark in this sub-section.

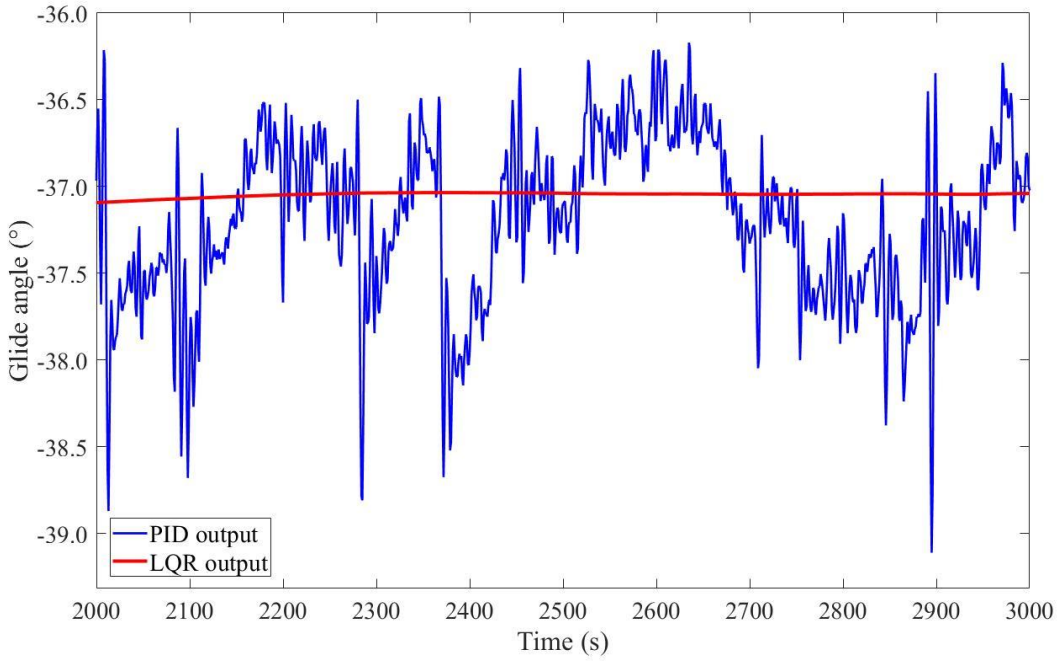

Figure 4.6 Output comparison for the -38° dive.

As highlighted in **Figure 4.6**, the PID controller does not mitigate the fluctuating response. These oscillations increase the power consumption, as the controller continuously spends energy on path correction. In this scenario, excessive actuator effort spent on course modification is not ideal since the glider's objective is to conserve energy while moving cargo

over longer distances. This glide is controlled with a PID controller that is aggressively tuned. As a result, the overall system response is not improved. There is, therefore, no room for improvement in tuning PID. Selecting a controller that causes fewer oscillations and reduces settling time for such applications is recommended.

To reduce fluctuations, LQR is tuned based on the system's response. As shown in **Equation 4.5**, the controller effort is lightly penalized in the M matrix. As a result, the controller responds rapidly, following the desired path while dramatically reducing the rise and settling times. A downside of this controller is the steady-state error in the response, which can be easily removed with optimized tuning, contrasting to the PID controller. However, as the gains selected for an LQR-type control are ideal in this scenario, the system becomes robust.

4.3 Summary

This chapter presents the control design of the USFG, which comprises maneuvering in ocean current for two separate controlled glides. Significant differences between LQR and PID controllers, which are mainstream in autonomous naval research applications, are highlighted. The LQR is the clear choice for the current application, as it improves the robust response of the USFG while reducing fluctuations. Also, the tuning method for both controllers is presented. PID requires more computational power to converge results, and the tuning method is complex compared to LQR. Additional details of this analysis can be found in the enclosed papers in **Appendix B – Appended Papers.**

Chapter 5 - Mechanical Design of the USFG

This chapter presents the mechanical design of the USFG, which can likely aid in establishing the operational or technical limits (if the glider has any). The design procedure is depicted in **Figure 5.1**

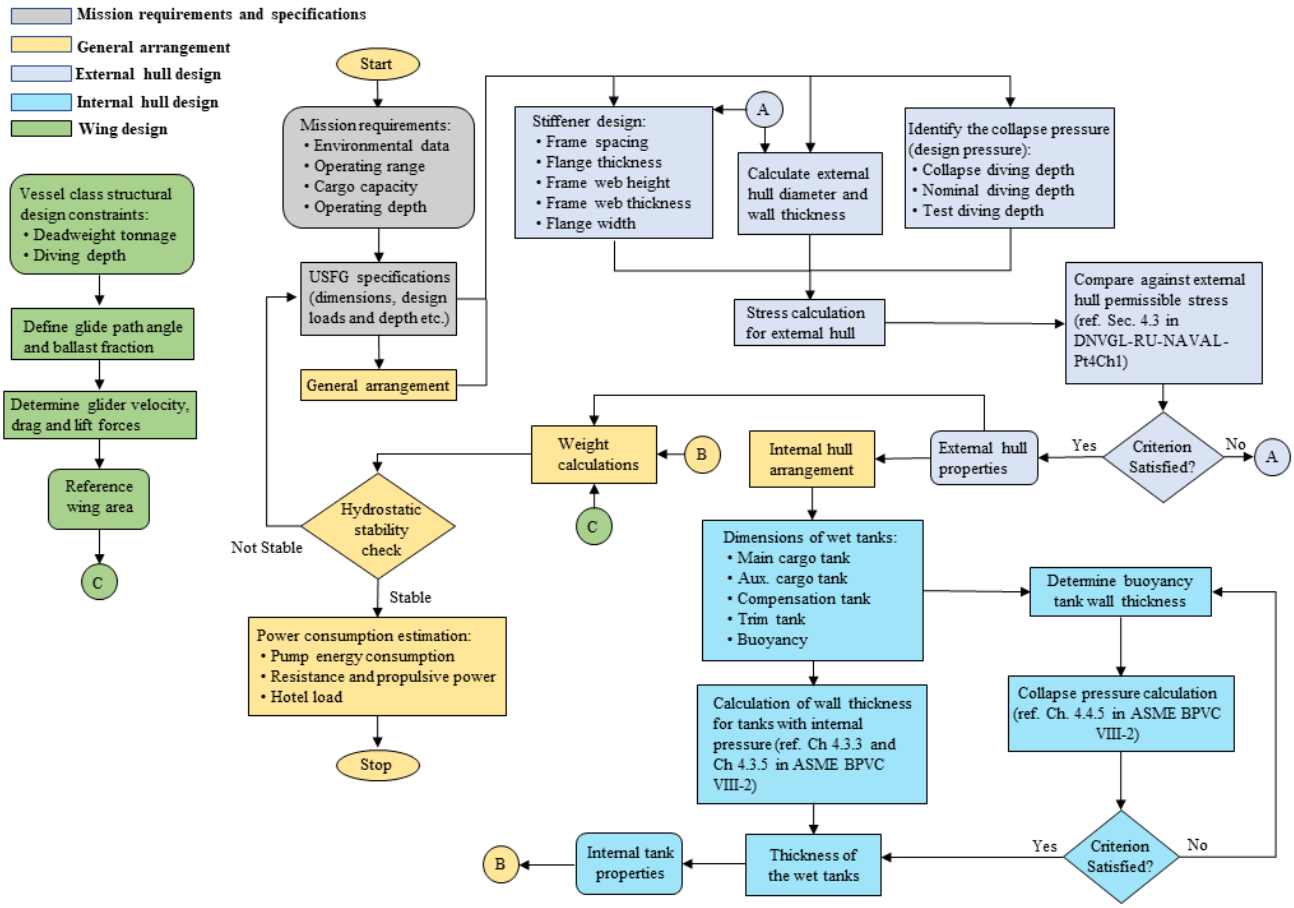

Figure 5.1 Design flow for USFG's mechanical design.

The requirements of the mission (Ref. **Chapter 2.2**) are used as the input in this design loop. After the following specifications have been assigned, the general arrangement or location of all the components of the USFG can be derived (Ref. **Chapter 2.3**). Then, based on the mission specifications and general arrangement, calculations for the exterior and interior hull can be carried out (Ref. **Chapter 5.2** and **5.3**). Afterwards, the hydrofoil reference area is calculated (Ref. **Chapter 5.4**). Moreover, the stability check (Ref. **Chapter 5.6**) is performed under certain hydrostatic load cases based on the weight calculations (Ref. **Chapter 5.5**). Lastly, power consumption (Ref. **Chapter 5.7**) can be obtained after the mechanical design has been derived. The mechanical design calculations are based on the American Society of Mechanical

Engineers Boilers and Pressure Vessel Code (ASME BPVC) VIII-2 (ASME, 2015) and DNV-RU-NAVAL-Pt4CH1 (DNV-GL, 2018), which are the revolutionary engineering codes and standards, respectively. Extensive details of this design can be found in **Paper C**, **Appendix B – Appended Papers**.

5.1 Structural Materials for the Mechanical Design

The materials used for the mechanical design of the USFG are listed in **Table 5.1**.

Table 5.1 Proposed design materials.

Sections	Material	Yield Strength	Tensile Strength
Exterior shell - aft compartment	VL D47	460 MPa	550 MPa
Bulkhead	VL D37	360 MPa	276 MPa
External shell - bow section	VL D47	460 MPa	550 MPa
External shell - mid-body	VL D47	460 MPa	550 MPa
Inner hull - buoyancy tube	SA-738 Grade B	414 MPa	586 MPa
Inner hull - trim tank	SA-738 Grade B	414 MPa	586 MPa
Inner hull - auxiliary cargo tank	SA-738 Grade B	414 MPa	586 MPa
Inner hull - comp. tank	SA-738 Grade B	414 MPa	586 MPa
Internal hull - main cargo tank	SA-738 Grade B	414 MPa	586 MPa

5.2 External Shell/Hull Design

A hull shaped like a torpedo is utilized for the USFG; this shell has a slenderness ratio of 1:9.7. This slender design induces two inherit advantages:

- This innovative design is an added benefit of not requiring any complex manufacturing procedures due to its simple shape.
- This unique design enables increased cargo-carrying capacity of the glider.

A stiffener is used to reinforce the external shell of the USFG; stiffener properties and illustration is presented in **Table 5.2**. Stiffeners utilized in this design procedure are per DNV-RU-NAVAL-Pt4CH1 (DNV-GL, 2018).

USFG contains free-flooded compartments, which are pressure vessels capable of withstanding the water pressure due to depth. Therefore, stresses for all the depths (test diving, collapse, and diving) for these compartments are calculated. Afterwards, these calculated stresses are checked against the permissible stresses stated in Chapter 4 in DNVGL Rules for Classification

for Naval Vessels, Part 4 Sub-surface ships, Section 1 Submarine (DNVGL-RU-NAVAL-Pt4Ch1).

Table 5.2 Stiffener properties (external shell).

Parameter	Symbol	Units	Value
Inner radius to the flange of the frame	R_f	[mm]	2533
Flange width	b_f	[mm]	80
Frame spacing	L_F	[mm]	1000
Frame cross-sectional area	A_F	[mm^2]	7.35
Flange thickness	s_f	[mm]	30
Frame web height	h_w	[mm]	165
Frame web thickness	s_w	[mm]	30

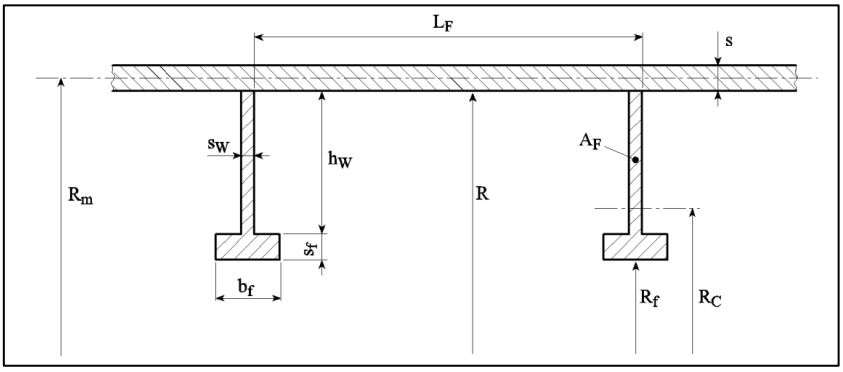

Figure 5.2 Illustration of stiffener for the external shell. (DNV-GL, 2018).

Table 5.3 USFG's external hull properties.

Sections	Elements	Units	Values
Free-flooding aft section	Material	-	VL D47
	Thickness	[m]	0.025
	Design collapse pressure	[bar]	40.000
	Steel Weight	[ton]	15.789
	Length	[m]	10.000
Free-flooding bow section	Material	-	VL D47
	Thickness	[m]	0.025
	Design collapse pressure	[bar]	40.000
	Steel Weight	[ton]	7.658
	Length	[m]	2.500
Flooded mid-body	Material	-	VL D47
	Thickness	[m]	0.011
	Design collapse pressure	[bar]	20.000
	Steel Weight	[ton]	66.842
	Length	[m]	37.500

Similarly, the design of the flooded mid-body compartment is finalized. Although this compartment is not responsible for bearing the hydrostatic loads, in case of accidents, i.e., breakdown of the vent on USFG, it may experience tremendous pressure. To prevent this, USFG is designed for a collapse pressure of 20 bars preventing any immediate structural damage. The derived external hull design is presented in **Table 5.3**. The mid-body weighs around 74 percent of the total structural weight of the glider.

5.3 Internal Shell/Hull Design

This section describes and derives the mechanical design of the internal tanks of the USFG, and the design is presented as per ASME BPVC Chapter 4, Section VIII, Division 2 (ASME, 2015).

For CO_2 loading, cargo tanks experience two pressures: the internal pressure caused by the cargo and the external hydrostatic pressure. These tanks are designed for a burst pressure ranging from 35 – 55 bars. The USFG experiences this situation during its surface operations (maintenance or refueling). For this scenario, an active pressure compensating system (ACPS) can be employed to tackle the pressure difference of 55 bars (Xing, Ong, et al., 2021).

The buoyancy tubes are designed to tolerate 20 bars of static water pressure. The free-flooded compartments (compensation and trim tanks) are the soft-pressure tanks that do not bear the hydrostatic pressure. Since these tanks are flooded, trim and compensation tanks should be designed for internal pressures. The shape and size of these tanks can be optimized to maximize the storage space. **Table 5.4** presents the details of the internal shell design.

5.4 Hydrofoil Design

The detailed design procedure for the wings of the USFG is depicted in **Figure 5.3**. The glider parameters used to calculate the reference wing area have been defined previously (Ref. **Figure 4.1**). Initially, the operating depth and vessel parameters are defined, which help to select an optimal glide angle. Once the glide angle has been defined, the velocities of the glider can be calculated to yield lift and drag force. Finally, the lift-to-drag ratio and the required reference area can be obtained from these forces.

Table 5.4 USFG's internal tank characteristics.

Sections	Elements	Units	Values
Buoyancy Tube (Total tanks = 8)	Material	-	SA-738 Grade B
	Total volume	[m^3]	25.574
	Acceptable collapse pressure	[bar]	7.000
	Hemispherical end wall thickness	[m]	0.002
	Length	[m]	28.000
	Thickness	[m]	0.004
	Steel weight	[ton]	1.134
	Diameter	[m]	0.390
Auxiliary Cargo Tank (Total tanks = 6)	Material	-	SA-738 Grade B
	Total volume	[m^3]	67.160
	Acceptable burst pressure	[bar]	55.000
	Hemispherical end wall thickness	[m]	0.008
	Length	[m]	28.000
	Thickness	[m]	0.004
	Steel weight	[ton]	24.322
	Diameter	[m]	0.735
Trim Tank (Total tanks = 2)	Material	-	SA-738 Grade B
	Total volume	[m^3]	50.000
	Acceptable burst pressure	[bar]	10.000
	Length	[m]	1.890
	Thickness	[m]	0.002
	Steel weight	[ton]	73.705
	Diameter	[m]	3.500
Compensation Tank (Total No.= 2)	Material	-	SA-738 Grade B
	Total volume	[m^3]	22.96
	Acceptable burst pressure	[bar]	8.000
	Length	[m]	1.750
	Thickness	[m]	0.002
	Steel weight	[ton]	33.561
	Diameter	[m]	3.750
Main Cargo Tank (Total tanks = 7)	Material	-	SA-738 Grade B
	Total volume	[m^3]	459.366
	Acceptable burst pressure	[bar]	55.000
	Hemispherical end wall thickness	[m]	0.009
	Length	[m]	28.000
	Thickness	[m]	0.017
	Steel weight	[ton]	119.859
	Diameter	[m]	1.500

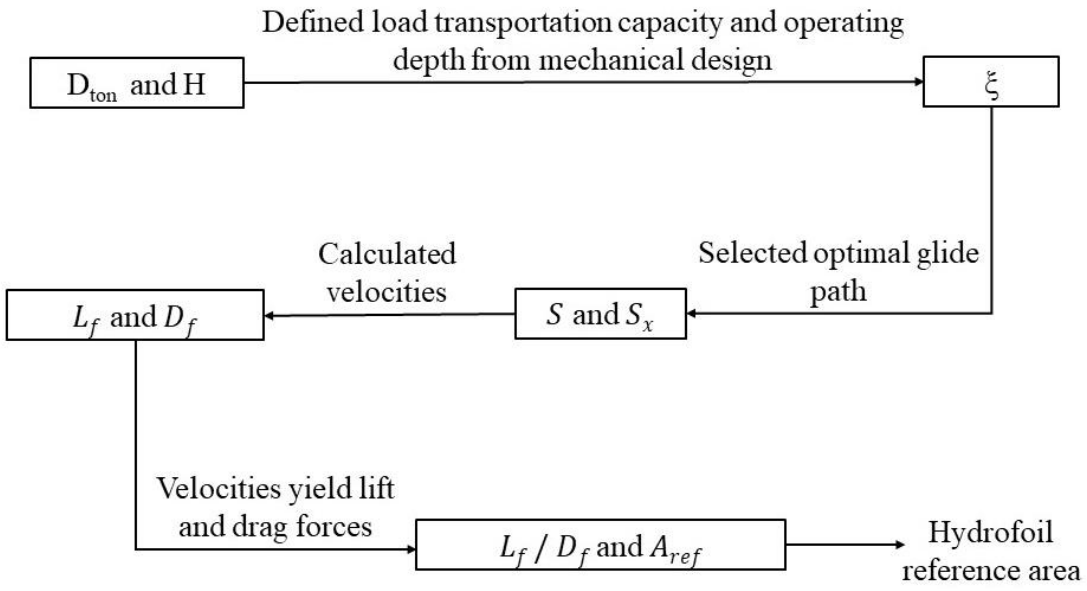

Figure 5.3 Design flow for hydrofoil's reference area.

The reference area for the hydrofoils of the USFG comes out to around 5 m^2. Detailed calculations for this section and the expressions are presented in **Appendix A - Calculation of Reference Wing Area**.

5.5 Weight Estimations

After the mechanical design has been concluded, the derived weight configuration for the USFG can be obtained. It must be noted that a targeted payload of around 45 percent can be transported by utilizing a double hull design combined with an ACPS. The weight estimation is presented in **Table 5.5**.

Table 5.5 USFG's weight configuration (CO_2 charged).

Module	Weight (tons)	%
Structure	419	30.42%
Permanent ballast mass	30	2.23%
Freight	612	44.45%
Compensation ballast	51	3.72%
Equipment	30	2.23%
Mid-body seawater	226	16.42%
Trim ballast mass	7	0.52%
Total	1379	100%

5.6 Stability Analysis

The intact stability of the USFG is verified subsequently after the weight estimations. This evaluation is done as per DNVGL-RUNAVALPt4Ch1 Section 3.5.2.3. As depicted in Figure 5.4, four different loading scenarios are used in this analysis.

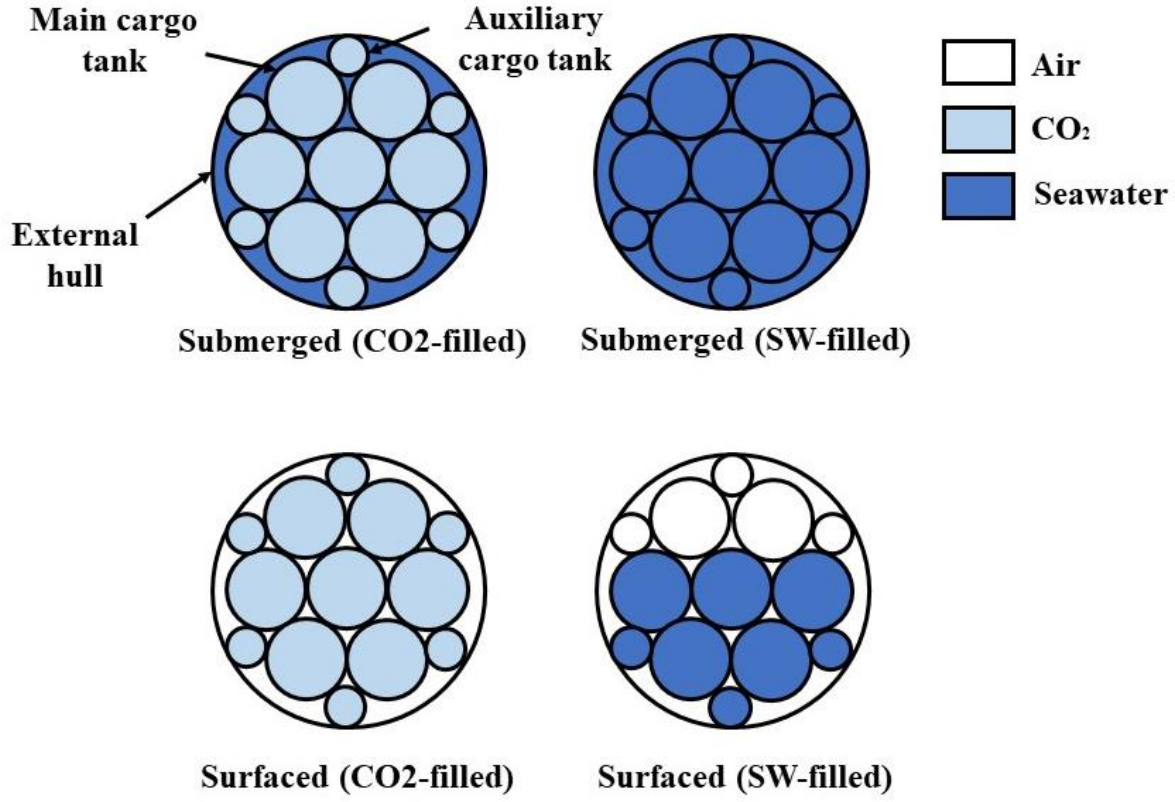

Figure 5.4 Loading scenarios of the USFG (Ma et al., 2021).

1. Surfaced (SW-filled): the USFG floats on the water's surface, while three out of six auxiliary and five main tanks are filled with heavy seawater/saltwater. The remaining tanks are empty. This situation arises during the initial and final phases of the CO_2 transportation cycle, correspondingly when the USFG surfaces to load and unload the cargo.

2. Surfaced (CO_2-filled): this case occurs after the tanks of the USFG are charged with CO_2 for transportation.

3. Submerged (CO2-filled): liquid CO_2 is filled in all 13 cargo tanks. At this point, the vessel is entirely underwater and filled with CO_2.

4. Submerged (SW-filled): this situation is observed after the USFG unloads the carbon dioxide at the injection site (subsea well). In this instance, the cargo tanks are charged with seawater during the unloading process.

The results of this analysis are depicted in **Table 5.6**.

Table 5.6 Hydrostatic stability study.

Parameters	Surfaced (SW-filled)	Surfaced (CO2-filled)	Submerged (CO2-filled)	Submerged (SW-filled)
G (x, y, z)	[-0.937, 0.00, 0.147]	[-1.032, 0.00, 0.276]	[-0.784, 0.00, 0.403]	[-0.829, 0.00, 0.460]
BG	3.807	5.252	0.405	0.460
B (x, y, z)	[-1.481, 0.00, 4.200]	[-1.481, 0.00, 5.500]	[-1.481, 0.00, 0.00]	[-1.481, 0.00, 0.00]
GM	0.393	0.248	0.405	0.460
M (x, y, z)	[0.00, 0.00, 0.00]	[0.00, 0.00, 0.00]	[0.00, 0.00, 0.00]	[0.00, 0.00, 0.00]
Effect	GM > 0.22 == OK	GM > 0.22 == OK	BG > 0.35 == OK	BG > 0.35 == OK

5.7 Power Utilization Analysis

This section presents the power consumption study of the USFG. The amount of energy utilized by the USFG during each mission is dependent on the glide path angle (Ref. to ξ in **Figure 4.1**) and the ballast fraction (representation of the size of ballast tanks). The USFG can change the gliding velocity by varying these two critical parameters.

A parametric study, shown in **Figure 5.5**, is performed to obtain an optimal ballast fraction (BF), which can yield a horizontal velocity (u_{USFG}) of 1 m/s. For every BF considered, the power consumed is calculated along with the glider's velocity.

Choosing the optimum glide path is vital for this analysis, as the USFG moves faster underwater with steep glide angles whereas utilizing more pumping work. On the other hand, shallow glide path angles spend less pump work, yielding lower glider speeds.

A BF of 0.15 percent paired with a gliding angle of 30° is selected from this parametric study. These parameters can achieve a glider speed of 1 m/s while utilizing 8 kW of power. It must be noted that smaller glide angles (<30°) are not chosen as they failed to achieve the desired targeted velocity. As for higher (>40°), the velocity curve becomes relatively flat while the power consumption increases noticeably. This trend serves no added advantage as the focal objective of the glider is to travel greater distances with a reduced amount of power utilization.

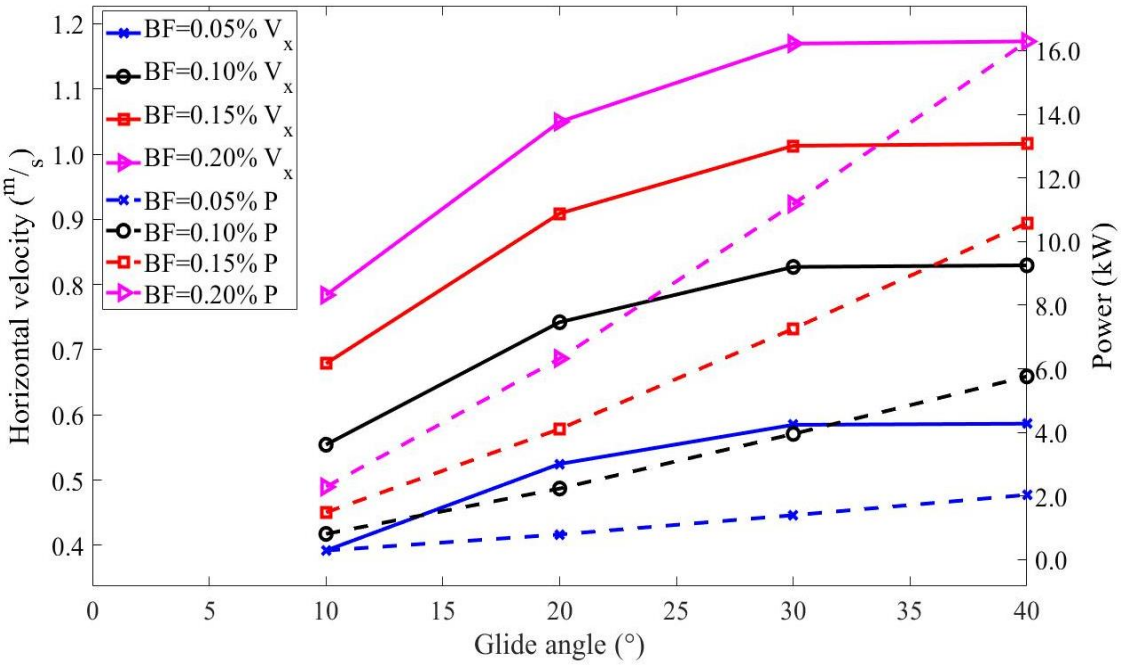

Figure 5.5 Horizontal velocity (S_X) vs power consumption.

5.8 Summary

This chapter presents the mechanical design of the UiS subsea-freight glider. The USFG aims to carry CO_2 for injection to the well sites, reducing the freight industry's overall carbon footprint. The mechanical design of the USFG is developed to promote research in underwater cargo-carrying vessels while also serving as a potential replacement for conventional transport methods, i.e., pipelines and tankers. A highlighting feature of the USFG is its ability to consume less power than the conventional transportation method. The final resulting design of the USFG is presented in **Table 5.7**.

Table 5.7 Design summary of the USFG.

Vessel Features	Value
Length [m]	50.25
Beam [m]	5.5
Total power consumptions [kW]	8
Range [km]	400
Lightweight [ton]	495
Deadweight [ton]	531
Displacement [ton]	1026
Lightweight [m^3]	483
Deadweight [m^3]	518
Displacement [m^3]	1001

Chapter 6 - Extreme Responses of the USFG

In this chapter, the averaged conditional exceedance rate (ACER) is employed to analyze the extreme surge responses of the USFG during a single cycle of the equilibrium glide. The single-cycle under scrutiny is depicted in **Figure 2.1**.

Extreme surge responses are crucial for the design of the USFG, as the controller on board is responsible for handling deviations during gliding. During transportation, the USFG is programmed to follow a pre-planned path which helps the vessel maintain its course and conserve energy. This pre-laid path is affected by the extreme surge motion of the glider. Any overrun from the targeted distance can likely result in additional power consumption. As mentioned earlier, the position tracking for underwater marine vehicles is only done at the start of the mission (Griffiths, 2002). Therefore, the USFG must steer clear of any divergence from the route, as it can cause loss of control of the vessel leading to a catastrophic failure.

This study is performed when the USFG maneuvers in an ocean current velocity of 0.5 m/s and 1.0 m/s. The innovative ACER method is utilized for the prediction of extreme responses. Former implementations in marine engineering include the evaluation of extreme sea states, including wind, wave, and current profiles (Gaidai, Naess, Karpa, et al., 2019; Gaidai, Naess, Xu, et al., 2019; Naess & Karpa, 2015; Yu et al., 2020) along with wave heights (Gaidai, Naess, Xu, et al., 2019; Gaidai et al., 2020). It has also been utilized for applications in structural analysis (Gaidai et al., 2021; Hui et al., 2019; Naess & Gaidai, 2008; Naess et al., 2010; Naess & Moan, 2013; Naess et al., 2008; Xu et al., 2019). The problem under attention is vastly non-linear; therefore, ACER is used for this study compared to other non-Monto Carlo-based methods. The data in this analysis is generated from time-domain simulations using the Simulink model presented previously (Ref. **Chapter 3**).

6.1 Extreme Response Prediction: Univariate Surge Analysis

As a part of this chapter, we analyze the arithmetic results of the ACER1D method, also known as univariate analysis. Accurate and precise prediction of extreme surge responses serves as an input for a reliable, safe, and robust design of the USFG.

This study extends the method for estimating the extreme surge responses of the USFG during its single equilibrium glide cycle. These responses are estimated while the USFG targets to

attain a pre-defined pitch angle (38°) and operating depth (200 meters) while maneuvering in the ocean current. The presented ACER method utilizes the available data efficiently and predicts the extreme surge responses precisely and accurately. It is established that the ACER method efficiently integrates the environmental disturbances while providing robust and accurate response values, given that the numerical data is exact.

Figure 6.1 shows the ACER1D response of surge motion with a 95 percent bounded interval or confidence interval (CI). The CI is indicated as dotted lines. The return periods used for this analysis are highlighted in **Table 6.1**. It must be noted that these return periods are used as targeted case studies. Moreover, the Gumbel plot for this analysis is depicted in **Figure 6.1**, and this fitted curve is extrapolated to analyze higher return periods (5-Year and 10-Year). The predictions highlighted in **Figure 6.2** can be compared against **Figure 6.1** (lower) since both plots represent the surge response in 1.0 m/s current velocity. Identical predictions of the surge motion, about 290 meters, are observed for a 3-Month return period for a current velocity of 1.0 m/s. It is also observed that the data points obtained from the 20 750-seconds simulations do not fit a straight line for Gumbel fit. Therefore, similar performance is monitored for all the return periods under consideration. In other words, all data points from the time series have not yet established the asymptotic generalized extreme value (GEV) condition. In addition, the 95 percent CI band from the ACER plot is prominently narrower than the one projected by the Gumbel plot. This narrow band highlights a distinct advantage of using the innovative ACER1D method.

The surge responses obtained from the predictions are more significant than the anticipated distance of 256 meters. This phenomenon is mutual for all the return periods highlighted in **Table 6.1**. The extreme values are about 1.1 to 1.2 times higher than the required distance for a 5-Year return period. For this purpose, a Luenberger observer design (Luenberger, 1971) can be implemented to cater to any overshoot or underrun (if present). Moreover, a slight variation in the surge responses is observed for all the return periods while moving across **Table 6.1**. In the case of both ACER and Gumbel methods, a variation of 6 meters is experienced between 3-Month and 5-Year return periods for a 1.0 m/s current velocity scenario. Similarly, an alteration of 3 meters is detected for both procedures for a 0.5 m/s current velocity. The Gumbel fit fails to provide accurate and precise estimations in contrast to the 95 percent CI band predicted by the ACER method.

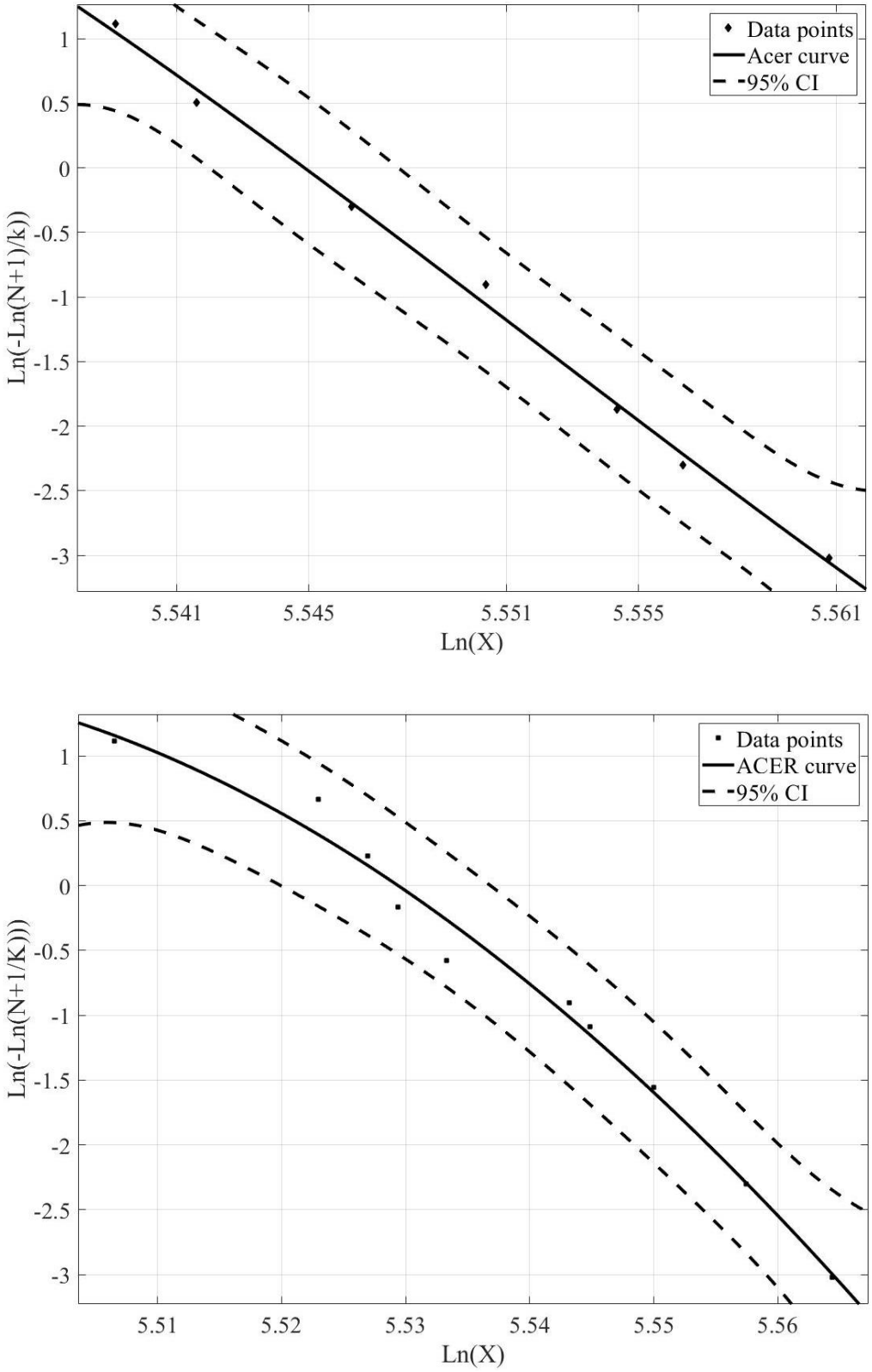

Figure 6.1 ACER1D extreme surge responses in log-scale. Upper: with a current velocity of 0.5 m/s; Lower: a current velocity of 1.0 m/s.

Table 6.1 Surge response (meters) predictions for five return periods.

Current velocity	Method	3-Month	6-Month	1-Year	2-Year	5-Year
0.5 m/s	ACER 95% CI	270.62 (245.01,307.87)	270.80 (245.18,308.07)	271.25 (245.58,308.58)	271.93 (246.20,309.36)	273.04 (247.20,310.62)
	Gumbel 95% CI	270.29 (203.77,317.27)	270.46 (203.90,317.47)	270.89 (204.23,317.98)	271.54 (204.72,318.74)	272.58 (205.50,319.96)
1.0 m/s	ACER 95% CI	290.99 (231.29,348.60)	291.49 (231.69,349.20)	292.76 (232.70,350.72)	294.68 (234.22,353.02)	297.82 (236.72,356.79)
	Gumbel 95% CI	288.49 (218.32,432.51)	288.93 (218.65,433.17)	290.03 (219.48,434.81)	291.69 (220.74,437.30)	294.37 (222.77,441.32)

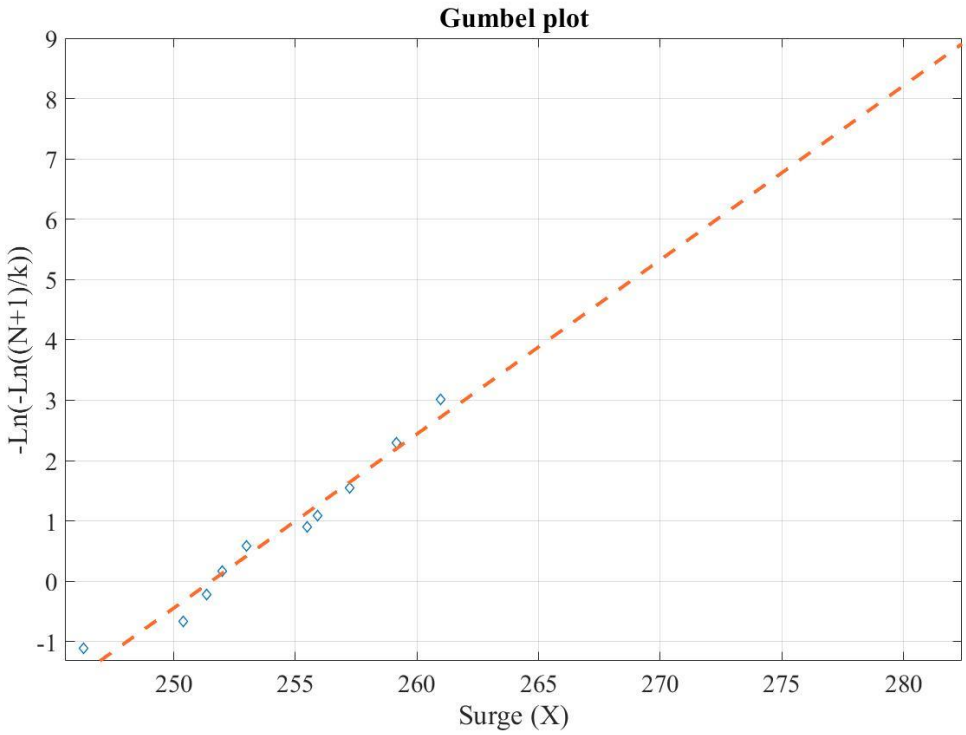

Figure 6.2 Gumbel plot for surge, dashed line specifies extrapolation toward a return period of 10-year. 20 750-seconds simulated responses. Current velocity of 1.0 m/s..

6.2 Summary

This chapter presents the study of the extreme responses of the surge motion during equilibrium gliding. It was discovered that the GEV condition in the data set had not been established for the 20 simulation cases. As a result, the Gumbel method did not successfully provide a straight line fit of the simulated data. Consequently, leading to a broad and non-accurate 95 percent bounded interval from the Gumbel pot. On the other hand, the ACER method was highly

efficient and accurate in predicting the responses, as indicated by the presented results. Detailed analysis can be found in **Paper D**, **Appendix B – Appended Papers**.

Chapter 7 - Conclusions and Recommendations

The baseline design of the UiS subsea-freight glider (USFG) for cargo and liquid carbon dioxide transportation is presented in this thesis. The USFG aims to carry CO_2 for injection to the well sites, reducing the freight industry's overall carbon footprint. The baseline design of the USFG is developed to promote research in underwater cargo-carrying vessels while also serving as a potential replacement for conventional transport methods, i.e., pipelines and tankers. The first part of the work presents a planar mathematical model of the USFG. Additionally, quality assurance has been completed for the presented model in the form of controller tuning. An in-depth study has compared two types of popular controllers used in marine applications, PID and LQR. This analysis favours LQR for the control of USFG rather than PID. This selection was made owing to LQR's simplified tuning method and reduced fluctuations in the output, which also takes less computational power to converge to results. For PID, excessive tunning is required, and even for high gain values, it fails to mitigate noise or oscillations effectively. The controller analysis presented is adaptable, as it is equally effective for various sizes and configurations of the USFG. The main details of the mechanical design are presented in the latter part of the work. The distinguishing feature of the USFG is its dual hull/shell design which utilizes an ACPS to reduce the overall structural weight. As for the concluding part of the work, it was proposed to utilize the state-of-the-art average conditional exceedance rate (ACER) design method to study the extreme surge responses (offset from the pre-planned surge motion also influences the heave motion of the vessel) while maneuvering in ocean current during the mission. The surge responses are studied in only the half cycle of the glide. It is observed that the extreme surge responses for all the return periods are higher, around 1.1 to 1.2 times than the mathematical 750-second response. These higher responses specify that an observer, commonly Luenberger Observer (Luenberger, 1971), can be integrated into the mathematical model of the USFG to ensure path-following even for extreme surge responses, such as depicted in **Table 6.1**.

Finally, for future work, a model predictive control (MPC) can be utilized to control the kinematics of the USFG instead of LQR or PID controller. It involves the accurate prediction of the output values by utilizing model measurements. Moreover, It is also possible to establish a structural design code explicitly tailored for the USFG to decrease the structural weight. The proposed ACER approach can also be applied to the complete equilibrium gliding path (1

complete cycle with turning motion) of the USFG (Ahmad & Xing, 2021). All of the presented suggestions can facilitate the USFG design to be evolved further. It can also contribute to optimized dynamic vessel parameters while minimizing probable damage to the glider.

References

Ahmad, U., & Xing, Y. (2021). A 2D model for the study of equilibrium glide paths of UiS Subsea Freight-Glider. IOP Conference Series: Materials Science and Engineering,

Ahmad, U., & Xing, Y. (2022). *UIS Subsea Freight Glider: controller design and analysis* International Conference on Offshore Mechanics and Arctic Engineering, Hamburg, Germany. (Under review)

Ahmad, U. N., Xing, Y., & Yucong Ma. (2022). UiS Subsea-Freight Glider: A Large Buoyancy Driven Autonomous Cargo Glider. *Journal of Offshore Mechanics and Arctic Engineering*.

Airfoil Tools. (2022). *NACA 4412 (naca4412-il)*. http://airfoiltools.com/airfoil/details?airfoil=naca4412-il

Allen, M., Antwi-Agyei, P., Aragon-Durand, F., Babiker, M., Bertoldi, P., Bind, M., Brown, S., Buckeridge, M., Camilloni, I., & Cartwright, A. (2019). Technical Summary: Global warming of 1.5° C. An IPCC Special Report on the impacts of global warming of 1.5° C above pre-industrial levels and related global greenhouse gas emission pathways, in the context of strengthening the global response to the threat of climate change, sustainable development, and efforts to eradicate poverty.

ASME. (2015). Boiler and Pressure Vessel Code, Section VIII, Division 2. In. New York: The American Society of Mechanical Engineers.

Åström, K. J., Hägglund, T., & Astrom, K. J. (2006). *Advanced PID control* (Vol. 461). ISA-The Instrumentation, Systems, and Automation Society Research Triangle Park.

Bae, Shin, S. B., Kwon, D. H., Joo, S. T., & G, M. (2014). An LQR controller for autonomous underwater vehicle. *Journal of Institute of Control, Robotics and Systems*, *20*(2), 132-137.

Bahlman, J. W., Swartz, S. M., Riskin, D. K., & Breuer, K. S. (2012). Glide performance and aerodynamics of non-equilibrium glides in northern flying squirrels (Glaucomys sabrinus). *Journal of the Royal Society, Interface*, *10*(80), 20120794-20120794. https://doi.org/10.1098/rsif.2012.0794

Burlacu, P., Dobref, V., Badara, N., & Tarabuta, O. (2007). A LQR controller for an AUV depth control. *Annals of DAAAM & Proceedings*, 125-127.

Carbon Capture and Storage Association [CCSA]. (2020). *What Is CCS?* Retrieved 2 February from http://www.ccsassociation.org/what-is-ccs/

Crippa, M., Guizzardi, D., Muntean, M., Schaaf, E., Solazzo, E., Monforti-Ferrario, F., Olivier, J., & Vignati, E. (2020). Fossil CO2 emissions of all world countries. *Luxembourg: European Commission*, 1-244.

DNV-GL. (2018). Rules for Classification, Naval Vessels, Part 4 Sub-Surface Ships (Chapter 1) Submarines. In.

DOF Subsea. (2018). *Glider AUV*. Retrieved 31 January from https://www.dofsubsea.com/rov/glider-auv/

Ellingsen, K. E., Ravndal, O., Reinas, L., Hansen, J. H., Marra, F., Myhre, E., & k. Sveberg. (2020). *RD677082 Subsea Shuttle System*.

Equinor. (2022). *Northern Lights CC*. Retrieved 1 February from https://www.equinor.com/en/what-we-do/northern-lights.html

Equinor Energy AS. (2019). *RD662093 Subsea Shuttle System*.

Ersdal, G. (2001). An overview of ocean currents with emphasis on currents on the Norwegian continental shelf.

EvoLogics. (2017). *EvoLogics BOSS - Manta Ray*. Retrieved 31 January from https://evologics.de/projects/boss

Fossen, T. I. (2011). *Handbook of marine craft hydrodynamics and motion control*. John Wiley & Sons.

Fullenbaum, R., Fallon, J., & Flanagan, B. (2013). *Oil & Natural Gas Transportation & Storage Infrastructure: Status, Trends, & Economic Benefits*. https://www.circleofblue.org/wp-content/uploads/2014/12/API-Infrastructure-Investment-Study.pdf

Gaidai, O., Naess, A., Karpa, O., Xu, X., Cheng, Y., & Ye, R. (2019). Improving extreme wind speed prediction for North Sea offshore oil and gas fields. *Applied Ocean Research*, *88*, 63-70.

Gaidai, O., Naess, A., Xu, X., & Cheng, Y. (2019). Improving extreme wind speed prediction based on a short data sample, using a highly correlated long data sample. *Journal of Wind Engineering and Industrial Aerodynamics*, *188*, 102-109.

Gaidai, O., Xu, X., Naess, A., Cheng, Y., Ye, R., & Wang, J. (2021). Bivariate statistics of wind farm support vessel motions while docking. *Ships and Offshore Structures*, *16*(2), 135-143.

Gaidai, O., Xu, X., Wang, J., Ye, R., Cheng, Y., & Karpa, O. (2020). SEM-REV offshore energy site wind-wave bivariate statistics by hindcast. *Renewable Energy*, *156*, 689-695.

Graver, J. G. (2005). Underwater gliders: Dynamics, control and design.

Griffiths, G. (2002). *Technology and applications of autonomous underwater vehicles* (Vol. 2). CRC Press.

Hui, G., Gaidai, O., Naess, A., Storhaug, G., & Xu, X. (2019). Improving container ship panel stress prediction, based on another highly correlated panel stress measurement. *Marine Structures*, *64*, 138-145.

Intergovernmental Panel on Climate Change. (2018). *Global warming of 1.5° C: an IPCC special report on the impacts of global warming of 1.5° C above pre-industrial levels and*

related global greenhouse gas emission pathways, in the context of strengthening the global response to the threat of climate change, sustainable development, and efforts to eradicate poverty.

Jacobsen, L., Lawrence, K., Hall, K., Canning, P., & Gardner, E. (1983). Transportation of LNG from the Arctic by commercial submarine. *Marine Technology and SNAME News*, *20*(04), 377-384.

Jacobsen, L. R. (1971). Subsea Transport of Arctic Oil-A Technical and Economic Evaluation. Offshore Technology Conference,

Langebrake, L. C. (2003). AUV sensors for marine research. *Technology and Applications of Autonomous Underwater Vehicles*, 245-277.

Luenberger, D. (1971). An introduction to observers. *IEEE Transactions on automatic control*, *16*(6), 596-602.

Ma, Y., Xing, Y., Ong, M. C., & Hemmingsen, T. H. (2021). Baseline design of a subsea shuttle tanker system for liquid carbon dioxide transportation. *Ocean Engineering*, *240*, 109891.

Mariano, A., Ryan, E., Perkins, B., & Smithers, S. (1995). The Mariano Global Surface Velocity Analysis 1.0. 61.

MathWorks. (2022). *Linearize Simulink Model at Model Operating Point*. https://se.mathworks.com/help/slcontrol/ug/linearize-simulink-model.html

Naess, A., & Gaidai, O. (2008). Monte Carlo methods for estimating the extreme response of dynamical systems. *Journal of engineering mechanics*, *134*(8), 628-636.

Naess, A., Gaidai, O., & Batsevych, O. (2010). Prediction of extreme response statistics of narrow-band random vibrations. *Journal of engineering mechanics*, *136*(3), 290-298.

Naess, A., & Karpa, O. (2015). Statistics of extreme wind speeds and wave heights by the bivariate ACER method. *Journal of Offshore Mechanics and Arctic Engineering*, *137*(2).

Naess, A., & Moan, T. (2013). *Stochastic dynamics of marine structures*. Cambridge University Press.

Naess, A., Stansberg, C., Gaidai, O., & Baarholm, R. (2008). Statistics of extreme events in airgap measurements. International Conference on Offshore Mechanics and Arctic Engineering,

National Centers for Environmental Information [NCEI]. *Greenland, Iceland, and Norwegian Seas Regional Climatology*. Retrieved 7 February from https://www.ncei.noaa.gov/products/greenland-iceland-and-norwegian-seas-regional-climatology

Nations, U. (2015). Paris Agreement—United Nations Framework Convention on Climate Change. *No. TIAS No. 16-1104*.

Norwegian Petroleum Directorate [NPD]. (2020). *Carbon Capture and Storage*. Retrieved 1 February from http://www.norskpetroleum.no/en/environment-and-technology/carbon-capture-and-storage

Palmer, A. C., & King, R. A. (2008). *Subsea pipeline engineering* (2nd ed.). PennWell.

Papanikolaou, A. (2014). *Ship design: methodologies of preliminary design*. Springer.

Sætre, R. (2007). *The Norwegian coastal current: oceanography and climate*. Akademika Pub.

Sherman, J., Davis, R. E., Owens, W., & Valdes, J. (2001). The autonomous underwater glider" Spray". *IEEE Journal of oceanic engineering*, *26*(4), 437-446.

Stommel, H. (1989). The slocum mission. *Oceanography*, *2*(1), 22-25.

Taylor, P. (2010). Energy Technology Perspectives. *International Energy Agency*.

Taylor, P., & Montgomery, J. (1977). Arctic submarine tanker system. Offshore Technology Conference,

Vestereng, C. (2019). *Shuttle tankers in Brazil*. DNV-Martitime Impact. Retrieved 30 January from https://www.dnv.com/expert-story/maritime-impact/shuttle-tankers-Brazil.html

Webb, D. C., Simonetti, P. J., & Jones, C. P. (2001). SLOCUM: An underwater glider propelled by environmental energy. *IEEE Journal of oceanic engineering*, *26*(4), 447-452.

WILSON, J. (2008). Shuttle tankers vs pipelines in the GOM frontier. *World oil*, *229*(4), 149-151.

Xing, Y. (2021). A conceptual large autonomous subsea freight-glider for liquid CO2 transportation. International Conference on Offshore Mechanics and Arctic Engineering,

Xing, Y., Ong, M. C., Hemmingsen, T., Ellingsen, K. E., & Reinås, L. (2021). Design considerations of a subsea shuttle tanker system for liquid carbon dioxide transportation. *Journal of Offshore Mechanics and Arctic Engineering*, *143*(4).

Xing, Y., Santoso, T. A. D., & Ma, Y. (2021). Technical–Economic Feasibility Analysis of Subsea Shuttle Tanker. *Journal of Marine Science and Engineering*, *10*(1), 20.

Xu, X., Gaidai, O., Naess, A., & Sahoo, P. (2019). Improving the prediction of extreme FPSO hawser tension, using another highly correlated hawser tension with a longer time record. *Applied Ocean Research*, *88*, 89-98.

Yu, S., Wu, W., Xie, B., Wang, S., & Naess, A. (2020). Extreme value prediction of current profiles in the South China Sea based on EOFs and the ACER method. *Applied Ocean Research*, *105*, 102408.

Appendix A - Calculation of Reference Wing Area

The hydrofoils reference area of 5 m^2 is derived based on Graver's work (Graver, 2005). The following parameters are used in the calculation of wing area.

- ***D_{ton}*:** described as DWT valued at 531 tons, is the amount of freight or cargo (CO_2 for this paper) that the USFG can transport.
- ***H*:** defined as nominal operating depth, estimated to be 200 m.
- ***BF*:** ballast fraction of 0.15 percent is preferred.
- ***ξ*:** the gliding angle of 30º is selected to conserve power while gliding at a constant speed.

The hydrofoil area can be calculated from these expressions:

$$BF = \frac{M}{D_{ton} \times 1000}$$ $$S = \sqrt[2]{\left(\frac{M \times g \times \sin\xi}{0.5 \times \delta \times D_c \times Vol^{\frac{2}{3}}}\right)}$$ $$u_{USFG} = S \times \cos\xi$$ $$D_f = S^2 \times 0.5 \times \delta \times D_c \times Vol^{\frac{2}{3}}$$ $$L_f = \frac{D_f}{\tan\xi}$$ $$A_{ref} = \frac{L}{S^2 \times 0.5 \times \delta \times L_c}$$	**Equation A.1**

Where M is the mass of the USFG, S is the velocity of the glider, g is the gravitational constant, δ is the density of water, D_c and L_c is the volumetric drag and lift coefficient of the USFG, Vol is the entire volume of the USFG, and L_f and D_f are the lift and drag forces, respectively.

The drag force is calculated to be 3907 Newtons, whereas the lift force comes out as 6767 Newtons for this case. It must be noted that the USFG attains a total horizontal speed of 1 m/s for these conditions.

Appendix B – Appended Papers

Paper A

A 2D model for the study of equilibrium glide paths of UiS Subsea Freight-Glider.

Usman Nawaz Ahmad and Yihan Xing.

Paper B

UIS SUBSEA FREIGHT GLIDER: CONTROLLER DESIGN AND ANALYSIS.

Usman Nawaz Ahmad and Yihan Xing.

Paper C

UiS Subsea-Freight Glider: A Large Buoyancy Driven Autonomous Cargo Glider.

Usman Nawaz Ahmad, Yihan Xing and Yucong Ma.

Paper D

Determination of extreme responses of USFG's equilibrium glide path hovering in ocean current.

Usman Nawaz Ahmad, Yihan Xing and Shuaishuai Wang.

A 2D model for the study of equilibrium glide paths of UiS Subsea Freight-Glider

U N Ahmad[1,*] and Y Xing[1]

[1] University of Stavanger, Norway

[*] usman0.21@hotmail.com

Abstract. A planar mathematical model for the analysis of equilibrium glide paths of the UiS subsea freight-glider (USFG) is presented. The model is developed using Simscape Multibody in MATLAB/Simulink to study the ever-changing dynamics of the glider. Motion along the heave and pitch direction is regulated by two separate PID controllers. Controllers are tuned for the optimal bandwidth and phase margin to provide the system with ideal gains which satisfy the system requirements. A wide-ranging sensitivity investigation is carried out on the USFG by changing the two key variables, pump flow rate and ballast fraction. The results reflect the advantages of using higher flow capacity and ballast fraction, which should be preferred according to the application, provided if there are no space and weight restrictions. Finally, different glide paths were simulated to observe that, controller gains obtained from the linear model can be improved to acquire better performance in terms of robustness and stability of the system.

1. Introduction

The subsea glider concept is fascinating owing to its efficient propulsion system. Envisaged by Stommel [1] in 1989, subsea gliders have come a long way from a concept to a real-world technology used for various purposes. This concept is utilized in Autonomous Underwater Vehicles (AUVs) which are employed to amass ocean data. They are usually deployed for numerous months during operation, covering hundreds of miles without any provision ships. Extensive research has been carried out on the design and control of underwater gliders, some examples include the DOF [2] and AUVAC subsea gliders [3]. Nevertheless, due to their limited size and load carrying capacity, these AUVs have not been utilized much for cargo transportation. To the author's knowledge, there has been only one cargo-carrying AUV so far which is developed by ISE Ltd, for the Spinnaker program in the 1990s [4]. Theseus was developed for cable-laying missions in the arctic to carry a payload of 660 kg over the range of 900 km. Further, equinor also suggested utilizing large subsea gliders for conveying freight [5]. However, this was just a proposal of concept without many technical details considered.

University of Stavanger Subsea Freight-Glider (USFG) as seen in Figure 1, was recently proposed by Xing [6] to utilize the ultra-efficient subsea glider principle for cargo transport. The main design parameters are listed in Table 1. As illustrated in Figure 2, it thrusts itself onwards following a sawtooth motion. In the upward cycle, it pumps out the ballast water such that the buoyancy force becomes positive and carries the glider to the desired operating depth. In the opposite direction, it will pump in ballast water and the vehicle gains weight. As a result, the buoyancy force becomes negative which lets the glider dive to its initial depth. The hydrodynamic wings generate lift and drag forces as the freight-glider cycles up and down, thereby propelling the vessel forward in the water. This entire process is repeated throughout the entire journey. This propulsion method uses energy only for regulating the ballast water between the tanks, while propulsion is indirectly

created by the wings. In doing so, it consumes minimal energy while carrying a huge quantity of payload. The USFG is aimed as an ultra-low-energy substitute to prevailing solutions as such pipelines, tanker ships, and bulk carriers. With its highly efficient propulsion, it can contribute to the reduction of ocean transport-related emissions (about 3 % of global carbon emissions) [7].

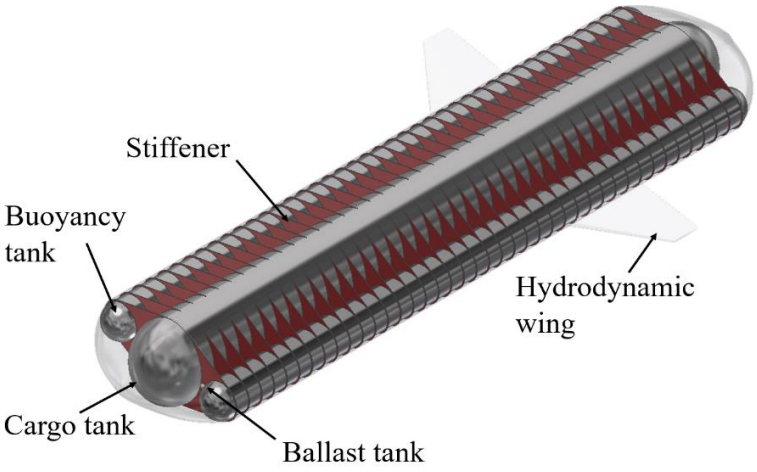

Figure 1. UiS Subsea Freight-Glider.

Table 1. Design parameters of UiS Subsea Freight-glider.

Parameter	**Value**	**Unit**
Vessel length	50	m
Cargo tank diameter	5.0	m
Buoyancy tank diameter	2.2	m
Deadweight ton	1533	ton
Structural weight	470	ton
Cargo weight	785	ton
Ballast fraction	0.15	%
Diving depth	200	m
Glide path angle	38	°
Wing area	20	m^2
Volumetric drag coefficient	0.1	-
Ballast pump capacity	2000	m^3/h
Pumping time / cycle	< 5% of half cycle	-
Horizontal speed	1	m/s
Average Power	< 10	KW
Net transport economy	< 0.5	-

Owing to its considerable size, controlling pre-programmed ballasting and de-ballasting system, which is being utilized in a massive, submerged structure is a technical problem requiring further investigations. Furthermore, due to the limitations imposed by environmental conditions, the glider faces two challenges: (a) lower maneuverability and (b) longer response time to control pitching angles and elevation. Therefore, a stable and robust control system is required to tackle any sort of variations experienced by the vessel.

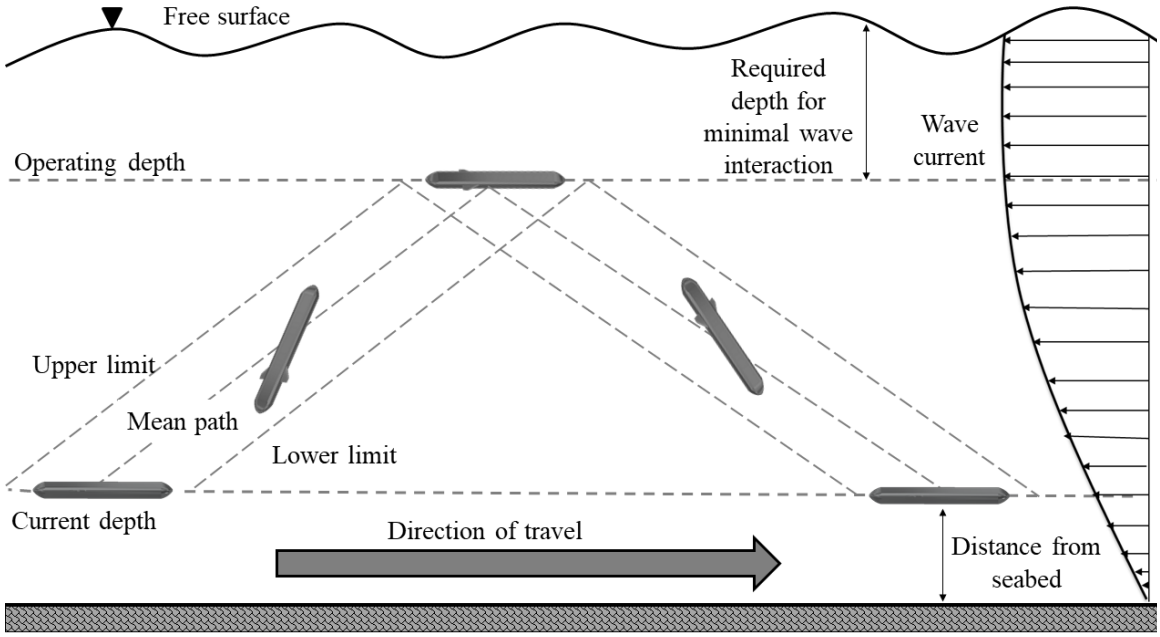

Figure 2. Equilibrium glide paths.

Previously, a significant amount of work has been done to scrutinize the three vital pillars or features of underwater vehicles: cargo or freight-carrying capability by LSE Ltd [4], autonomous or self-directing ability by Fossen[8] and equilibrium glides by Graver [9]. This paper combines these critical domains to study the equilibrium gliding paths for an autonomous underwater vehicle capable of carrying 785 metric tons as highlighted in Table 1.

This paper concerns modeling the dynamics of the USFG to analyze the control system for ballasting and flight path. The aim is to develop a dynamic model to cater for buoyancy and hydrodynamic forces to investigate the equilibrium glides for USFG, which involves the sawtooth gliding path in a 2D plane. While carrying cargo the USFG has to take a pre-planned path to maximize its travel range as illustrated in Figure 2. The ability to navigate accurately is quite critical when it comes to the design of the underwater glider. Maintaining the desired path can likely aid in energy conservation since we do not want to exceed the one-fourth part of the pre-determined energy budget as studied by Langebrake [10]. For this purpose, the glider must keep itself within the range of the planned path and avoid any deviations, since position tracking is only performed during the initial stages for autonomous vehicles as highlighted by Gwyn Griffiths *et al.* [11]. After the system is modeled, a few vital studies including, controller tuning and sensitivity analysis, are carried out. This allows the author to further augment the performance of the mathematical model for the performance of the USFG. Finally, various glide paths are simulated against the base case to investigate different operating conditions. This is done to study the importance of optimal controller gains for the desired response.

2. Ballasting system

Normally in an ordinary AUV, the net buoyancy force is regulated by altering the ballast volume, whereas motion in the direction of pitch and roll is adjusted by regulating the center of mass with the aid of a mass actuator. This method cannot be applied to enormous freight-carrying gliders such as the USFG. The mass that needs to be actuated is considerably heavy and the conventional techniques would require a substantial hydraulic network. Moreover, when it comes to the control of glider dynamics a quick response system is needed to efficiently tackle any changes, i.e., a sluggish response system is not desired. To achieve good response times, USFG exploits a coalescence of ballast tanks for gliding and ailerons for control of motions like pitch and roll as illustrated in Figure 3.

The Ballast system for heave and pitch motion is controlled by two separate proportional-integral-derivative (PID) controllers. Controller gains are adjusted with the aid of the PID tuner in Simulink. Moreover, the extended details concerning the model and the tuning of these controllers are discussed in the upcoming sections. The scope of this work is limited to a two-dimensional problem but, it can be easily expanded to a three-dimensional model. Figure 3 shows the ballast system used to control the heave and pitch motion of the glider. Motion along the heave direction is varied by the large buoyancy tank located at the center of gravity (COG) of the vessel, which controls water with the aid of a pump onboard. Desired pitch angles are attained by pumping water in and out of the two secondary ballast tanks simultaneously. It must be noted that these tanks are connected to form a network as indicated in Figure 3.

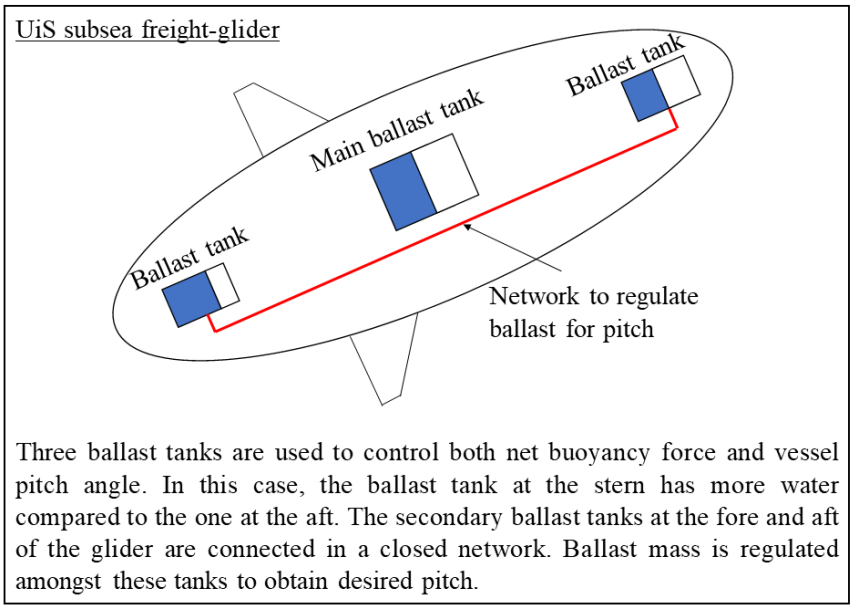

Figure 3. The control scheme of the UiS subsea freight-glider.

3. Simulink/Simscape implementation

A mathematical model of the UiS subsea freight-glider has been developed in MATLAB Simscape Multibody also referred to as SimMechanics. The Simscape model is depicted in Figure 4.

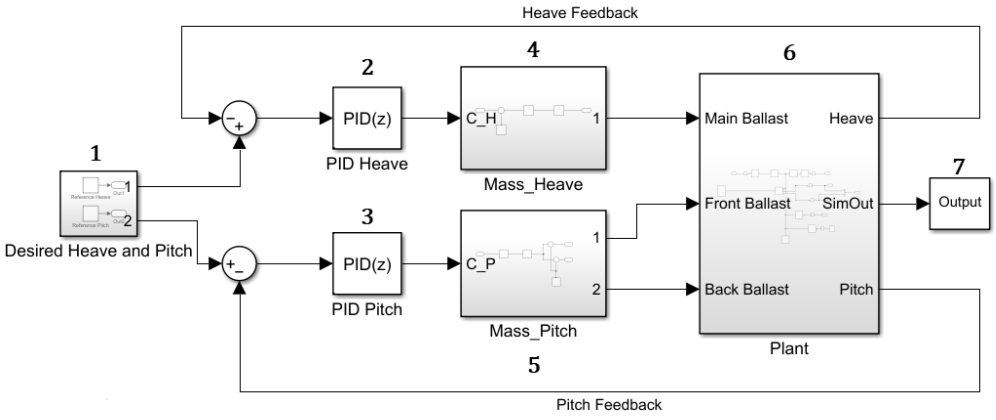

Figure 4. Simscape dynamic model.

The Simscape model for the UiS subsea glider consists of the subsequent key parts as characterized in Figure 4.

- Sub-system 1: Delivers required values for heave and pitch angles provided by the pilot.
- Sub-system 2: PID controller for heave response.
- Sub-system 3: Pitch motion PID controller, it must be noted that; independent controllers are used for actuation of the glider for pitch and heave motion.
- Sub-system 4: Manages the main ballast tank mass which controls the up and down motion of the glider. It also encompasses saturation (*bounds the ballast value*) for the main ballast tank and rate limiter (*limits the pump flow rate*).
- Sub-system 5: Fluctuates the ballast mass between two secondary tanks, i.e., Front and Back ballast tanks, it does so to control the pitch angles of the glider. It comprises the rate limiter (*controls mass being pumped in or out of the secondary tanks*) and as well as the saturation block (*confines the secondary tank capacity).*
- Sub-system 6: Termed as plant block in Figure 4, it represents the two-dimensional dynamic model of the UiS subsea freight-glider.
- Sub-system 7: Prompts and stores the results to MATLAB workspace for post-processing.

It must be noted that a control state is programmed to control the motion of the vessel during gliding in the sawtooth path. It is implemented in such a way that, when the value of the state is returned as "1" the USFG is programmed to glide upwards to the required elevation while moving forward. Similarly, when the value is "-1" it glides downwards to the initial depth.

3.1. Plant model

The plant model (represented by block 6 in Figure 4) is fully described in the upcoming text, Figure 5 presents a systematic view of the entire plant block.

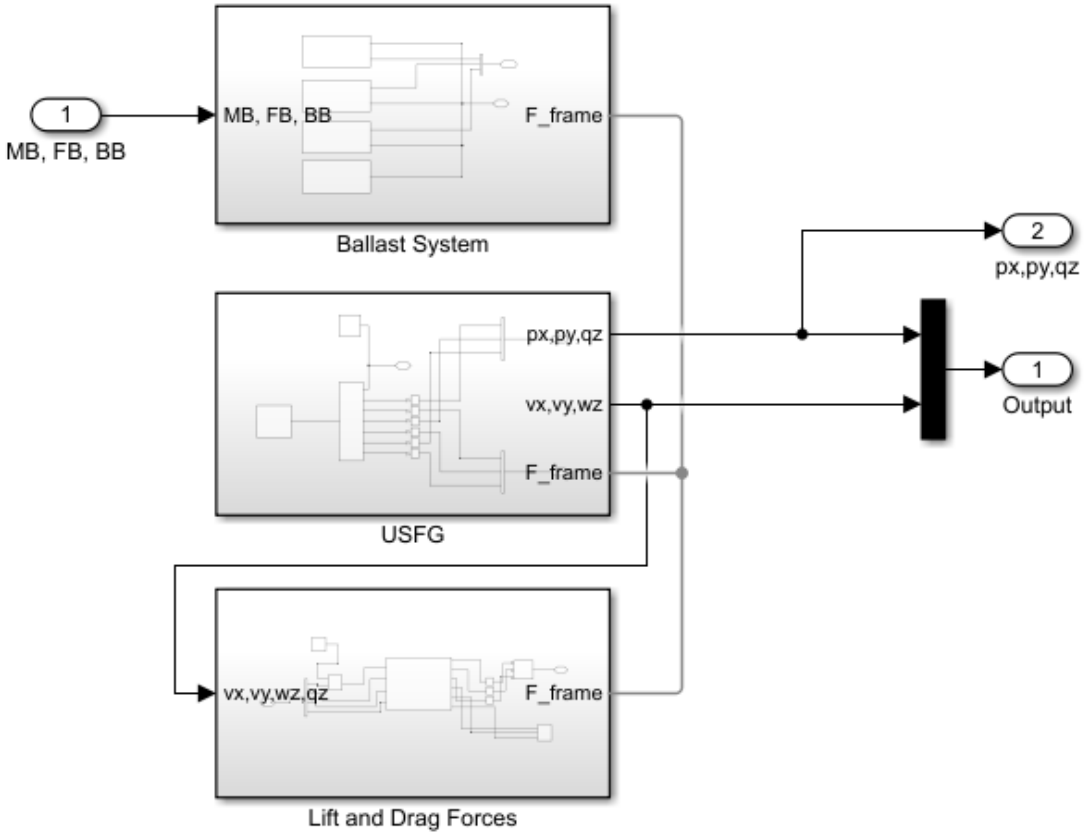

Figure 5. Plant model.

The following three main blocks are represented for the plant model:

- Ballast system: This block is used to model the dynamics of the ballast system in USFG. It takes in the control inputs for ballasts (Main, Front, and Back) and delivers them as an input

for forces to the USFG block. Furthermore, it also provides the glider with the buoyancy force.

- USFG: Contains a two-dimensional rigid body having three degrees of freedom in *x, y*, and *z* directions. Equations of motion will be solved in this block by Simulink based on the forces implemented on the body.
- Lift and Drag forces: Based on the angle of attack of the incoming flow, lift, drag, and rotational torque are calculated by taking into account the velocity of the USFG along with pitch angles. These forces then serve as an input to the USFG block. The lift and drag coefficients are a function of angle of attack (α) and are calculated using the equations (1) and (2):

$$C_L = 5(\alpha^2) + 10(\alpha) \tag{1}$$

$$C_D = 0.4(\alpha^2) + (\alpha) + 0.1 \tag{2}$$

4. Control theory and controller tuning

As stated previously, this work will limit its scope to a 2D dynamic problem for the UiS glider, i.e., only motions in heave and pitch direction are studied whereas, motion along the other axes is not considered here. Furthermore, few assumptions are ensured for added simplifications:

- The USFG is considered to be in hydrodynamic equilibrium. Leading to no coupling in the hydrodynamic terms due to symmetry, as all the forces act on the center of gravity (COG) of the glider.
- UiS subsea glider functions far off the region where wave effects are dominant: loading due to waves is insignificant in addition, currents are not considered.

4.1. Proportional-integral-derivative controller

Proportional-integral-derivative (PID) type control is adopted for the system under consideration, owing to its popularity amongst autonomous underwater and marine vehicles for varying the motion and obtaining desired performance of the vessel along the axis under consideration. To adduce, pitch motion for Slocum [12] is regulated by implementing a proportional controller to control internal kinetic mass.

The Control system for the glider is depicted in Figure 6 below, two PID controllers are used to control heave and pitch separately and the glider block represents the system dynamics. Desired response for operating conditions, i.e., heave and pitch, is generated from the pilot block which is then fed to the error detector. Afterward, it is then processed by the controller to produce a stimulating signal which is transformed into the desired motion.

The main task is to control the heave along with pitch motion of the USFG, which is achieved by designing a PID controller based on single input and output. For instance, if $U(s)$ in equation (3) depicts a transfer function of a particular control loop and $U_c(s)$ in equation (4) characterizes a PID based controller:

$$U(s) = K_p(1 + \frac{1}{T_i s} + T_d s) \tag{3}$$

T_d, T_i and K_p are called derivative time, integrator time, and proportional gain, respectively. These are the parameters that can be tuned for a PID controller to get the optimal performance. Whereas, in time-domain, it is expressed as:

$$u(t) = K_p\, e(t) + K_i \int_{to}^{t} e(\tau) d\tau + K_d \dot{e} \tag{4}$$

where $K_i = K_p/T_i$ is called the integral gain and $K_d = K_p T_d$ is termed as derivative gain. Error signal $e(t)$, is the difference between the desired value and the actual value of the output signal.

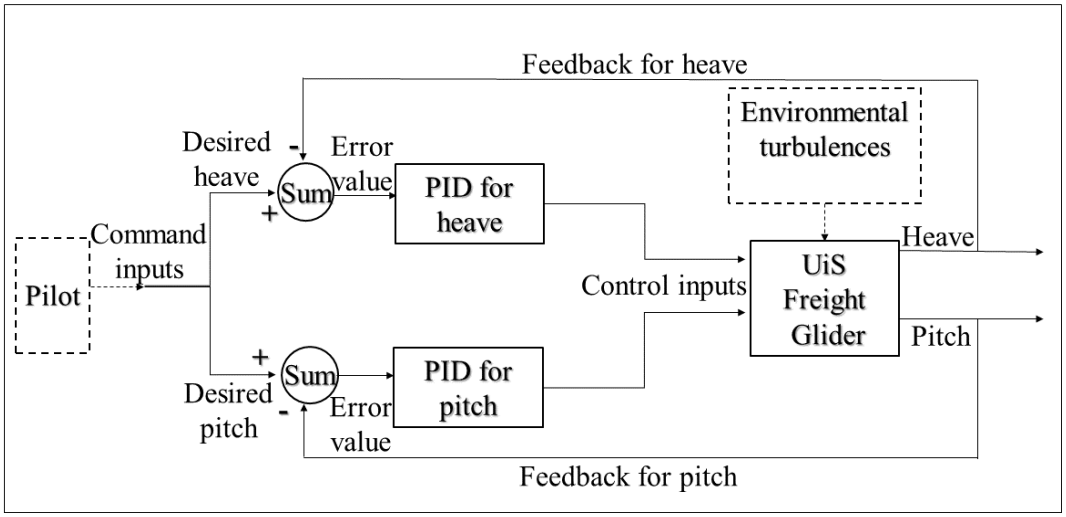

Figure 6. Control block for the glider system.

4.2. Controller Tuning

Gains for the PID controller are tuned by linearized analysis of the system along with experiments and experience of the control engineer. MATLAB transfer function-based PID Tuner App is used for this paper. The basic tuning principles for the utilized method are highlighted in Åström and Hägglund [13]. For tuning purposes, the tuner app utilizes a model which is linearized for a functional point. System step or impulse response can be obtained by altering the phase margin and bandwidth of the signal in the frequency domain, by doing this; the equivalent tuner gains can be acquired automatically. Consequences of varying the bandwidth and phase margin on different parameters like percentage overshoot (yield value which surpasses its final time-dependent value), rise time (time required by the signal to move from 10% to 90% of the yielding value), and settling time (time taken by the oscillating signal to reach 2% of the final value) are discussed in the following sections.

4.2.1. Effects of phase margin. Phase margin, which is defined as the negative phase disturbance that compels the system to be slightly stable. Figure 7 underneath displays a step plot presenting the contrast between changing the phase margin from 50° to 90° for block and tuned response respectively for heave and pitch motions.

Increasing the phase margin expands the transient behavior of the response, making the system more robust as the percentage overshoot is significantly reduced. Whereas, controller gains are reduced consequently, as seen in Table 2, leading to the increased rise time and the settling time, resulting in a less aggressive control system. Contrary behavior is observed if the phase margin is reduced which can be seen in terms of block response in Figure 7.

Table 2. PID gains for phase margin behavior.

Gains	Tuned (Heave)	Block (Heave)	Tuned (Pitch)	Block (Pitch)
P	164	1662	28	284
I	0.19	19	0.03	3.27
D	31229	29478	5329	5031

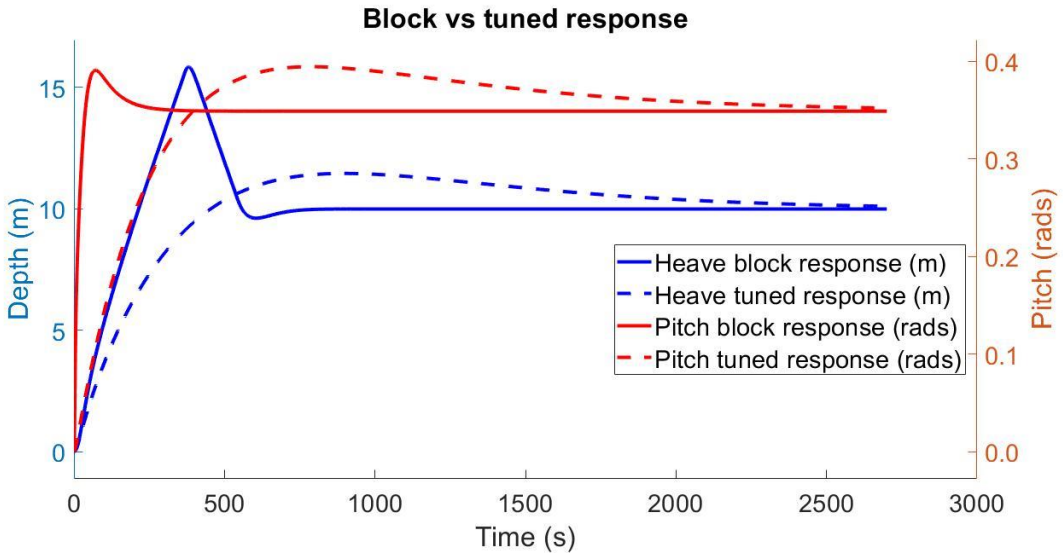

Figure 7. Response for varying phase margin.

4.2.2. Effects of bandwidth. Bandwidth sometimes referred to as response time, is defined as how fast the system retorts to changes in the input or desired conditions. Figure 8 beneath demonstrates control loops' step plot representing distinction amongst shifting response time from 0.20 for block response to 0.35 seconds for the tuned signal.

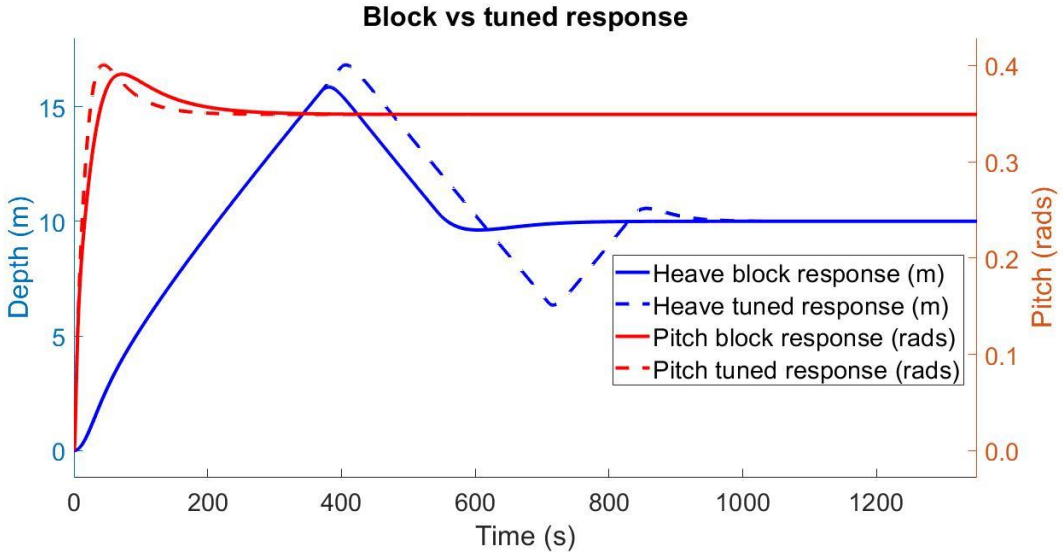

Figure 8. Varying bandwidth response.

Increasing the bandwidth of the controller for the tuned response makes the system more aggressive and agile to changes. It was observed that increasing the bandwidth to a larger value doesn't always help, instead of increasing it beyond a certain threshold induces oscillations (a reference to the tuned signal of heave in Figure 8) and makes the system unstable. Furthermore, rise time and response time are reduced as a consequence of higher controller gains (K_p, K_i, K_d) as illustrated in Table 3. On the other hand, contradicting behavior can be seen with the block response in Figure 8 in which the system is relatively lagging due to increased rise and settling time along with lower gains. As for overshoot, it can be noticed that for both cases it is quite similar, in other words, bandwidth, in this case, doesn't influence the peak of the response.

Table 3. PID gains for response time performance.

Gains	Tuned (Heave)	Block (Heave)	Tuned (Pitch)	Block (Pitch)
P	4956	2333	846	284
I	93	34	16	3.27
D	51727	37367	8827	5031

Subsequent conclusions were drawn:

- Phase margin decreases overshoot, whereas bandwidth has no effect over it.
- Bandwidth, when increased minimalizes rise time, while no change is observed with varying phase margin.
- The bandwidth of 0.3 rad/s and phase margin of 90 degrees is selected from the tuning exercise.

5. Sensitivity analysis

This exercise is performed to study how the vessel response changes over time for varying ballast fraction (*BF*) and pumping capacity (*Cp*) of the pump. The focal idea behind this is to formulate few cases, as illustrated in Table 4, to study the effects of changing ballast fraction (*proportion of dead mass used for ballast*) and pumping volume (*Volumetric flow rate of ballast*) of the pump on the dynamics of the glider.

Table 4. Characteristics of sensitivity study.

Case no.	Ballast Fraction (BF) %	Pump Flowrate (Cp) m^3/h
Case 1	0.15	2000
Case 2	0.075	1000
Case 3	0.30	4000

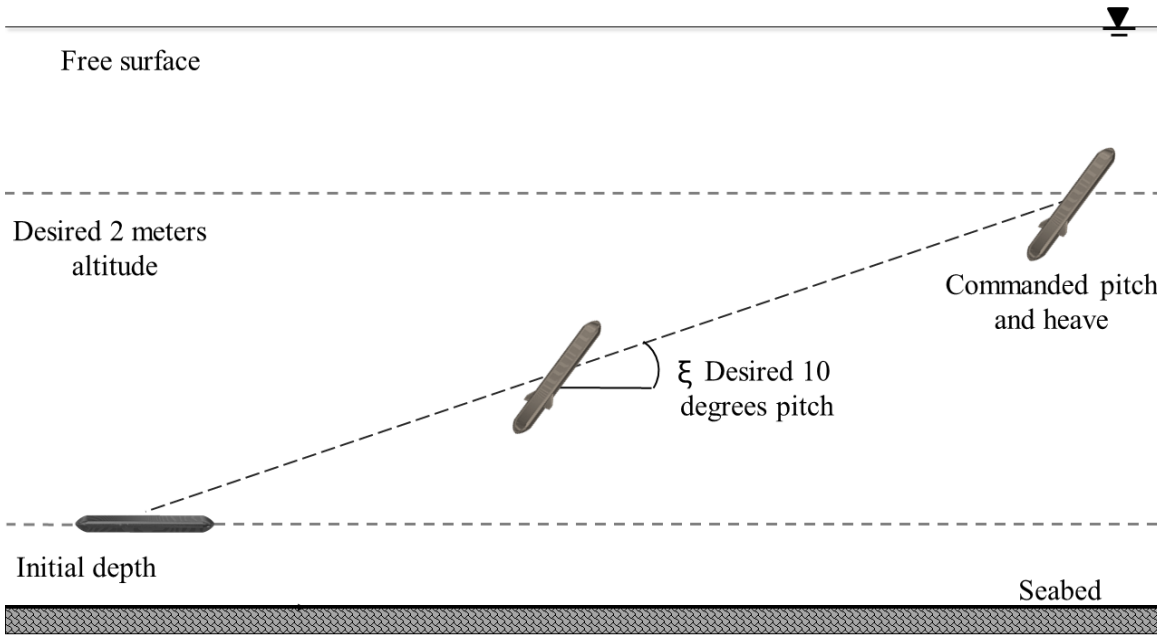

Figure 9. Test case simulation.

As a test case, the glider is instructed to attain an altitude of 2 meters long with a pitch angle of 10 degrees as depicted in Figure 9. Each case highlighted in Table 4 above was simulated to study how sensitive the USFG is to deviations in two vital parameters.

Figure 10 shows the discrepancies amongst diverse heave responses of the glider under various conditions mentioned earlier, it must be noted that the output signal is not plotted for the entire time series for better visualization and comprehension.

Output response for the 3rd case has the best performance amongst the three cases, this is because the glider generates more buoyancy force consequently due to higher ballast fraction. Moreover, as a result of increasing pump flow rate, ballast is changed efficiently and quickly, which translates to the glider attaining the desired heave and pitch quickly with no fluctuations. On the other hand, oscillations can be seen for the 2nd case in the output response making the system unstable and less robust to changes. It takes excessive time by the glider with adverse overshoot and undershoot to settle on its desired state if these conditions are used. The first case, as proposed by Xing [6] is only used as a benchmarking tool to study the effects of increasing ballast fraction and flow rate on the glider and vice versa.

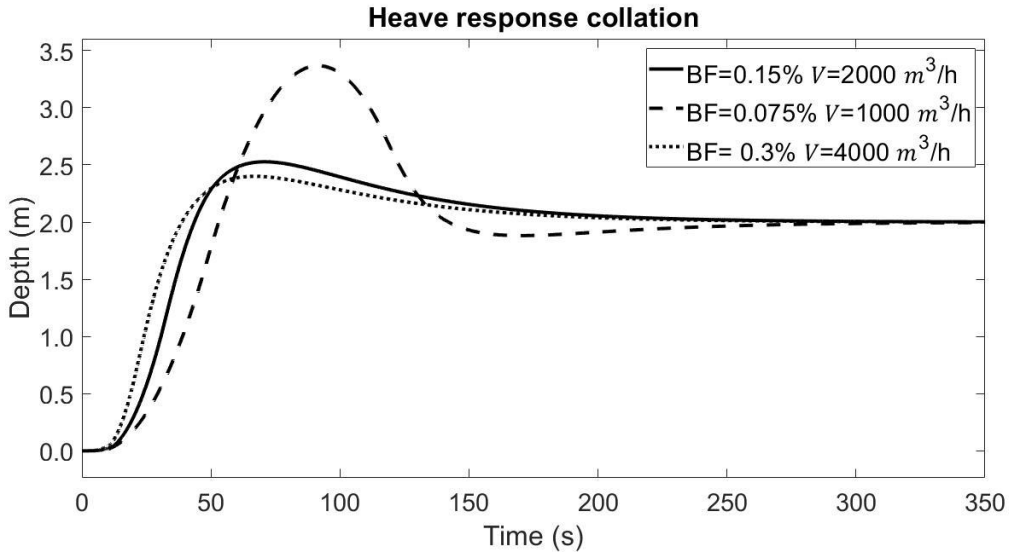

Figure 10. Heave responses for the scenarios.

The advantage of using a ballast fraction of 0.30% and a volumetric flow rate of 2000 $\frac{m^3}{h}$, i.e., Case 3, is two folds: the ability of the system to handle disturbances is significantly improved: enhanced robustness, along with faster response time. Contrarily, there are some added shortcomings, using a large pump for higher flow rates along with bigger and bulkier ballast tanks to accommodate for increased ratio. In the author's opinion, it is better to select a low power pump and small ballast tanks, i.e., 1st case, since there is not much of a variance between the results of both cases as seen in Figure 10 above.

6. Case studies

To completely define a glider, its steady glide paths must be clearly described. For this purpose, few test cases, presented in Table 5, were set up to fully understand the changing behavior of the glider concerning controller gains.

The variables studied for this analysis are the diving depth and the required pitch angles attained by USFG for the glides. The initial or base case termed as Case A signifies that the glider tries to achieve the height of 200 meters while pitching at an angle of 38˚with the tuned gains chosen earlier. Moreover, it is used for benchmarking other cases operating under various conditions.

Table 5. Simulated cases.

Case name	Required depth (m)	Pitch angle (deg)	Bandwidth (rad/s)	Phase margin (deg)
Case A	200	38	0.2	90
Case B	200	19	0.3	90
Case C	200	19	0.4	90

7. Results and discussions

7.1. Effects of tuning

The results of different tuning cases for glide paths in vertical planes are presented in Figure 11 along with time series for pitch response of the USFG in Figure 12.

Reducing the bandwidth affects the system response critically as depicted in Figure 11 and Figure 12 for Case B. Lowering the bandwidth value leads to poor system response, as it becomes slower and also shows excessive overshoot and undershoot from target values. This can also be seen in the pitch response, where it takes greater time for the system to obtain the desired pitch angle.

Case C, being the ideal amongst the alternatives has the smallest response time due to aggressive tuning. It can be seen in the plots below that for this particular case the glider is quick to respond to changes in the heave and pitch motions. Moreover, for this case, deviations in the upper and lower limits are also condensed leading to reduced overrun and undershoot. Gains obtained for this case enable the system to follow the intended path closely as compared to the alternatives. Further optimizing these gains can reduce the error significantly, thus leading to enhanced performance of the USFG while gliding.

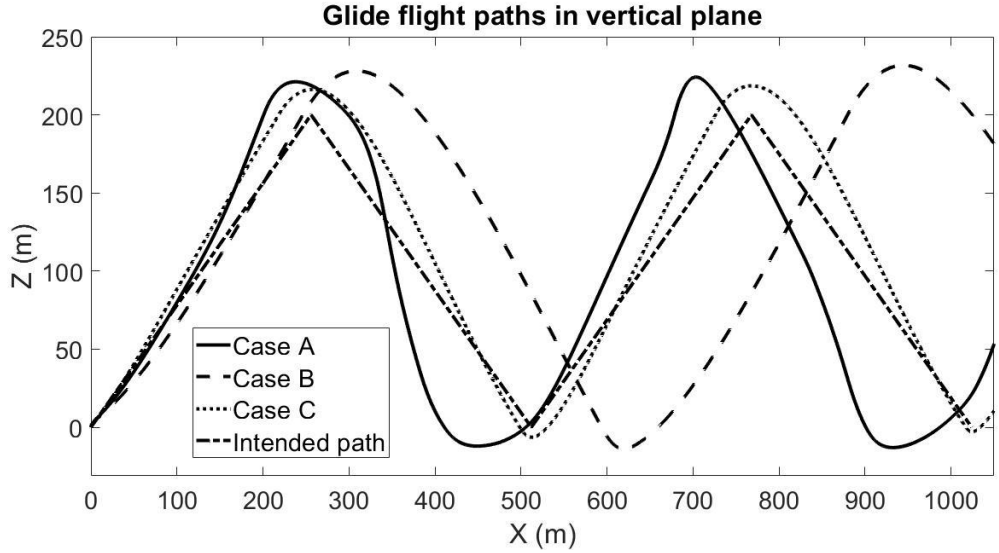

Figure 11. Glider path in a vertical plane from simulation.

Case A represents the base case gains, these controller gains were obtained in section 4.2. . It can be seen in the figure above that even the best PID gains i.e., Case C, obtained from the linear model of the system i.e., the USFG model, failed to follow the intended path. Moreover, the responses are quite slow for disturbances introduced into the system as compared to the desired case.

An error of 13 to 8 % is induced into the system for gains of Case B and Case C respectively. Also, this is likely to induce adverse effects on the glider trajectory, since at every oscillation the glider travels a significant amount of distance which was not initially intended. This is due to

excessive overshoot and undershoot induced by the controller parameters and can offset the USFG from its course by a compelling margin.

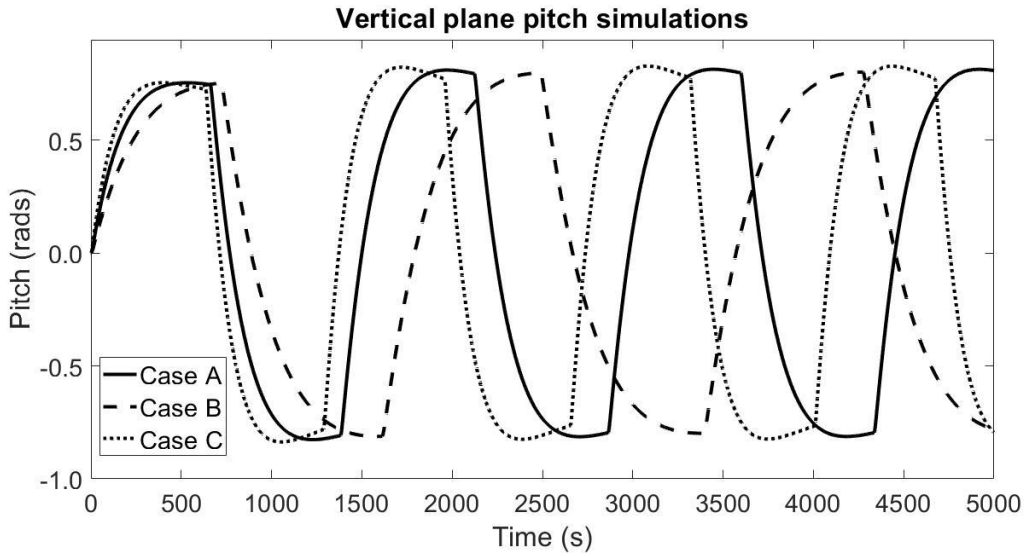

Figure 12. Vertical plane pitch state.

7.1. Best controller gains

Selecting the best parameters for $(K_p,\ K_i, K_d)$ for both the controllers is a challenging and cumbersome task, but it can be done with excessive research and further developments. Following observations are made in response to selecting the best gains:

- Increasing the phase margin to the maximum value of 90° can minimize the overshoot but it does not completely diminish it as even the best gains still have an 8% overshoot.
- Improving the value of bandwidth to a certain limit i.e., 0.4, can help with the system response; making it agile, afterwards, it has no effect.

8. Conclusions

This study presents a 2D mathematical model of the UiS subsea freight-glider. Along with the model, quality assurance for the presented model has also been completed in the form of controller tuning and sensitivity analysis. The results from the case studies convey that tuning the system only by utilizing time responses obtained from a linearised model does not yield the best results. Lastly, it was observed that enhanced performance can be obtained by re-tuning the controllers for higher bandwidth, leading to better system response.

Since the equilibrium glides for the USFG should stringently follow the planned path shown in Figure 2, optimization of the PID controllers to allow for enhanced, robust, and optimal controls will lead to ideal performance. This will be the target study for future work.

References

[1] Stommel H 1989 The Slocum mission, *Oceanogr.* **2**(1), 22–25.

[2] DOF Subsea *Glider AUV Project.* Accessed 07.07.2021 from http://www.dofsubsea.com/rov/glider-auv/.

[3] AUVAC *AUV System Spec Sheet*. Accessed 07.07.2021 from https://auvac.org/23-2/.

[4] Ferguson J S 2003 *Cargo Carrying AUVs: Technology and Applications of Autonomous Underwater Vehicles* (London: Taylor and Francis Group).

[5] Equinor 2020 *RD 677082 Subsea Shuttle System 2020.*

[6] Xing Y 2021 A conceptual large autonomous subsea freight-glider for liquid CO2 transportation, *Proc. 40th Int. Conf. Ocean Offshore Arct. Eng.* (Virtual: Jun 21 – 30, 2021).

[7] Reducing greenhouse gas emissions from ships International Maritime Organisation. Assessed 21.07.2021 from https://www.imo.org/en/MediaCentre/HotTopics/Pages/Reducing-greenhouse-gas-emissions-from-ships.aspx.

[8] Fossen T 1995 *Guidance and Control of Ocean Vehicles* (New York: John Wiley and Sons).
[9] Graver J G 2005 *UNDERWATER GLIDERS: DYNAMICS, CONTROL AND DESIGN* (Princeton University: Ph.D. thesis).
[10] langebrake L C 2003 *AUV Sensors for Marine Research: Technology and Applications of Autonomous Underwater Vehicles* (London: Taylor and Francis Group).
[11] Griffiths G et al. 2003 *Logistics, Risks And Procedures Concerning AUVs: Technology and Applications of Autonomous Underwater Vehicles* (London: Taylor and Francis Group).
[12] Webb D C, Simonetti P J, and Jones C P 2001 SLOCUM: an underwater glider propelled by environmental energy," *IEEE J. of Oceanic Eng.* **26**(4), 447-452.
[13] Åström K J and Hägglund T 2006 *Advanced PID Control* (ISA - The Instrumentation, Systems and Automation Society).

Proceedings of the ASME 2022 41st International Conference on Ocean, Offshore and Arctic Engineering
OMAE2022
June 5-10, 2022, Hamburg, Germany

OMAE2022-79448

UIS SUBSEA FREIGHT-GLIDER: CONTROLLER DESIGN AND ANALYSIS

Usman Nawaz Ahmad
University of Stavanger
Stavanger, Norway

Yihan Xing*
University of Stavanger
Stavanger, Norway

ABSTRACT

The UiS subsea freight-glider (USFG) is a novel 785 DWT large cargo-carrying underwater autonomous vehicle. It uses variable buoyancy propulsion, i.e., it glides forwards using generated lift and drag forces at the hydrofoils while ascending and descending in water. This propulsion method is ultra-efficient and can transport cargo over long distances with minimal energy consumption. For USFG to operate with maximum speed and enhanced range, a robust, reliable, and accurate control is important as this results in a precise navigation system that would allow for its gliding motion to be extremely efficient. During long-distance voyages, a robust control system based on a feedback loop provides enhanced utility against any external uncertainties or environmental disturbances. The purpose of this work is to implement a control methodology that is based on feedback from the model. This approach removes the need for excessive tuning of controllers for any changes in operating conditions. Moreover, dynamic states, i.e., velocities, can be determined by designing an observer which can be used to predict the motion of the USFG in a planar axis. The gliding paths of USFG in the vertical plane are analyzed along with the observability and controllability of the steady equilibrium glides. For this purpose, the control system is designed with two different controllers, PID and LQR, which control the heave and pitch of the vehicle. Finally, a comprehensive comparison study is presented, which highlights the key differences for the controllers for tunning and rise time. This can also help in designing the ideal control for the required application.

Keywords: Large AUV gliders, Control system, Maritime transportation, Subsea technology, LQR, PID

NOMENCLATURE

AUVs	Autonomous underwater vehicles
BF	Ballast fraction
DWT	Dead-weight ton
D	Drag force
F_b	Buoyancy force
K_p	Proportional gain
L	Lift force
LQR	Linear-quadratic regulator
M_b	Main ballast tank mass
M_s	Secondary ballast tank mass
PID	Proportional-integral-derivative
SST	Subsea shuttle tanker
SIMO	Single input multiple outputs
SISO	Single input single output
T_i	Integrator time
T_d	Derivative time
UiS	University of Stavanger
USFG	UiS subsea-freight glider
V	Glide velocity
V_r	Required velocity
V_x	Horizontal glide velocity
V_z	Vertical glide velocity
V_{x_e}	Horizontal velocity estimate
V_{z_e}	Vertical velocity estimate
W	Weight
$\dot{x}_{DR}$	Horizontal dead-reckoned velocity
x'	Required path of USFG
z'	Perpendicular distance from the path
α	Angle of attack
θ	Pitch angle
θ_r	Required gliding angle
$\dot{\theta}$	Pitch rate
ξ	Glide path angle
ξ_r	Required glide path angle

*yihan.xing@uis.no

1. INTRODUCTION

The UiS subsea-freight glider (USFG) as illustrated in FIGURE 1 was proposed by Xing [1]. It is a 785-dead-weight ton (DWT) cargo-carrying glider which utilizes an ultra-efficient propulsion system instead of typical thruster or propeller-based systems. The propulsion system is based on the principle of variable buoyancy, it allows the USFG to glide in the water owing to its large hydrodynamic wings spanning an area of 20 m^2. Consequently, a large amount of cargo can be conveyed autonomously by resourcing the energy efficiently while traveling long distances. The USFG can be used as a cost-effective substitute to long subsea pipelines, which have massive maintenance and laying costs, as well as the conventional tankers or crude carrying ships. The USFG is anticipated to have the same cost per ton of CO_2 as compared to the subsea shuttle tanker studied by Xing et al. [2].

The USFG is novel and unique due to its buoyancy-driven mechanism of propulsion which allows the glider to propel itself for longer missions. The concept of efficient gliding has already been introduced and researched quite expansively in autonomous underwater vehicles (AUVs); especially underwater gliders that can log ocean data for months without the need of any support or accompanying vessel. These gliders include DOF [3] and AUVAC [4], however, they are not designed to carry cargo. To the authors' knowledge, there has only been one cargo-carrying AUV, Thesus which is developed by LSE ltd. in the late 1990s for the Spinnaker project [5]. Thesus is a cable-laying vessel, capable of carrying 660 kg while having a range of 900km. The subsea shuttle tanker proposed by Equinor [6] and discussed in Xing et al. [7] and Ma et al. [8] also highlighted the potential use of gliders to carry a payload.

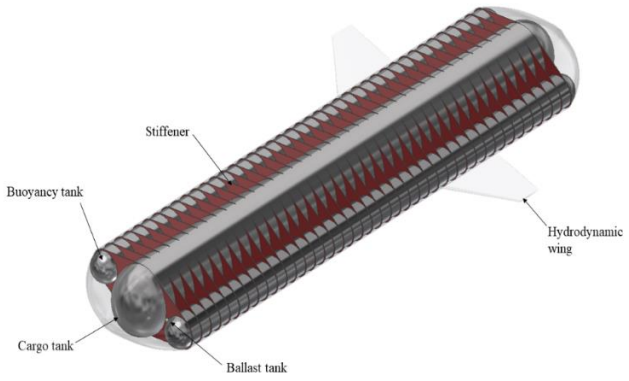

FIGURE 1: UIS SUBSEA GLIDER

FIGURE 2 illustrates the basic principle of the USFG. The USFG glide path resembles a sawtooth motion as it is based on two cycles: upward and downward. During the initial cycle, the ballast water is pumped into the system increasing the overall weight of the vehicle which in terms generates a negative force of buoyancy causing the glider to dive down to the desired depth. In the upwards cycle, the USFG sheds weight by pumping out the ballast water making the overall system positively buoyant, and upward acting buoyancy force carries the vehicle to the initial depth, thus completing a single cycle or one equilibrium glide. The large spanning hydrodynamic wings are responsible for generating sufficient drag and lift force to propel the USFG frontward during its cyclic motion. These two cycles are repeated throughout the entire mission of the glider making it extremely energy efficient as the hydrodynamic wings are responsible for generating thrust whereas a reduced amount of energy is being depleted by the pumps to vary ballast. TABLE 1 presents the vital design parameters of the glider. Due to its innovative propulsion system, the USFG has a lower carbon footprint as compared to conventional transport vessels and can contribute to the decrease of transport emissions (roughly about 3% of the carbon emissions globally) [9].

TABLE 1: DESIGN PARAMETERS OF USFG

Parameter	Value	Unit
Vessel length	50	m
Cargo tank diameter	5.0	m
Buoyancy tank diameter	2.2	m
Deadweight ton	1533	ton
Structural weight	470	ton
Cargo weight	785	ton
Ballast fraction	0.15	%
Diving depth	200	m
Glide path angle	38	°
Wing area	20	m^2
Volumetric drag coefficient	0.1	-
Ballast pump capacity	2000	m^3/h
Pumping time / cycle	< 5% of half cycle	-
Horizontal speed	1	m/s
Average Power	< 10	kW
Net transport economy	< 0.5	-

Xing [1] studied and proposed the unique concept of USFG with the help of design optimization methods. Design margins were included in this study by using probabilistic analysis. This analysis highlights the use of USFG for CO_2 transportation among marginal subsea fields, as stand-alone pipelines are not a cost-effective solution. Work by Ahmad and Xing [10] presents a planar model for the USFG developed in MATLAB to capture the dynamics of the system. Tunning and sensitivity studies were performed which aids in selecting optimal controller gains for the equilibrium gliding path taken by the glider. This paper builds on this previous work done by the authors to further optimize the control of the freight-glider.

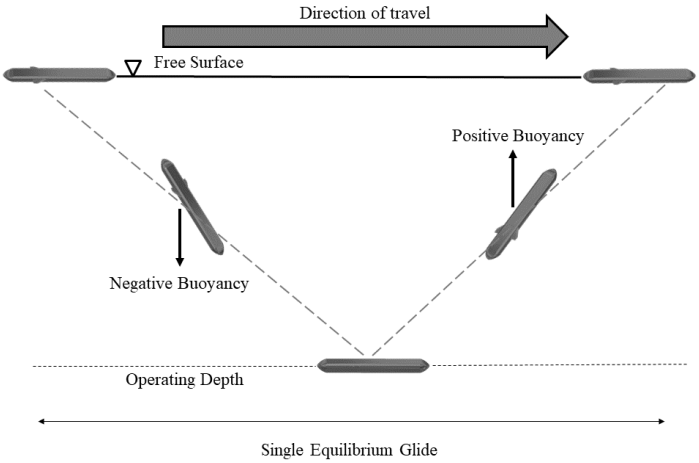

FIGURE 2: USFG's WORKING PRINCIPLE

2. STEADY GLIDE PLOTS

This section presents the steady glide plots of the USFG. The purpose of this analysis is to establish the required ballast fraction and the diving or gliding angle essential for achieving the glider velocity (V) of 1 m/s. Ballast fraction (BF), is the percentage of the mass of water used for pumping ballast in and out of the tanks. BF is varied for different glide path angles i.e., 10º, 20º, 30º, and 40º as shown in FIGURE 3. Whereas V_x is the velocity of the glider in the horizontal axis.

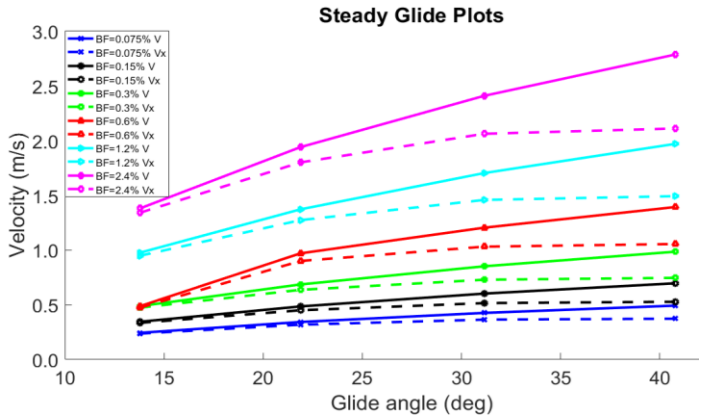

FIGURE 3: GLIDE SPEEDS VS GLIDE PATH ANGLE

Ballast fraction (BF) of 0.6 % along with glide angles of 30º and 40º gives velocities in the required range for the current application. Higher ballast fractions are not chosen as they will increase the pumping capacity, requiring a higher flow rate pump which has the potential to drain more energy. Increased pitching angles of the USFG are not preferred, i.e., greater than 40º, as they might proportionally increase the actuator capacity, which means more electrical power consumed on the vessel. Both, ballast fractions and glide angles can also affect the equipment weight of the vessel significantly.

For a design glide velocity (V) of 1 m/s, Ref. Xing [1], the corresponding glide angle and ballast fraction are 38 ° and 0.6 % respectively.

3. CONTROLLED GLIDING IN A TWO-DIMENSIONAL PLANE

This section focuses on assessing the linear observability and the ability of the USFG to be controlled during the steady planar gliding paths. Generally, a glide path is well-defined by the required gliding angle of the path θ_r and the required velocity V_r of the glider. FIGURE 4 depicts α (angle of attack), L (Lift force), D (Drag force), and θ (pitch angle).

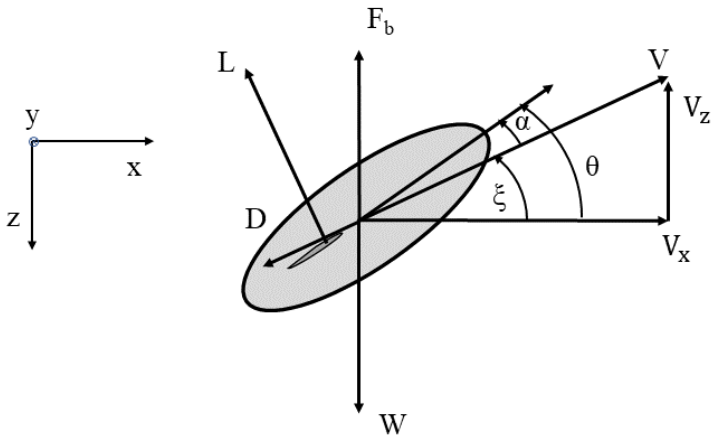

Figure 4: USFG's PARAMETERS IN THE VERTICAL PLANE

Glide path angle and the gliding speed of the vehicle is:

$$\xi = \theta - \alpha \tag{1}$$

$$V = \sqrt{(V_X{}^2 + V_Z{}^2)} \tag{2}$$

The equations of motion in this system can be expressed as:

$$\begin{aligned} W(\dot{u} + wq - xq^2 + z\dot{q}) &= \sum X_e \\ W(\dot{w} + uq - zq^2 + x\dot{q}) &= \sum Z_e \\ I_{yy}\dot{q} + W[z(\dot{u} + wq) - x(\dot{w} - uq)] &= \sum M_e \end{aligned} \tag{3}$$

Whereas forces and moments are expressed by (X, Z, and M) and velocities by (u and w) along with accelerations (u̇ and ẇ). Equation 3 contains inertial terms on the left side along with external forces in heave (Z_e), surge (X_e), and pitch (M_e) directions.

Equation 4 represents the coordinates (x', z') whereas x' overlaps with the required path taken by the USFG while z'measures the glider's vertical distance to the anticipated path.

Two objectives for gliding motions are defined as:

- **M01** Preliminary objective is to control the velocity and path of the USFG's gliding motion. As for this scenario, x and z are not measured.
- **M02** Secondary task is to control USFG to glide along a straight path or line as shown in FIGURE 5. For this case, z' is the critical parameter for control application as the aim is to minimize it and achieve $z' = 0$ without considering x'.

$$\begin{bmatrix} x' \\ z' \end{bmatrix} = \begin{bmatrix} \cos \xi_r & -\sin \xi_r \\ \sin \xi_r & \cos \xi_r \end{bmatrix} \begin{bmatrix} x \\ z \end{bmatrix} \quad (4)$$

The state dynamics of z' can be modeled by:

$$\dot{z}' = \sin \xi_r \, (V_x \cos \theta + V_z \sin \theta) + \cos \xi_r \, (-V_x \sin \theta + V_z \cos \theta) \quad (5)$$

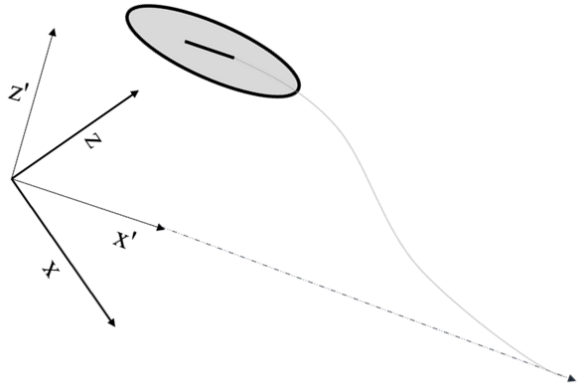

Figure 5: OBJECTIVE M02 IN 2D PLANE

3.1 Linearization

The two-dimensional mathematical model presented by Ahmad and Xing [9] is linearized along two different glide paths of 30° and 40° highlighted in TABLE 2. The goal is to extract the linear model of the dynamic system as a state-space model. For single input multiple outputs system (SIMO), the state-space equations are given by:

$$\frac{dx_1}{dt} = Ax_1 + Bu_1 \quad (6)$$

$$\frac{dx_2}{dt} = Ax_2 + Bu_1 \quad (7)$$

$$y_1 = Cx_1 + Du_1 \quad (8)$$

$$y_2 = Cx_2 + Du_1 \quad (9)$$

where $x_{1,2}$ are state variables of the system, u_1 and $y_{1,2}$ are scalar matrices that signify the inputs and outputs respectively.

Linearization is done for the mathematical model at a model operating point [11] with the aid of the model linearizer tool in Simulink. Open-loop input is configured as shown in FIGURE 6 which is taken as output just after the sum block. Output signals from the plant block are marked as open-loop outputs. After the operating points are configured a Bode plot is plotted along with the generation of the linear model. This is done to generate ***A*** and ***B*** matrices.

USFG's design characteristics, i.e., if it is controllable or observable, can be checked with the help of the obtained linearized state-space model. The design process can be automated for different gliding paths of the USFG, which is another application of this linearization technique. This can be done by applying the Routh criterion to the state-space variable of the gliding path, i.e., glide angle or ballast mass, in the ***A*** matrix: which in terms specifies the stability of the system.

3.2 Controllability

This section examines the steady gliding paths of the USFG for their controllability. After linearization, the stability of the vehicle is assessed by evaluating the linear controllability. It must be noted that the same procedure can be implemented to any sort of underwater marine vehicle provided the Simulink model is available.

The two-dimensional model presented by Ahmad and Xing [10] is directly controllable for the four intended paths listed in TABLE 2. That is to say, the matrices ***A*** and ***B***, when calculated at any of the specified conditions of the equilibrium glide paths, satisfy the rank condition for the controllability matrix, i.e., the rank of matrix ***A*** equals the rank of the controllability matrix. The linearization performed in the previous section considers the conditions for the state variable z', this signifies that controllability also covers the variable z' of the system. Consequently, a controller can be designed for the USFG which can accomplish objectives M01 and M02.

TABLE 2: STEADY GLIDE PATHS FOR THE USFG

Parameter	30° Downwards	30° Upwards	40° Downwards	40° Upwards
θ_r (deg)	-30.00	30.00	-40.00	40.00
α_r (deg)	4.65	-4.65	2.04	-2.04
ξ_r (deg)	-35.35	35.55	-42.04	42.04
V_r (m/s)	0.35	0.35	0.80	0.80

3.3 Observability

Observability for the various glide conditions highlighted in TABLE 2 is analyzed in this section. For M01, variable z' is not required for this application since only the USFG's velocity and the direction of travel are controlled for each glide path. The dynamic model of the USFG is entirely observable with regards

to M_b and M_s (variable mass for main ballast and secondary ballast tanks). That is because the rank of matrix $\boldsymbol{B}$ equals the rank of observability matrix. For this scenario, detection of θ pitch angle, $\dot{\theta}$ pitch rate and the velocity components V_x and V_z are not required. Consequently, a mathematical observer can be designed which corresponds with M_b and M_s to approximate θ, V_x, V_z and $\dot{\theta}$ which are the unmeasured variables or states of the USFG. This has the benefit of evaluating the velocity components V_x and V_z as θ pitch angle is commonly measured, as for $\dot{\theta}$ pitch rate it's generally easy to measure using onboard instruments. The multi-dimensional model of the USFG, if restricted to state variables θ, M_s and M_b are fully observable.

High precision can be obtained in M01 by employing a dynamic observer. By doing this, the observer approximates the variables or states of the vehicle, and the accuracy of the entire process may be significantly enhanced. Moreover, contemporary measurement methods induce some simplifications to the system for measurement of states, i.e., constant angle of attack of the vehicle. For instance, Slocum utilizes velocity calculated from depth measurements, global positioning system (GPS) locations, quantified pitch angles θ and implicit angle of attack to compute the horizontal motion throughout gliding as highlighted by Webb and Jones [12]. Similarly, for the Spray glider, the horizontal distance during the gliding is measured depending on constant attack angle, pitch, and heading as discussed by Sherman et al. [13].

To accomplish M02 that is, to control the motion of the glider along a straight path, z' should be measured. From Equation 4, it is seen that z' is dependent on horizontal state-space variable x (cannot be measured) and the depth coordinate z, which can be measured without any difficulty. The state-space variables M_s and M_b along with the estimation of z are not enough for observing x. To measure the trajectory of USFG x(t), measurements at initial conditions are required, making x non-observable. Moreover, an observer cannot be designed to detect z' but, the horizontal position or motion of the vehicle can be dead reckoned with the aid of velocity approximations from the mathematical observer by using initial GPS measurements. In this way, an error ($z' - z'_{DR}$) can be inducted into the state variable z'. Finally, M02 can then be accomplished by introducing the inferred z'_{DR} as feedback into the control loop which enables the USFG to glide along the commanded or required route. The dead-reckoned velocity in the horizontal direction, $\dot{x}_{DR}$ is given by:

$$\dot{x}_{DR} = V_{x_e}\cos\theta + V_{z_e}\sin\theta \qquad (10)$$

x_{DR} can then be obtained by integrating Equation (10) which is then used to deduce z'_{DR}. The glide parameters, ξ_r, θ and z are defined by the glide path taken by the glider and can be easily measured. Whereas velocity estimates V_{x_e} and V_{z_e} can be acquired from the observer. The dead-reckoned parameter z'_{DR} is given by.

$$z'_{DR} = \sin(\xi_r\, x_{DR}) + \cos(\xi_r\, z) \qquad (11)$$

For linearization to be effective, the observed variables V_{x_e} and V_{z_e} will tend to close in on the actual state-space variables V_x and V_z when the glider is adjacent or sufficiently close enough to the desired path. On the other hand, if there is an error consequently the result will be, $z' - z'_{DR} \neq 0$. Moreover, this error is a function of state variables and is sensitive to external environmental disturbances.

4. CONTROLLER ARRANGEMENT: PID VS LQR

This section discusses the design of two controllers commonly used in marine vehicles, PID and LQR. The given task or objective is to pitch the USFG to an optimal glide angle of 38 ° as highlighted by graver in his Ph.D. thesis [14] as stably as possible without utilizing excessive actuator power. Both controllers are designed to be robust to the applied application. Noise is artificially generated into the system to mimic the external disturbances from the environment. The following objectives must be fulfilled.

- **M03** the glider must attain an angle of -38° (clockwise pitching direction) while diving downwards to the required operating depth. This objective is designed to act as a benchmarking tool while selecting the optimal controller as well as the controller gains.

4.1 SIMULINK MODEL

SimMechanics or MATLAB Simscape Multibody is employed to model the dynamics of the USFG. FIGURE 6 displays the Simscape model.

The key parts as highlighted in the figure above are discussed below.

- Block 1: Represents the PID controller to regulate the pitch response.
- Block 2: Termed as a manual switch, as the name suggests it acts as a lever to switch between PID or LQR based control.
- Block 3: The heave mass block regulates the mass into and out of the main ballast tank which aids the glider to move in the heave direction. It does so with the aid of lift and drag forces generated by the large hydrodynamic wings. It also contains a rate limiter along with a saturation block to have enhanced control over the tank.
- Block 4: Similar to block 4 the pitch mass block controls the mass of ballast between the two secondary tanks. These tanks influence the pitching motion or angles of the glider.
- Block 5: Linear quadratic regulator (LQR), is simply a gain that is multiplied by the state space variables and then fed into a closed-loop.
- Block 6: Depicted as plant block which represents the planner model of the USFG to capture the dynamics.

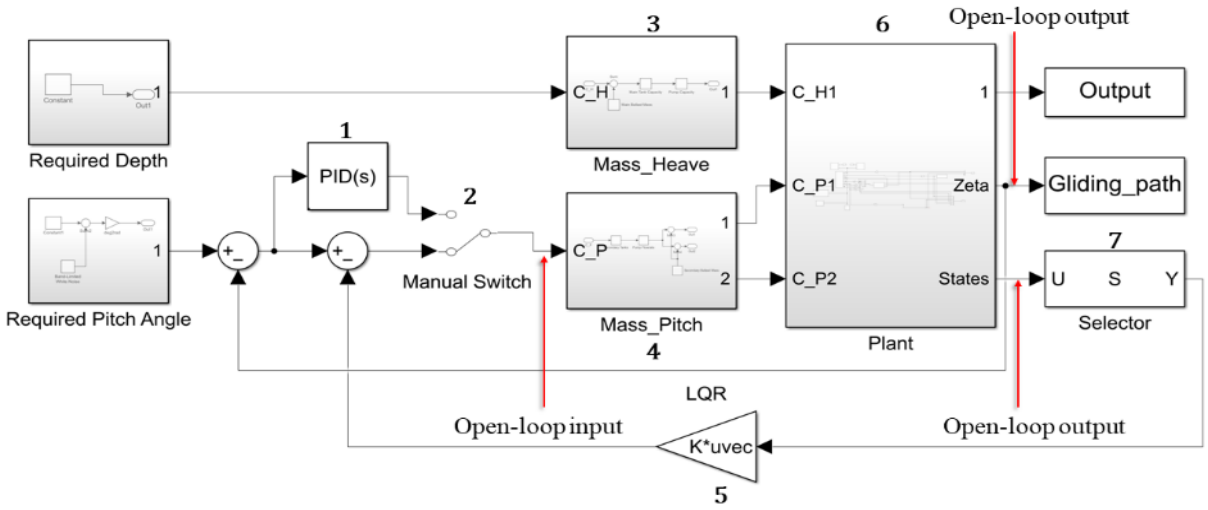

Figure 6: SIMULINK MATHEMATICAL MODEL

- Block 7: The selector block takes the states of the system and orders them in a specific vector format to be processed further. Subsequently, these states are multiplied by the K matrix to form an LQR type control.

4.2 PID

Proportional-integral-derivative (PID) controller is the most opted controller when it comes to marine vehicle applications. Slocum also utilizes such a type of control to switch the position of moving mass onboard [15].

The purpose of the PID is to control the pitching motion of the USFG in a closed feedback loop to form a single input single output (SISO) system. The glide path angle (ξ) acts as the feedback, that is the motion along the pitch direction is controlled by the glide angle. To illustrate, if P(s) represents the transfer function of a specific control loop so $P_c(s)$ in Equation (12) gives the PID controller.

$$P_c(s) = K_p\left(1 + \frac{1}{T_i s} + T_d s\right) \qquad (12)$$

$$p(t) = K_p\, e(t) + K_i \int_{to}^{t} e(\tau)d\tau + K_d \dot{e} \qquad (13)$$

K_p, T_i and T_d are termed as proportional gain, integrator, and derivative time correspondingly. To enhance the PID performance these constraints should be tuned for the system to improve the overall performance. Equation (13) represents $P_c(s)$ in the time domain. As for Equation (13), integral gain ($K_i = K_p/T_i$) and derivative gain which is represented by $K_d = K_p T_d$ and e(t) is the error signal which shows the difference between the desired and output values. The implementation of the PID controller can be seen in FIGURE 6.

4.3 PID CONTROLLER TUNNING

To tune the gains of PID a system should be analyzed linearly. The said feature PID tuner in MATLAB is used for this work. The tuner app distinctly utilizes the transfer function of the given control loop to tune the system at a given operating point, i.e., V = 1 m/s and zeta = 38 °. The block or corresponding output is obtained by varying the bandwidth (a measure of how quickly the system responses to fluctuations in the input conditions) and phase margin (value of phase disturbance that induces the control system to be somewhat stable). By changing the phase margin and bandwidth the corresponding PID gains can be obtained from the tuner app. This also changes some vital characteristics of the system like rise-time, settling-time, and percentage overshoot.

The characteristic phase margin bandwidth along with gains for both tunning cases are mentioned in TABLE 3.

TABLE 3: TUNNING GAINS FOR PID

Gains	**Case-A-1**	**Case-B-1**
P	329	2035
I	3	12
D	8359	76742
N	23	115
Bandwidth (rad/s)	0.2	1.0
Phase Margin (deg)	60	90

4.4 LQR

The Linear quadratic regulator or formally known as LQR is a well-established and tested technique to stabilize the closed-loop performance of the system. It does by generating controller gains that provide optimal performance to the designed system. LQR has been a popular choice when it comes to underwater vehicles. It has been utilized for depth-control of autonomous vehicles by Burlacu et al. [16] along with steering control by Seol et al. [17].

LQR or full-state feedback method is used for the analysis in which the USFG is linearized around an operating point for a downward glide of 38 º while achieving a velocity of 1m/s. The controller is designed based on $\boldsymbol{A}$ and $\boldsymbol{B}$ or linearized system matrices obtained from Section 3. This method involves a conventional control design technique that reduces a cost function formed based on an alleviated control law. This function is dependent on the subjective sum of the square of the variables that are input into the system along with states. The function is given by Equation (14).

$$N = \int_0^{\infty} \delta x^T Q \delta x + \delta u^T R \delta u \, dt \qquad (14)$$

$\boldsymbol{Q}$ and $\boldsymbol{R}$ are termed state and control cost penalty matrices. To prevent large variations in the ballast mass which would surpass the physical restrictions of the USFG reasonable values for $\boldsymbol{Q}$ and $\boldsymbol{R}$ were chosen. This also makes sure that the dynamics of the USFG are well-behaved. The states linked to the glider's velocity, acceleration, and pitching angles are weighted

significantly for the system. By doing this the expected or required values of the state, which also cater for the maxima's, are also considered.

The equivalent control law implemented for the system is $\boldsymbol{u = -K\delta x}$, here MATLAB is employed to calculate the gain matrix K as depicted in FIGURE 6. Moreover, weights of $\boldsymbol{Q}$ and $\boldsymbol{R}$ along with sensitivity study of the LQR are done in the succeeding section.

4.5 LQR TUNNING

The linear quadratic regulator is tuned based on the state-space matrices $\boldsymbol{A}$ and $\boldsymbol{B}$. The glider is tuned by adjusting the weights of $\boldsymbol{Q}$ and $\boldsymbol{R}$ matrices. This is an iterative process and does not follow any hard and fast rules or any strict technique. To tune the weights, a complete understanding of the system dynamics is a must. Response time should be observed as compared to the desired performance of the system, which allows the designer to fine-tune the weights consequently.

Moreover, Bryson's method is used here to adjust the weights of the USFG plant. By implementing this technique, $\boldsymbol{Q}$ and $\boldsymbol{R}$ matrices can be tuned manually according to the desired response. The weights of the $\boldsymbol{Q}$ matrix govern the tolerable error in the two output states and the $\boldsymbol{R}$ matrix regulates the control effort. USFG's dynamics are given by equation (15). The weights are expressed in TABLE 4.

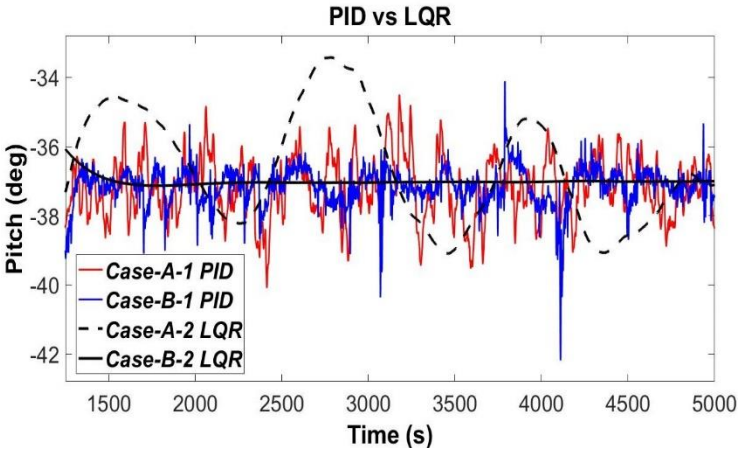

Figure 7: PITCH REPONSE PID vs LQR

$$\begin{bmatrix} \dot{\theta} \\ \ddot{x} \\ \ddot{y} \\ \ddot{\theta} \end{bmatrix} = [A] \times \begin{bmatrix} \theta \\ \dot{x} \\ \dot{y} \\ \dot{\theta} \end{bmatrix} \qquad (15)$$

TABLE 4: WEIGHTS OF STATE AND CONTROL COST

Gains	Q	R
Case-A-2	diag (0,0,0,10^2)	diag (1)
Case-B-2	diag (0,0,0, 10^3)	diag (0.01)

It must be noted that the authors have prioritized control cost over state cost. For the case of USFG, which is designed to follow a particular pitch angle (38 º) the cost concerning the pitch acceleration is penalized heavily, i.e., 10^3. This is done to minimize the state-space error and the oscillations in the output response. The effects of tunning are discussed in the following section which will consider the response and settling time while accessing the final weights.

5. RESULTS AND DISCUSSION

This chapter summarizes the key aspects from the tunning of PID and LQR controller highlighted earlier (Ref. to Section 4). FIGURE 7 represents the comparison of response between using PID and LQR (Ref. TABLE 3 and 4) performed for the

objective M03, which requires the USFG to pitch at an angle of -38 º with minimal actuator effort.

5.1 PID CASES

The PID tuner reports that the percentage overshoot decreases from 42 % to 13.5 % when going from *Case-A-1 PID* to *Case-B-1 PID*. This can also be observed in FIGURE 7 which highlights the larger peak for the latter case. This also affects the settling time for the response drastically by increasing from 15.4 seconds to 163 seconds for *Case-B-1 PID* and *Case-A-1 PID* respectively as reported by the PID tuner.

Increased peak or percentage overshoot can have a negative effect on the gliding dynamics. As the aim is to conserve power on-board while gliding for a longer duration of time. So, it is not efficient to spend extensive actuator effort or power to stabilize the system to the required value.

Case-B-1 PID is tuned with aggressive gains which cause the system to fluctuate. These aggressive gains do not improve or add value to the system's performance, which is not true for most cases. So, *Case-A-1 PID* is preferred over the other as the system performs better with these gains with less overshoot and fluctuations in the required pitch value.

Excessive oscillations can be observed for the tuned cases of PID, which is responsible for higher settling times. For an ideal case the percentage overshoot, rise, and settling time should be minimized for well-behaved system dynamics.

5.2 LQR CASES

Tunning of LQR is different as compared to the PID, as for LQR we set the system performance by penalizing the control loop accordingly.

For *Case-A-2 LQR* the $\boldsymbol{R}$ matrix is penalized heavily whereas, the pitch as highlighted by Equation (15) is not. These state and control cost values induce fluctuations into the system, consequently, this increases the settling time to the desired value. Rise time is minimized as the control cost is penalized to quickly achieve a certain pitch angle; this makes the system robust in following the pilot command. The peak as observed from FIGURE 7 also increases significantly.

The other tunning case, *Case-B-2 LQR*, follows the desired objective smoothly without any excessive oscillations or peaks. This increases the rise time of the signal which is highly influenced by the $\boldsymbol{Q}$ matrix. If control cost is penalized lightly the rise time increases thus increasing the slope of the signal. The gains selected for this case are best amongst the alternatives.

5.3 RISE TIME STUDY

A rise time study as depicted in FIGURE 8 was formulized to see the pitch response for all tunning cases. Initially, the USFG is allowed to settle at a pitch angle of 38 º, the pilot then commands it to pitch at 35 º and then finally to its mean pitch position. PID as previously established is quick to respond to changes, but the output is noisy and contains oscillations, which is not ideal in this case. As for LQR, the rise time is increased as compared to PID from 250 s to around 800 s. This increase in rising time is acceptable, as the objective is to design a robust and stable controller which can pitch the USFG to the desired angle without inducing any oscillations.

Moreover, penalizing θ heavily introduces significant damping in the system. This tunes the controller aggressively which doesn't permit the USFG to obtain the desired pitch angle.

6. CONCLUSION

A comprehensive study has been presented comparing two types of popular controllers used in marine applications, PID and LQR. This analysis results in favor of LQR for the control of USFG rather than PID. LQR was chosen to owe to its simplified tuning method and reduced fluctuations in the output it, also takes less computational power to converge to results. For PID, excessive tunning is required, and even for highly aggressive gains, it fails to mitigate noise or oscillations effectively. Finally, this analysis is equally effective for various sizes and configurations of the USFG.

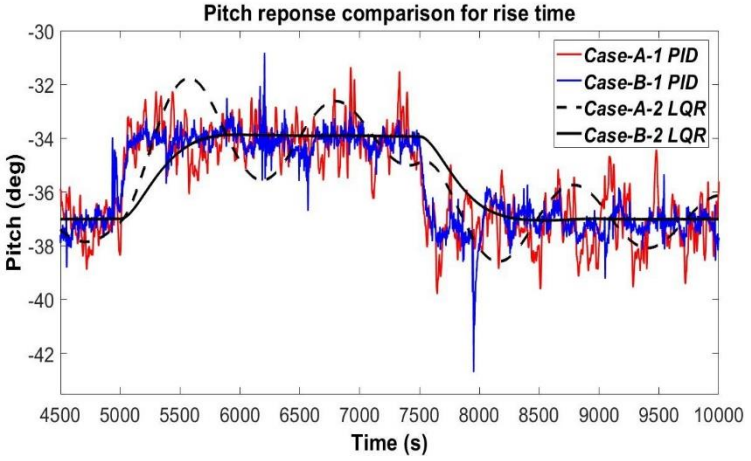

Figure 8: RISE TIME FOR TUNNING CASES

REFERENCES

[1] Xing Y., A conceptual large autonomous subsea freight-glider for liquid CO2 transportation, Proceedings of 40th International Conference on Ocean Offshore Arctic Engineering, Virtual: Jun 21 – 30, 2021.

[2] Xing Y., Santoso T. A. D. and Ma Y. Technical – economic feasibility analysis of Subsea Shuttle Tanker. Journal of Marine Science and Engineering, Sep 2021.

[3] DOF Subsea, Glider AUV, assessed 20.10.2021 from http://www.dofsubsea.com/rov/glider-auv/

[4] AUVAC, AUV System Spec Sheet, assessed 20.10.2021 from https://auvac.org/23-2/.

[5] Ferguson J. S., Cargo Carrying AUVs: Technology and Applications of Autonomous Underwater Vehicles, Taylor and Francis Group, London, 2003.

[6] Equinor, RD 677082 Subsea Shuttle System, 2020.

[7] Xing, Y., Ong, M.C., Hemmingsen, T., Ellingsen, K.E., Reinas, L., 2021. Design considerations of a subsea shuttle tanker system for liquid carbon dioxide transportation. Journal of Offshore Mechanical and Arctic Engineering, 143 (4), 045001, https://doi.org/10.1115/1.4048926.

[8] Ma, Y., Xing, Y., Ong, M.C. et al. (2021) Baseline design of a subsea shuttle tanker system for liquid carbon dioxide transportation. Ocean Engineering, 240, 109891, https://doi.org/10.1016/j.oceaneng.2021.109891.

[9] Reducing greenhouse gas emissions from ships International Maritime Organisation, assessed 21.10.2021 from https://www.imo.org/en/MediaCentre/HotTopics/Pages/Reducing-greenhouse-gas-emissions-from-ships.aspx.

[10] Ahmad U. N. and Xing Y., A 2D model for the study of equilibrium glide paths of UiS Subsea Freight-Glider, COTech conference, Stavanger, Norway, 2021.
[11] Linearize Simulink model using model, https://se.mathworks.com/help/slcontrol/ug/linearize-simulink-model.html, assessed 5th Oct 2021.
[12] D. Webb and C. Jones. Personal communication, 2001-2004.
[13] J. Sherman, R. E. Davis, W. B. Owens, and J. Valdes. The autonomous underwater glider 'Spray'. IEEE Journal of Oceanic Engineering, Special Issue on Autonomous Ocean Sampling Networks, 26(4), Oct 2001.
[14] Graver, J.G., Underwater Gliders: Dynamics, Control and Design, Ph.D. Thesis, Princeton University, 2005.
[15] Webb D. C., Simonetti P. J., and Jones C. P., SLOCUM: an underwater glider propelled by environmental energy, IEEE Journal of Oceanic Engineering 26(4), 447-452, 2001.
[16] Burlacu P., Dobref V., Badara, N., and Tarabuta O., "A LQR controller for an AUV depth control", Annals of DAAAM & Proceedings, 2007, accessed on 02.11.2021 from https://link.gale.com/apps/doc/A177174526/AONE?u=anon~ea514c0a&sid=googleScholar&xid=037efc6c.
[17] Seol B. S., Dong H., Soon T. K., and Moon G. J., "An LQR Controller for Autonomous Underwater Vehicle". Journal of Institute of Control, Robotics, and Systems, 2014.

UiS Subsea-Freight Glider: A Large Buoyancy-Driven Autonomous Cargo Glider

Usman Nawaz Ahmad
University of Stavanger
Stavanger, Norway

Yihan Xing[1]
University of Stavanger
Stavanger, Norway

Yucong Ma
University of Stavanger
Stavanger, Norway

ABSTRACT

This work presents the baseline design for the autonomous subsea vehicle capable of travelling at a lower speed of 1 m/s with an operating range of 400 km. Owing to UiS subsea-freight glider's (USFG) exceedingly economical and unique propulsion system, it can transport various types of cargo over variable distances. The primary use-case scenario for the USFG is to serve as an autonomous transport vessel to carry CO_2 from land-based facilities to subsea injection sites. This allows the USFG to serve as a substitute for weather-dependent cargo tankers and underwater pipelines. The length of the USFG is 5.50 m along with a beam of 50.25 m, which allows the vessel to carry 518 m^3 of CO_2 while serving the storage needs of the carbon capture and storage (CCS) ventures on the Norwegian continental shelf. The USFG is powered by battery cells, and it only consumes a little less than 8 kW of electrical power.

[1] Corresponding author: yihan.xing@uis.no

Along with the mechanical design of the USFG, the control design is also presented in the final part of the paper. The manoeuvring model of the USFG is presented along with two operational case studies. For this purpose, an LQR and PID-based control system is designed, and a detailed comparison study is also shown in terms of tuning and response characteristics for both controllers.

1 INTRODUCTION AND FRAMEWORK

Pipelines transport most of the oil and gas produced from the offshore platforms to the land-based facilities [1]. Subsea pipe laying technology is well-known and has improved significantly since it was first installed and used during World War II by the United Kingdom [2]. Economic and technical problems induce various limitations on this transportation technology. The primary disadvantage is the installation costs. As for remote fields, these costs can be exceptionally high as they intensify with the increased length of the pipeline. Apart from that, deep-water activities such as pipeline inspection are quite costly and challenging. From a financial outlook, pipeline maintenance entails a complete or fractional shutdown, which is not feasible for marginal oil and gas fields. Tanker ships, specifically shuttle tankers, are frequently utilized [3]. A subsea pipeline is an attractive solution for large offshore fields with higher revenue due to the reduced number of step-outs in the operations [4]. Using shuttle tankers provides enhanced flexibility in various situations, i.e., increased demand, as it can swiftly be deployed to the desired location. As for accidents or any unforeseen events, it is advantageous to use tankers instead of conventional pipelines, as an auxiliary ship can be sent quickly. Though, large tanker operations are weather restricted and dependent. Dynamic loads highly influence them in harsh

weather situations from the environment, such as wind and wave loads. To tackle these potential problems, UiS subsea-freight glider (USFG) (illustrated in Fig 1) was introduced, which is a 531-deadweight tonnage (DWT) underwater glider [5] combining the economy and feasibility of the tanker ships along with the underwater capability of submarines. It also serves as an effective alternative to existing technologies for CO_2 transportation. Moreover, it is expected that the cost per ton of transporting CO_2 is comparable to that of the subsea shuttle tanker (SST) as considered by Xing et al. [6].

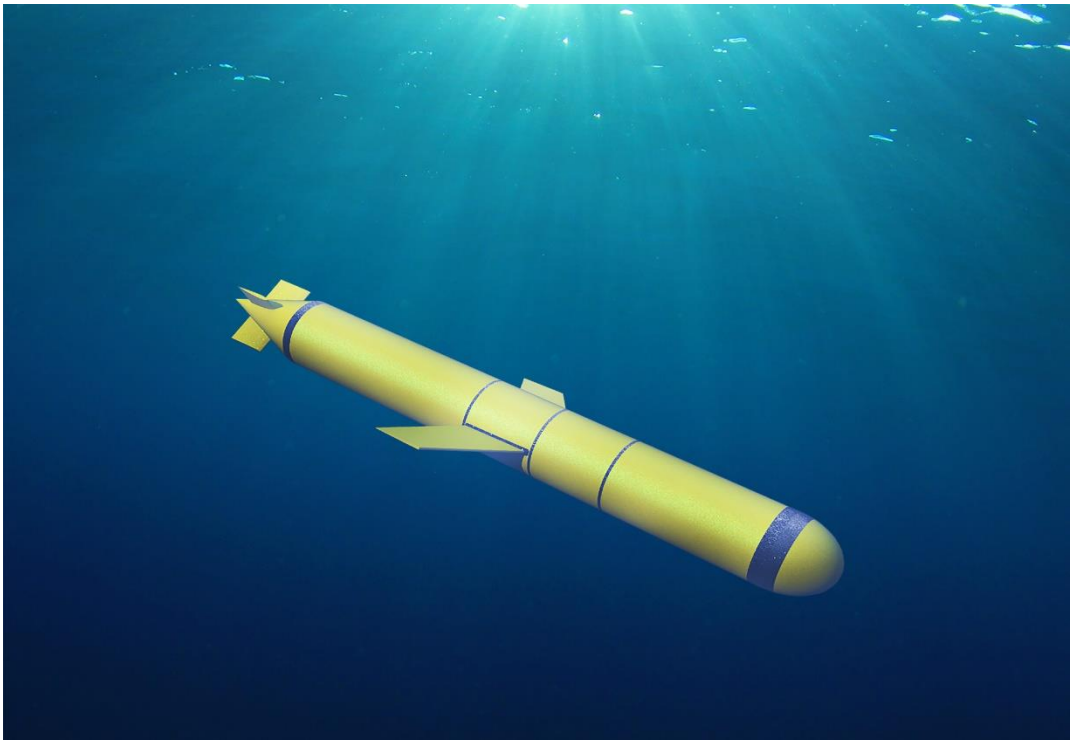

Fig 1 Illustration of UiS subsea-freight glider.

1.1 Earlier Studies in Autonomous and Underwater Cargo Vessels

In 1989, Henry Stommel [7] presented his work on an autonomous observation system intended to collect ocean data. It consisted of "1000 neutrally buoyant floats formally called

Slocums" they moved through the ocean by varying their ballast and steered with hydrodynamic wings. It was originally named Slocum after Joshua Slocum, the first sailor to sail around the world by himself. The initial concept, as proposed by Stommel, has come a long way from small-scale observation floats to Autonomous Underwater Vehicles (AUVs) such as Manta Ray AUV [8] and Glider AUV [9] from Skandi explorer gliders. However, these AUVs have not been utilized for transporting cargo as they are limited by size and loading capacity. Primary cases of underwater vessels with cargo-carrying capabilities date to the 1970s, where Taylor et al. [10] and Jacobsen [11] presented submarines capable of carrying 20,000 to 420,000 DWT of crude oil in the Arctic region. After that, Jacobsen et al. [12] presented in the year 1983 two enormous submarine tankers with the ability to transport 727,400 and 660,000 DWT of Liquefied Natural Gas (LNG). As a result of the Spinnaker program in the 1990s [13], LSE Ltd. developed the Theseus to carry 660 kg of cable to a distance of 900 km. Recently Equinor [14][15], proposed an autonomous freight-carrying tanker to transport hydrocarbon along with the necessary tools required for subsea operations and CO_2. Moreover, Ellingsen et al. [15] also proposed a large underwater glider that serves as an efficient method to transport cargo. Reposed to the previous work, Xing [5] presented to utilize an ultra-efficient freight-carrying glider to transport CO_2 while consuming an average power of 10 kW. The abovementioned research by Ellingsen et al. and Xing were concept proposals and did not divulge any technical details. This work will cover the critical considerations relating to the baseline design of the USFG followed by well-defined design specifications, which will remove all the knowledge barriers as previously defined. The authors will extend upon the work presented by Xing [16] and Ma et al. [17].

1.2 The UiS Subsea-Freight Glider (USFG)

The USFG is a novel and unique concept owing to its state-of-the-art propulsion system, which varies buoyancy to generate thrust with large hydrodynamic wings instead of using conventional propulsion methods, which consumes significantly more power. Table 1 presents the critical design parameters of the glider. The path taken by the glider is represented in Figure 2, which is formally known as the equilibrium gliding path, the sawtooth pattern [18].

Table 1. Characteristics of USFG.

Parameter	Value	Unit
Net transport economy	< 0.5	-
Pumping time / cycle	< 5% of half cycle	-
Structural weight	419	ton
Vessel length	50.25	m
Volumetric drag coefficient	0.1	-
Wing area	5	m^2
Horizontal speed	1	m/s
Glide path angle	38	°
Average Power	< 8	kW
Ballast fraction	0.15	%

Ballast pump capacity	2000	m^3/h
Deadweight ton	531	ton
Diving depth	200	m

The USFG sails by utilizing its ballast tanks. This process is illustrated in Figure 2. Initially, the ballast water is pumped out of the tanks. This produces a negative pitch angle (bow heading up) and a positive net buoyancy. As a result, the glider becomes lightweight, consequently producing positive buoyancy. The glider, therefore, ascents with an angle of attack. As a result, the relative velocity between the glider and seawater generates a lift force pointing forward and propels the USFG to move towards its desired direction. Similarly, the vessel's weight can be increased by pumping in ballast, generating negative buoyancy and positive pitch angle, which permits the glider to return to its initial depth while moving ahead. Propulsion is generated by the hydrodynamic wings, which give rise to lift and drag forces while the glider cycles in this to-and-fro pattern while also moving forward. This process is repeated through the entire mission of the USFG, and it minimizes the energy usage onboard as the pumps only require power to regulate water amongst the tanks.

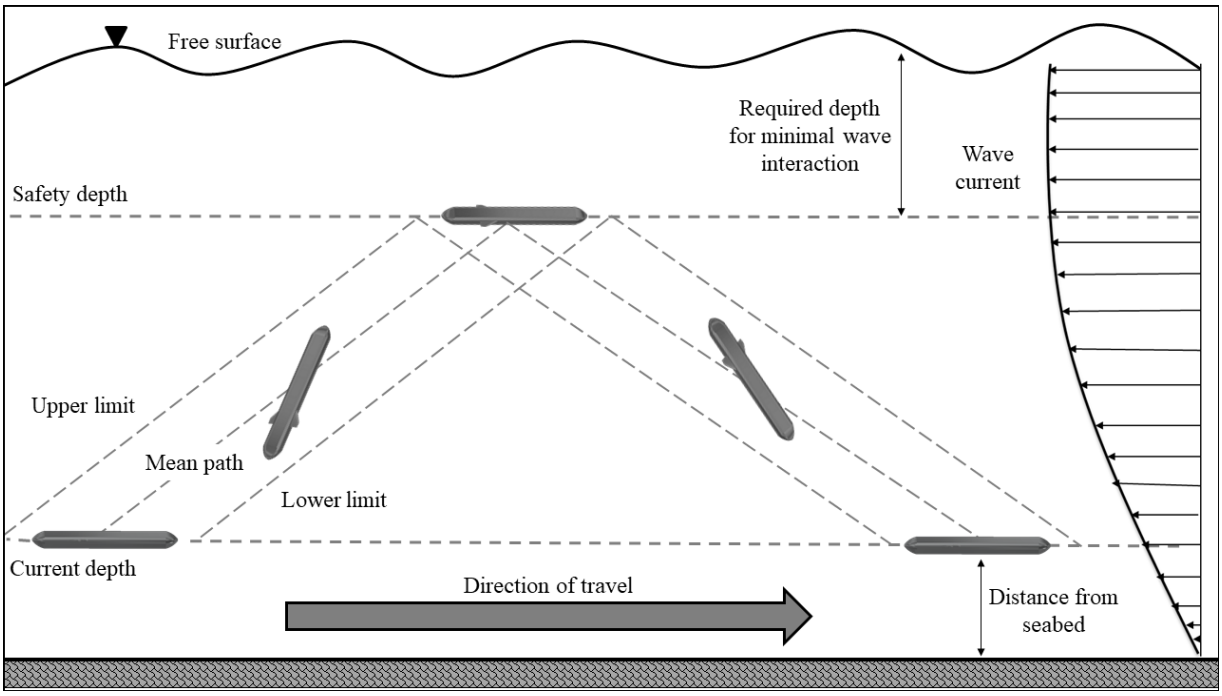

Figure 2 Equilibrium glide paths.

Generally, underwater gliders manoeuvre in the water by regulating the net buoyancy via changing the ballast volume. At the same time, the roll and the pitch motion of the vessel are controlled by employing a mass actuator. This mechanism is not feasible for large cargo-carrying gliders, as increased size and freight tonnage demand a mammoth actuating and hydraulic network. For the glider dynamics, a swift but robust response system is required to cater to any changes in the operating conditions. The USFG controls the roll and pitch motion with its ailerons combined with varying ballast mass of the tanks to obtain desirable response times, as demonstrated in Figure 3.

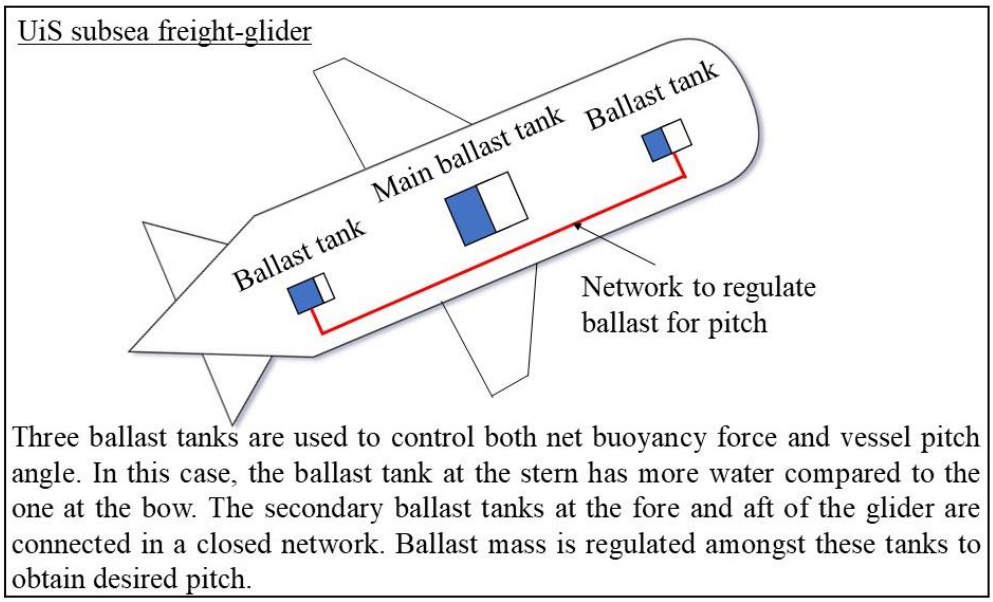

Figure 3 Ballasting system for USFG – top view of the glider.

Two individual proportional-integral-derivative (PID) controllers manage the ballast system on the USFG for pitch and heave motion. A large ballast tank indicated as the main ballast tank in Figure 3 allows the glider to move in the heave direction by controlling the ballast water with a pump onboard. The two secondary ballast tanks located at the fore and aft of the vessel control the pitch angle of the vessel as they are connected in a closed network.

1.3 Use-case Scenario

Figure 4 represents the role of the USFG in the supply chain operations for marine carbon capture and storage (CCS). The USFG is designed to transport CO2 from land or offshore-based facilities to be injected directly into the seabed using subsea wells. It does so while

carrying out the entire mission autonomously. As the USFG can operate in any climate conditions: it does not restrict its operations in extreme sea states.

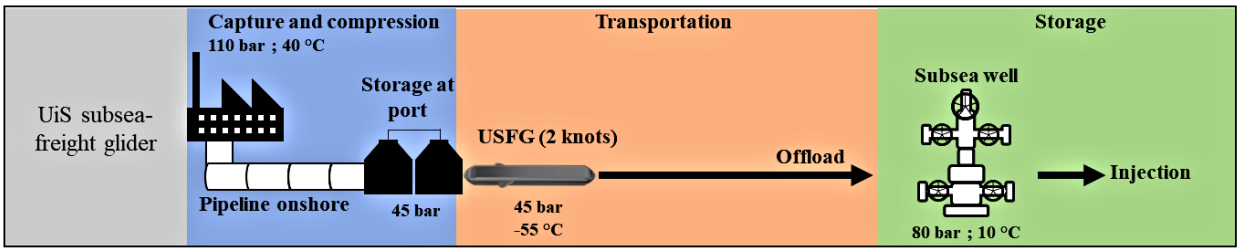

Figure 4 Marine CCS process utilizing USFG.

The baseline design for the glider is planned to be employed in the Norwegian sea CCS projects, Utgard, Snøhvit, and Sleipner offshore fields [19]. These projects involve capturing the CO_2 generated by the oil and gas exploration and production activities while injecting it into the petroleum reservoir. The location of these projects is illustrated in Figure 5. Together with these ventures, Equinor [20] aims to start the Northern Lights Project by 2024, which aims to transport CO_2 generated from land-based industrial activities to be injected into the Utsira formation on the Troll field. The initial design target for the USFG is to be technically feasible for these CCS ventures. Nevertheless, it can easily be configured to be utilized anywhere in various conditions around the globe. Although the study in this work targets CO_2 as the primary cargo but due to its diverse applications, the USFG can also be employed to carry various subsea tools, hydrocarbons, and electricity (by stand-alone battery cells).

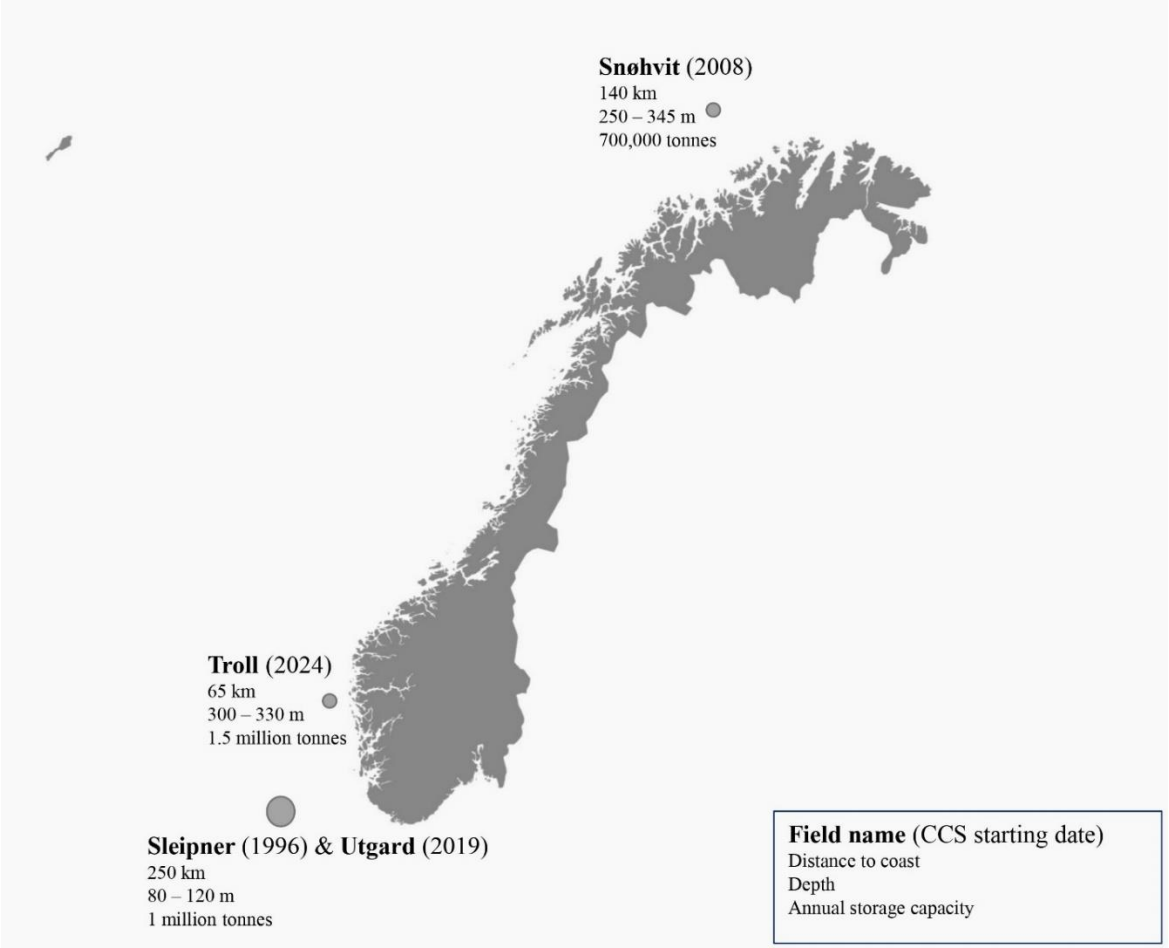

Figure 5 Norwegian sector storage sites for the CCS projects [19],[20].

The USFG can play a vital role in alleviating global warming in several ways. Due to increasing energy demand, the concentration of CO2 in the air is projected to increase two folds by the year 2100 in contrast to the level in 1960 [21]. The CO_2 emissions for transportation activities are zero as the vessel is powered by a battery instead of conventional power sources. This enhances the sustainability value of the shipping industry as it accounts for nearly 3.3% of the hydrocarbon-based CO_2 emissions [22]. Moreover, the vast amount of CO_2 produced from industrial activities worldwide can be captured and stored. This permits the USFG to utilize

small-scale subsea fields as permanent sites for the storage of CO_2, consequently meeting the future requirements of CCS by creating more storage sites [23].

2 BASELINE DESIGN OF THE USFG

The baseline design of USFG is a 531-DWT autonomous glider spanning over a length of 50.25 m with a beam of 5.50 m capable of transporting 518 m^3 of CO_2. It does so while gliding at a 1 m/s (2 knots) with an extended range of 216 nautical miles (400 km).

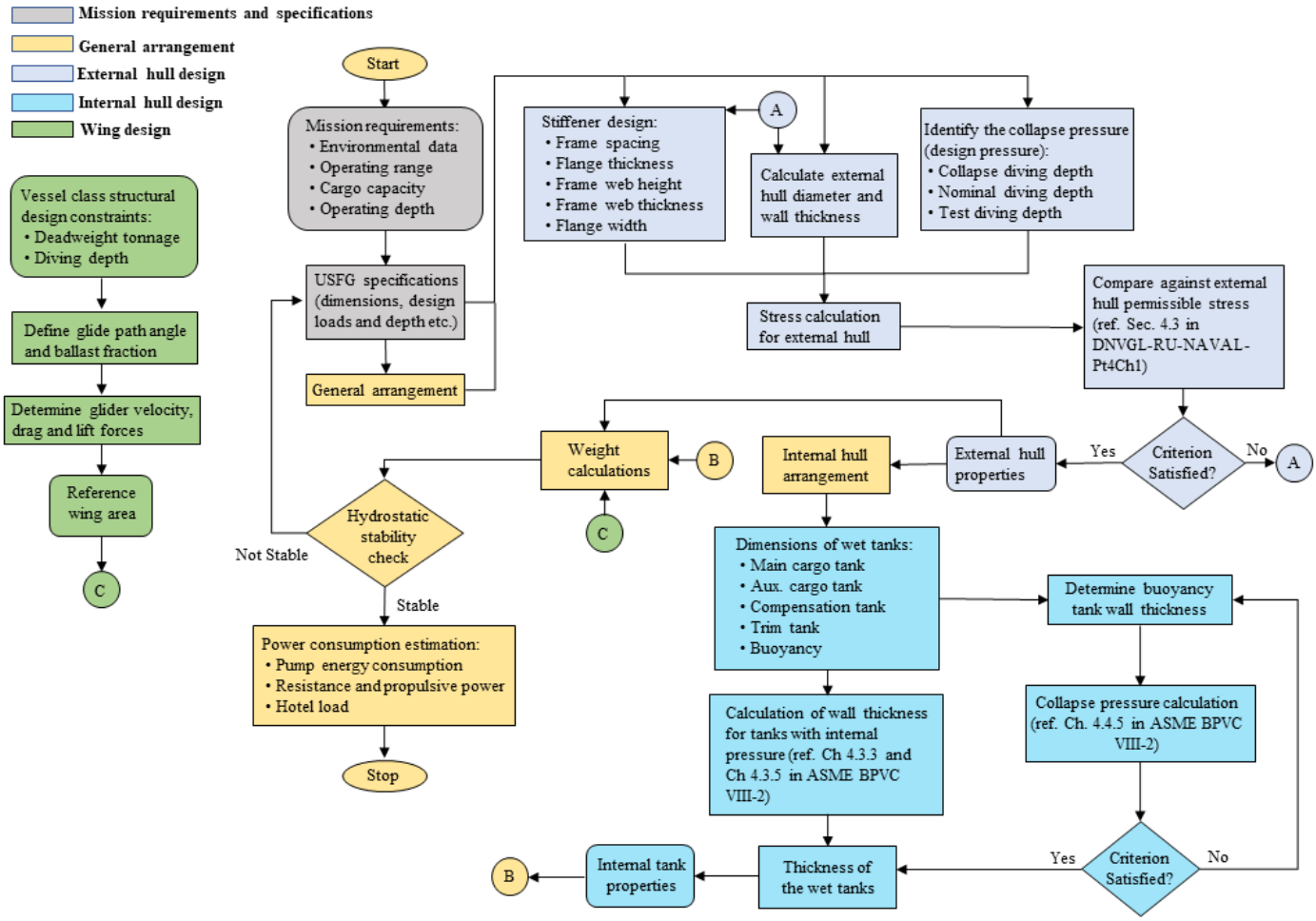

Figure 6 Design flow for USFG baseline design.

This analysis presents the baseline design of the USFG to study this innovative concept and establish its technical and operational limits (if they exist). The mechanical design procedure is highlighted in Figure 6.

As specified by each mission, the assignment requirements serve as an input to the design loop followed by the glider specifications (Section 2.2). It involves the environmental conditions/data, operating range, cargo capacity, and operating depth. Consequently, the USFG specifications are defined: probable load effects, required range, CO_2 cargo properties, and required speed. The general system gives the location and arrangement of all the components of the USFG (Section 2.3). Based on the arrangement and specifications of the USFG, the interior and exterior structural calculations are carried out (Section 2.4). The mechanical design calculations are based on the American Society of Mechanical Engineers Boilers and Pressure Vessel Code (ASME BPVC) VIII-2 [24] and DNV-RU-NAVAL-Pt4CH1 [25], which are the pioneering industrial codes and standards, respectively. The reference area for the wings (Section 2.6) is calculated by the method introduced in Xing et al. [5]. Furthermore, the stability criterion (Section 2.8) is also checked against the hydrostatic properties obtained from the preceding sections. The design loop is an iterative process meaning the dimensions of the glider are adjusted until the stability criterion is not satisfied. Finally, after the final design has been obtained, the amount of power consumed can be obtained (Section 2.9). The extensive details of the design process are in Ma et al. [17].

The aim is to transport a payload that is 50% of the displacement, and it is done by utilizing an Active-Pressure Compensating System (APCS) and a double hull design for the USFG. By employing an APCS, the external loads from the pressure on the external hull can be restricted.

By doing this, the external hull design can be less conservative: as it is not designed to sustain the complete hydrostatic pressure due to the operating water depth. Xing et al. [16] and Ma et al. [17] described this system in more detail. The 50% target is maintained, making the glider economically feasible.

2.1 Mission requirements and USFG Specifications

The mission requirements and the specifications of USFG set the basis for the entire design process. The baseline parameters for the design of USFG are given in Table I.

Table I Design parameters of USFG.

Characteristics	**Value**	**Unit**
Functional depth	200	[m]
Determined range	400	[km]
Operating speed	2	[knots]
Cargo pressure	35 - 55	[bar]
Freight temperature	0 - 20	[°C]
Current velocity	1	[m/s]
Collapse depth	400	[m]

The USFG is designed to carry 531-tons of CO_2 with each trip. It can easily be scaled up to meet the increasing demands of the CCS markets worldwide. Instead of employing a large vessel to carry a huge amount of CO_2 daily, several USFGs can be deployed at the same time

to carry the same amount of payload. This can also be a cost-effective solution as the operations and maintenance costs for smaller vessels are substantial compared to large ones.

The operating temperature for the baseline USFG ranges from 0 to 20 °C, which is the range for aquatic ambient temperature. For reference, the temperature in the Norwegian sector (0–10° E, 60–70° N) varies between 2 °C and 12 °C [26]. The design speed for the current is set at 1 m/s; this allows the authors to represent maximum-average current speeds for the Norwegian coast and the North Atlantic region. At the same time, the seasonal normal current speed in the North Sea is observed around 0.2 m/s [27],[28],[29].

To prevent impact from any floating structures or ships on the water's surface, a safety depth of 40 m is defined, which is also illustrated in Figure *2*. This can also minimize the dynamic loads on the USFG from the waves, hence rendering it weather independent. The nominal diving depth is defined based on the retrievable depth from any situations that yield control loss. USFG has a nominal depth of 200 m while transporting CO_2. Thus, the operating depth range of the USFG is between 40 to 200 m. The test diving and collapse depths are 250 m and 400 m, respectively, which are 1.25 and 2.00 times the operating depth and in agreement with Table 1 in DNV-RU-NAVAL-Pt4CH1 [25]. The CCS sites' depth descriptions considered in this work, along with the depths of USFG, are illustrated in Figure 7.

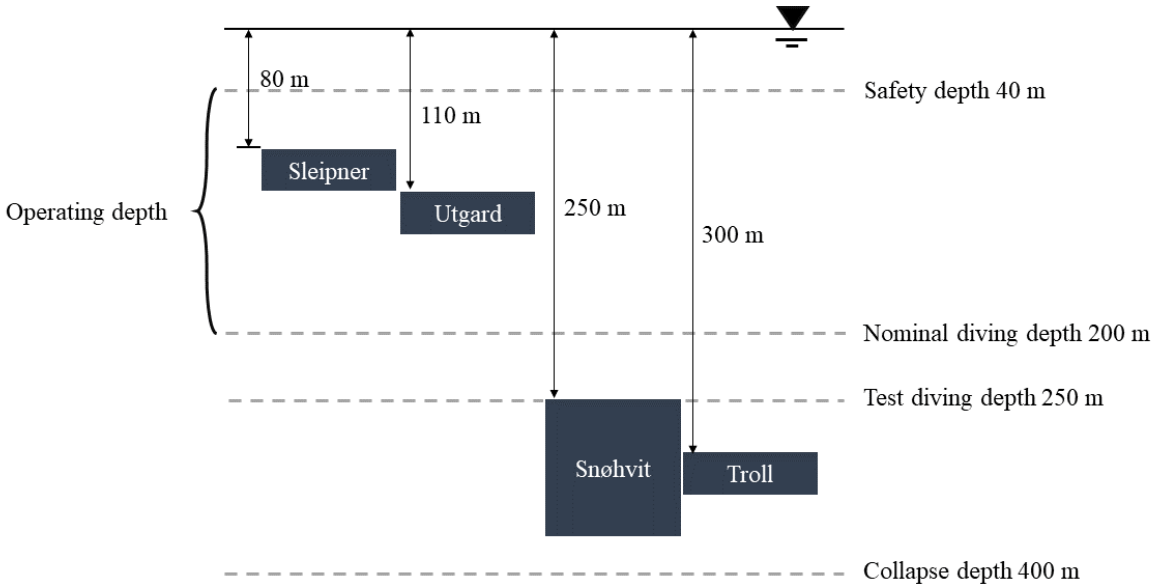

Figure 7 CCS sites depth with USFG depth definitions.

The range of USFG, which is 400 km, is designed such that it can complete a one-sided trip to Utgard and Sleipner storage sites. Moreover, a two-way trip can also be accomplished for Troll and Snøhvit fields. For the former case, the USFG can be docked and charged at offshore Utsira High facilities (Gina Krog, Ivar Aasen, and the Edvard Grieg fields) which are powered from the onshore grid with the help of Johan Sverdrup field.

2.2 General Arrangement of the USFG

As shown in Figure 8, the general arrangement drawing depicts the internal tanks and compartments of the external hull.

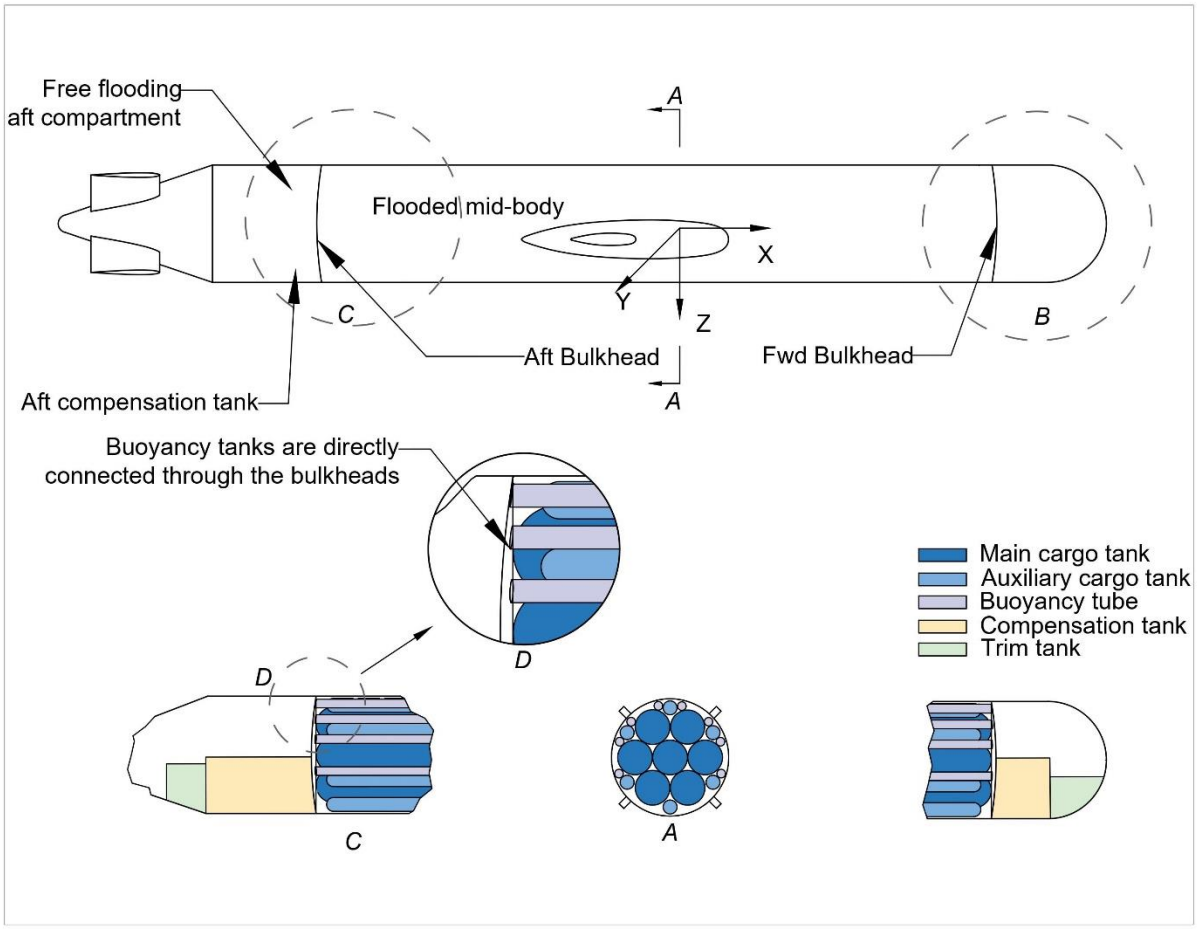

Figure 8 USFG's general arrangement.

To achieve low drag resistance, a torpedo-shaped geometry is employed for the external hull of the USFG. It consists of a cylindrical mid-body, a conical-shaped aft, and a hemispherical designed bow. The aft and the bow sections of the USFG weigh about 23% of the total steel weight, which is used to manufacture the external hull in the baseline USFG. A dual-hull/shell design is employed for the cylindrically formed mid-body to circumvent the design for collapse failure under pressure. The mid-body external hull is free from differential loading, i.e., hydrostatic pressure. The four bulkheads on the USFG are utilized to reinforce the

pressure hulls (buoyancy tubes and cargo tanks) and isolate the free-flooded compartment from the mid-body, the flooded section. The buoyancy tubes and the cargo tanks, as illustrated in Figure 8, are the small-scale pressure hulls capable of withstanding collapse and burst pressures.

The external shell or hull of the USFG comprises three different sections: (a) a flooded mid-body in the centre of the vessel which holds piping, buoyancy, and cargo tanks, and it is the largest compartment on the vessel by capacity; (b) a free flooded compartment located at the stern, which encompasses all the equipment that are susceptible to moisture including, rudder controls, gearbox, battery, aft compensation and trim tanks, and motor; (c) a free flooding compartment at the fore which incorporates, the control station, pumps for unloading CO_2, sonar, sensors, fore trim tank, radio, and fore compensation tank. Pressure vessels are an integral part of the USFG, and there are five different kinds of internal pressure vessels onboard, buoyancy tubes, trim tank, main cargo tank, compensation tank, and auxiliary cargo tank.

- *Buoyancy tubes:* To make the USFG neutrally buoyant, eight vacant buoyancy tubes are utilized, which are supported by the bulkheads and have the same span as the main cargo tanks. They are placed at the upper section of the USFG. They are designed to bear collapse pressure.
- *Trim tanks:* There are two trim tanks onboard the USFG, one at the cone in the stern and the other in the fore hemisphere. These tanks aid in achieving a neutral equilibrium position along the length direction. This is done by adjusting the

centre-of-gravity (COG) of the vessel directly below the centre-of-buoyancy (COB). Both trim tanks are connected in a closed-loop to regulate the water. Since the tanks are in a flooded mid-body section, they are designed to handle the internal hydrostatic pressure. As a result, they are free from external hydrostatic pressure.

- *Main and supplementary cargo tank:* The USFG has 13 cargo tanks arranged in a rotational symmetry, as shown in Figure *8*, which comprise six auxiliary and seven main cargo tanks. All the cargo tanks have a cylindrical shell and hemispherical heads.
- *Compensation tank:* To provide stability to the USFG, two compensation tanks are used for various hydrostatic loading scenarios. They aim to vary the overall weight of the vessel along with moment (trim) to achieve neutral buoyancy. Compensation tanks along with cargo and trim tanks are designed to withstand burst pressure.

2.3 Structural materials for mechanical design

Materials used in USFG and their graded strength are given in Table 3.

Table 3 USFG's proposed design materials.

Sections	Material	Yield Strength	Tensile Strength
Exterior shell - aft compartment	VL D47	460 MPa	550 MPa
Bulkhead	VL D37	360 MPa	276 MPa

External shell - bow section	VL D47	460 MPa	550 MPa
External shell - mid-body	VL D47	460 MPa	550 MPa
Inner hull - buoyancy tube	SA-738 Grade B	414 MPa	586 MPa
Inner hull - trim tank	SA-738 Grade B	414 MPa	586 MPa
Inner hull - auxiliary cargo tank	SA-738 Grade B	414 MPa	586 MPa
Inner hull - comp. tank	SA-738 Grade B	414 MPa	586 MPa
Internal hull - main cargo tank	SA-738 Grade B	414 MPa	586 MPa

2.4 External shell/hull design

A torpedo-shaped shell is employed for the USFG, having a diameter to length ratio (slenderness ratio) of 1:9.7. This design reduces the manufacturing difficulty of the vessel while optimizing the slenderness of the structure to obtain maximum cargo capacity and reduced drag resistance. The external hull is reinforced by utilizing a stiffener. The properties of the stiffener are highlighted in Table . It must be noted that the stiffeners are used conferring to the calculation procedure in DNV-RU-NAVALPt4Ch1 [25]. Following are the various compartments in the external hull of the USFG.

Table 4 Stiffener properties (external shell).

Elements	**Symbol**	**Units**	**Value**
Inner radius to the flange of the frame	R_f	[mm]	2533
Flange width	b_f	[mm]	80
Frame spacing	L_F	[mm]	1000

Frame cross-sectional area	A_F	[mm^2]	7.35
Flange thickness	s_f	[mm]	30
Frame web height	h_w	[mm]	165
Frame web thickness	s_w	[mm]	30

- The allowable stresses at the collapse, operating, and test diving depths are 415 MPa, 203 MPa, and 418 MPa, respectively.
- Pressure hulls that are designed to withstand hydrostatic pressure are called free flooded compartments. Stresses at various depths (collapse, diving, and test diving) for the compartments are calculated and compared against the allowable stresses in Chapter 4 in DNVGL Rules for Classification for Naval Vessels, Part 4 Sub-surface ships, Section 1 Submarine (DNVGL-RU-NAVAL-Pt4Ch1) [25].
- As stated previously, a similar method is utilized to design a flooded mid-body compartment. Though, this section of the hull does not have to handle the pressure due to the weight of the water on the structure. So, for any accidental or unforeseen load scenarios, namely, vent breakdown, a collapse pressure of 20 bars (200 m) is used to avert instantaneous mechanical or structural failures. Table presents the derived external hull design for USFG. The mid-body accounts for 74 % of the total structural weight, as this section is a substantial part of the baseline USFG design.

Table 5 USFG's external hull properties.

Sections	**Elements**	**Units**	**USFG**
Free-flooding aft section	Material		VL D47
	Thickness	[m]	0.025
	Design collapse pressure	[bar]	40.000
	Steel Weight	[ton]	15.789
	Length	[m]	10.000
Free-flooding bow section	Material		VL D47
	Thickness	[m]	0.025
	Design collapse pressure	[bar]	40.000
	Steel Weight	[ton]	7.658
	Length	[m]	2.500
Flooded mid-body	Material		VL D47
	Thickness	[m]	0.011
	Design collapse pressure	[bar]	20.000
	Steel Weight	[ton]	66.842
	Length	[m]	37.500

2.5 Internal shell/hull design

The internal tanks onboard the USFG are described in this section, and designed per ASME BPVC Chapter 4, Section VIII, Division 2 [24].

- Trim and compensation tanks (free flooded compartments) do not have the requirement to withstand external pressure, making them soft tanks. They are designed to tackle stresses from the hydrostatic pressure (internal pressure) that arises due to the flooded mid-section of the USFG. To obtain a practical sizing parameter for volume and weight, both tanks are assumed to be of cylindrical geometry. The shape of these tanks can be optimized to avail the storage space in the compartment efficiently.
- As for the buoyancy tanks/tubes, the design allows the tubes to endure a 20-bar hydrostatic pressure corresponding to an operating depth of 200 m.
- Cargo tanks that are employed for CO_2 storage are subjected to internal tank pressure and external static pressure from the fluid (water). They have a design burst pressure of 55 bar. This design situation only occurs when the USFG surfaces for routine tasks, such as maintenance, etc. Accordingly, the pressure difference rises to 55 bar because external pressure is 0 bar gauge (barg). An APCS can be utilized to avoid failure due to collapse; extended details can be found in work by Xing et al. [16] and Ma et al. [17].
- Table 6 presents the derived internal tank design for USFG.

Table 6 USFG's internal tank characteristics.

Sections	**Elements**	**Units**	**USFG**
Buoyancy Tube (Total tanks = 8)	Material		SA-738 Grade B
	Total volume	[m^3]	25.574
	Acceptable collapse pressure	[bar]	7.000
	Hemispherical end wall thickness	[m]	0.002
	Length	[m]	28.000
	Thickness	[m]	0.004
	Steel weight	[ton]	1.134
	Diameter	[m]	0.390
Auxiliary Cargo Tank (Total tanks = 6)	Material		SA-738 Grade B
	Total volume	[m^3]	67.160
	Acceptable burst pressure	[bar]	55.000
	Hemispherical end wall thickness	[m]	0.008
	Length	[m]	28.000
	Thickness	[m]	0.004
	Steel weight	[ton]	24.322
	Diameter	[m]	0.735
Trim Tank (Total tanks = 2)	Material		SA-738 Grade B
	Total volume	[m^3]	50.000
	Acceptable burst pressure	[bar]	10.000

	Length	[m]	1.890
	Thickness	[m]	0.002
	Steel weight	[ton]	73.705
	Diameter	[m]	3.500
Compensation Tank (Total No.= 2)	Material		SA-738 Grade B
	Total volume	[m^3]	22.96
	Acceptable burst pressure	[bar]	8.000
	Length	[m]	1.750
	Thickness	[m]	0.002
	Steel weight	[ton]	33.561
	Diameter	[m]	3.750
Main Cargo Tank (Total tanks = 7)	Material		SA-738 Grade B
	Total volume	[m^3]	459.366
	Acceptable burst pressure	[bar]	55.000
	Hemispherical end wall thickness	[m]	0.009
	Length	[m]	28.000
	Thickness	[m]	0.017
	Steel weight	[ton]	119.859
	Diameter	[m]	1.500

2.6 Wing design

The design procedure for the wings is highlighted in Figure 9. Glider parameters are defined in Figure 10, with Fb being the buoyancy force and W being the overall weight of the vessel. The vessel class (cargo carrying capacity) is defined along with the nominal operating depth of the USFG, which serves as the basis for selecting an optimal glide path angle. From the gliding angle, velocities of the USFG can be calculated, which further yields drag and lift forces. Lastly, the hydrofoil's reference area and lift to drag ratio can be decided.

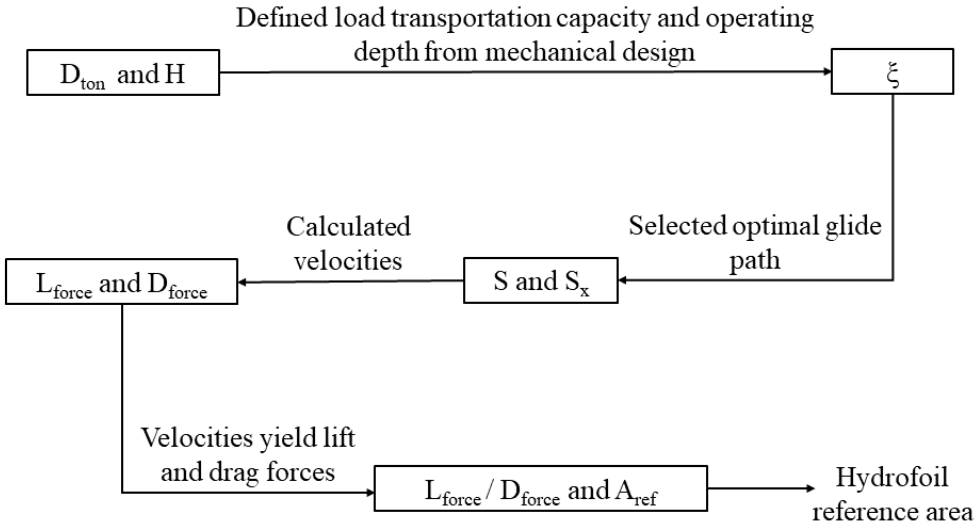

Figure 9 USFG's global parameters.

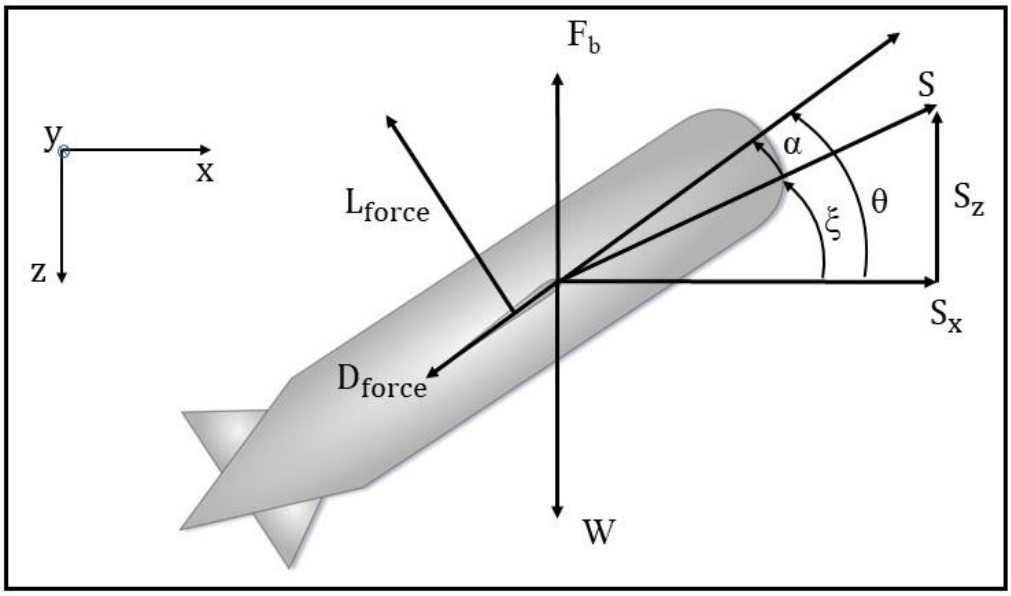

Figure 10 USFG's gliding parameters – side view of the glider.

The hydrofoil reference area comes out to be around 7 m^2 by following this procedure. Detailed calculations and the nomenclature for this section can be found in **Appendix A. Calculation of reference wing area**.

2.7 Weight estimations

After the mechanical design has been finalized (Ref. Section 2.3-2.6), weight calculations for the USFG can be performed. Weight and storage capacity for CO_2-filled scenarios are given in. Subsequent weight definitions are employed to be used in USFG:

- The permanent ballast onboard is 2% of displacement.
- The targeted CO_2 load or payload is 44% of displacement.
- The trim (moment) ballast onboard is 0.5% of displacement.
- The weight of the machinery onboard the vessel is 2% of displacement.

Table 7 USFG's weight configuration (CO_2 charged).

Module	Weight (tons)	
	USFG	
Structure	419	30.42%
Permanent ballast mass	30	2.23%
Freight	612	44.45%
Compensation ballast	51	3.72%
Equipment	30	2.23%
Mid-body seawater	226	16.42%
Trim ballast mass	7	0.52%
Total	**1379**	**100%**

2.8 Hydrostatic stability study

After the weight estimations, criteria for intact stability are checked under DNVGL-RUNAVAL-Pt4Ch1 Section 3.5.2.3. The classification chosen is for submarines with a displacement ranging between 1000-2000 tons [25]. For USFG, the metacentric height (GM) should exceed 0.22 m, and the distance between the centre of gravity (G) and centre of buoyancy (B) must be higher than 0.35 m. This section considers four cases of hydrostatic loading, which are as follows.

1. *Surfaced (SW-filled)*: the USFG is floating on the water's surface, while three out of six auxiliary and five main tanks are filled with heavy seawater/saltwater. All

the remaining tanks aboard the vessel are bare. This scenario is observed at the start and end of the CO_2 transportation cycle when the USFG surfaces to load and unload the cargo, respectively.

2. *Surfaced (CO_2-filled)*: this scenario occurs after the tanks of the USFG are filled with CO_2. At this point, the USFG is ready to dive to the nominal operating depth.
3. *Submerged (CO_2-filled)*: liquid CO_2 is filled in all the 13 cargo tanks (main and auxiliary). At this stage, the USFG is fully submerged and loaded with CO_2.
4. *Submerged (SW-filled)*: this case arises after the USFG has unloaded the CO_2 at the subsea well. The vessel is submerged as the cargo tanks are replaced with seawater during unloading.

Table 8 outlines the results from this section. Finally, extended details for this check can also be found in Xing et al. [6] and Ma et al. [17].

Table 8 Hydrostatic stability study.

	USFG			
	Surfaced (SW-filled)	**Surfaced (CO_2-filled)**	**Submerged (CO_2-filled)**	**Submerged (SW-filled)**
CoG (x, y, z)	[-0.937, 0.00, 0.147]	[-1.032, 0.00, 0.276]	[-0.784, 0.00, 0.403]	[-0.829, 0.00, 0.460]
BG	3.807	5.252	0.405	0.460
CoB (x, y, z)	[-1.481, 0.00, 4.200]	[-1.481, 0.00, 5.500]	[-1.481, 0.00, 0.00]	[-1.481, 0.00, 0.00]
GM	0.393	0.248	0.405	0.460
M (x, y, z)	[0.00, 0.00, 0.00]	[0.00, 0.00, 0.00]	[0.00, 0.00, 0.00]	[0.00, 0.00, 0.00]

Effect	GM > 0.22 == OK	GM > 0.22 == OK	BG > 0.35 == OK	BG > 0.35 == OK

2.9 Power utilization analysis

The amount of power consumed is a function of the glide path (Ref. to ξ in Figure *10*) along with the ballast fraction (BF): the ballast tank size, as the USFG, can vary the speed with which it glides. To better visualize the system's performance, two glide path angles are considered; an angle that gives maximum horizontal velocity for the USFG and a shallower gliding angle.

As the USFG glides faster, it needs to incline at steeper angles while pumping in ballast more frequently to travel the required distance. Shallow glide angles generally result in a comparatively slow equilibrium glide, yielding low horizontal speeds. However, there is an added benefit of utilizing less pumping power/work while travelling a great amount of distance horizontally. As for steep gliding angles, higher horizontal velocity can be achieved by pumping in more ballast water, highlighted by graver [30]. This expands extensive energy on the pump onboard the vessel, leading to more pump work.

With the increase in BF, the horizontal velocity of the USFG also rises. Hence, USFG can be designed to travel much faster by selecting higher BFs. By doing this, the required pumping power will also be considerably increased. A parametric study is done to achieve the optimal BF that limits the pumping work and the pump's size. For each BF, the horizontal glider velocity is calculated and plotted against the consumed power as shown in Figure 11.

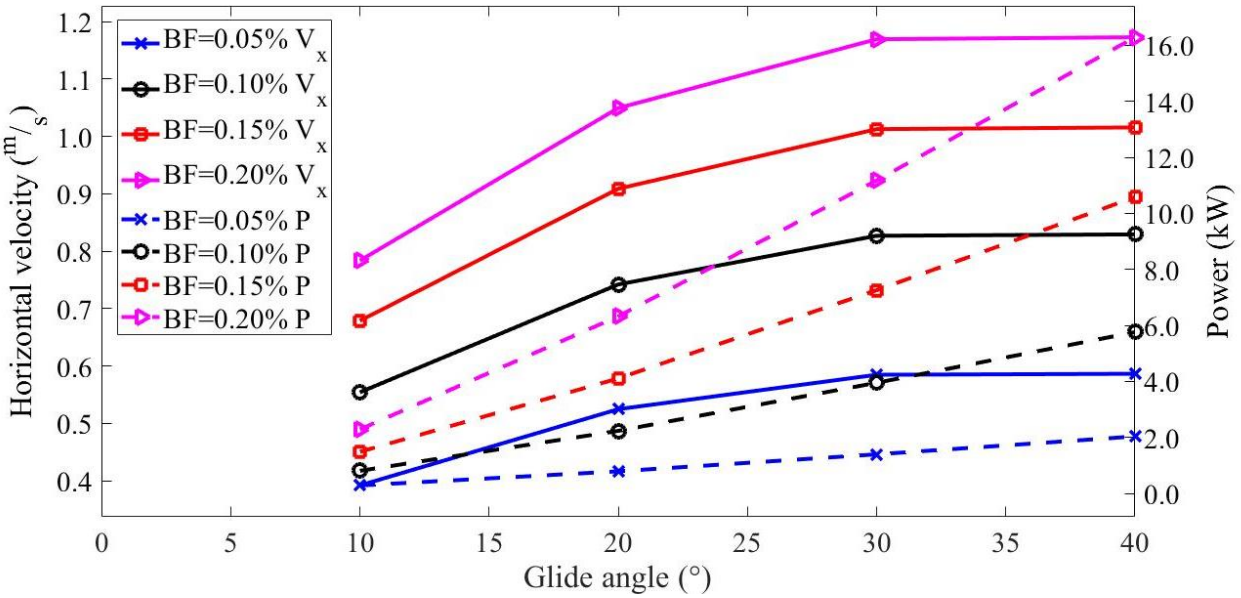

Figure 11 Horizontal velocity vs power consumption.

Depending on the USFG's mission, a desired operational gliding angle must be selected. This is dependent on a quid pro quo between the maximum horizontal glide-velocity and the required pumping work. From Figure 11, a balance between a steep and shallow glide angle must be struck to have an optimal speed and consume minimum power. So, a glide angle of 30° along with a BF of 0.15% is chosen as it caters to the required velocity (1 m/s) of the USFG while consuming a smaller amount of power (<8kW). Lower gliding angles are not considered as they fail to achieve the targeted velocity, even though the power consumption for smaller angles is quite insignificant. As for higher gliding angles, moving from 30° to 40°, the amount of power consumed becomes substantial, and the velocity difference is relatively minimal. Moreover, there is no added advantage of choosing a steeper glide angle than 30° rather than just increasing the pumping work.

3 DYNAMIC RESPONSE OF THE USFG

3.1 Coordinate system

To fully describe and understand the dynamics of the USFG, two-coordinate frames are defined, i.e., body-bound and earth frames. The body-bounded frame (O_b, X_b, Y_b, Z_b) of the USFG is located at its centre-of-gravity (G). Its motion involves a local north, east, and down coordinate system (O_E, X_E, Y_E, Z_E). The centre-of-buoyancy (B) is located accurately above the G and at the geometric centre of the USFG; this ensures enhanced stability of the vessel. The motion and its direction along the six degrees of freedom and the frames are highlighted in Figure 12.

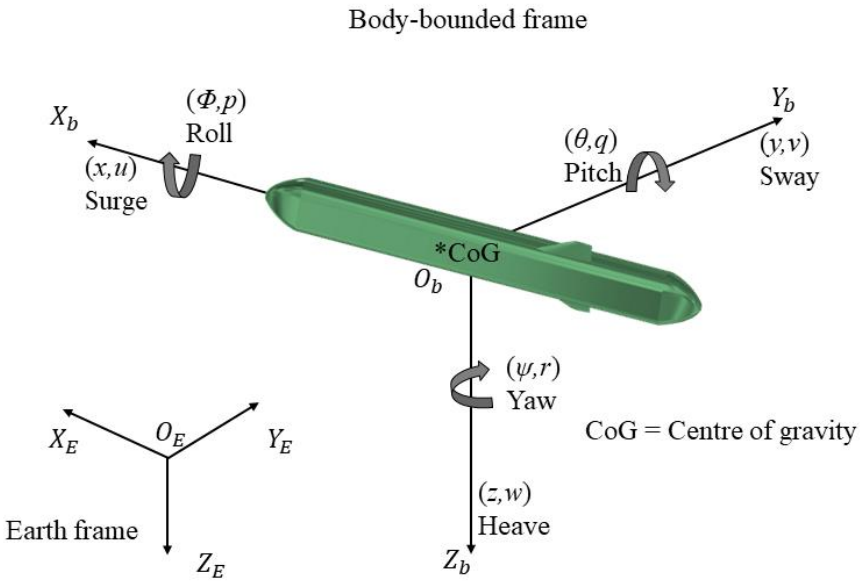

Figure 12 Coordinate system.

3.2 Modeling of USFG

3.2.1 Simulink/Simscape model

SimMechanics is utilized to capture the dynamics of the USFG. Figure 13 depicts the dynamic model of the USFG in the Simscape environment.

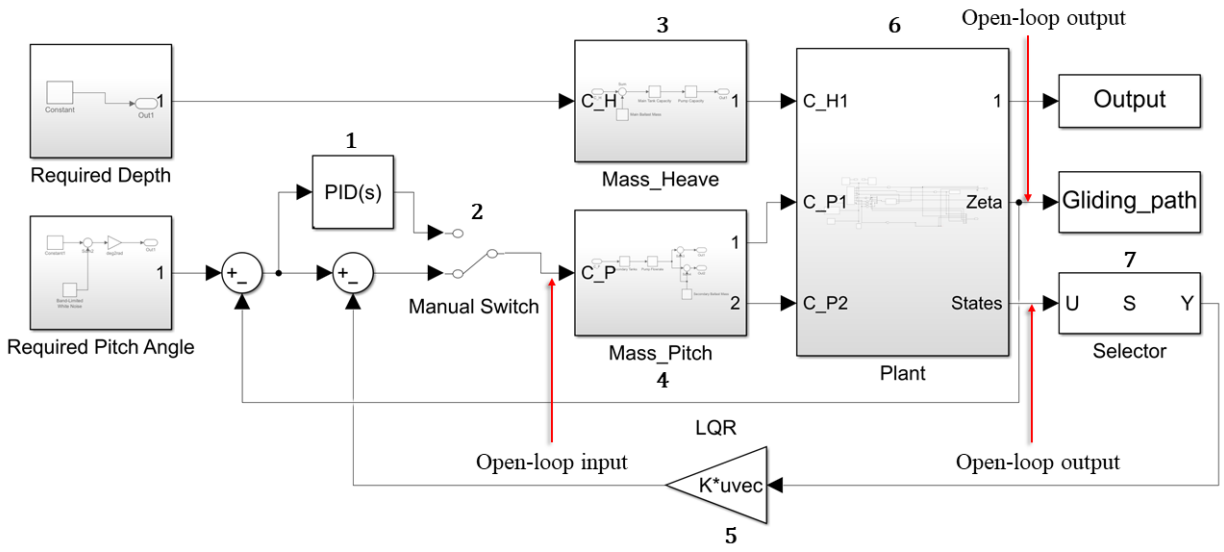

Figure 13 Mathematical model of the USFG.

The central blocks that are used to model the vessel, as highlighted in Figure 13 are elaborated below.

- *Block no.1:* this is the Proportional-integral-derivative (PID) type control that adjusts the pitch motion of the glider. Moreover, it can also be easily tuned to regulate the heave motion of the vessel.
- *Block no.2:* a manual switch that can direct power between the linear quadratic regulator (LQR) and PID controllers.

- *Block no.3:* termed as the heave block. Its purpose is to vary the ballast mass into the ballast tanks. This allows the glider to travel along the vertical direction with the help of lift and drag forces that are generated owing to its large hydrofoils. A saturation (limits the amount of ballast into the tanks) and a rate-limiter (bounds the volumetric flowrate) block is also confined in this sub-system.
- *Block no.4:* the pitch block that is responsible for varying the ballast among the secondary tanks of the glider. This allows the USFG to pitch forward or backwards, depending upon the configuration.
- *Block no.5:* this is the LQR type controller that simply multiplies the gain obtained from system optimization with the states of the system. More details of the controller are discussed in subsequent sections.
- *Block no.6:* the plant block represents the plant model of the glider. This block is discussed briefly in the next section.
- *Block no.7:* This block aims to arrange the state variables in a definite vector. An LQR type control is formed when this vector is multiplied by the gain matrix (K) to form a closed loop.

3.2.2 Plant block/model

This section describes the plant block depicted in Figure 13 as *block no.6*. A systematic configuration of the block is presented in Figure 14 below. The three main blocks that comprise the plant block are as follows:

- *USFG:* this block contains a two-dimensional (2D) rigid body that is allowed to move in three degrees of freedom (*x*, *y*, and *z*). Based on the forces acting on the glider, the following equations of motion will be solved:

$$W(\dot{u} + wq - xq^2 + z\dot{q}) = \sum X_e \tag{1}$$

$$W(\dot{w} + uq - zq^2 + x\dot{q}) = \sum Z_e \tag{2}$$

$$I_{yy}\dot{q} + W\lfloor z(\dot{u} + wq) - x(\dot{w} - uq)\rfloor = \sum M_e \tag{3}$$

While X and Z represent forces and moment is expressed as M. Velocities are expressed as u and w (x and z-direction) and similarly acceleration by u̇ and ẇ. Equations (1-3) encompass external forces in pitch (M_e), heave (Z_e), and surge (X_e) as presented on the right-hand side and inertial terms on the other side.

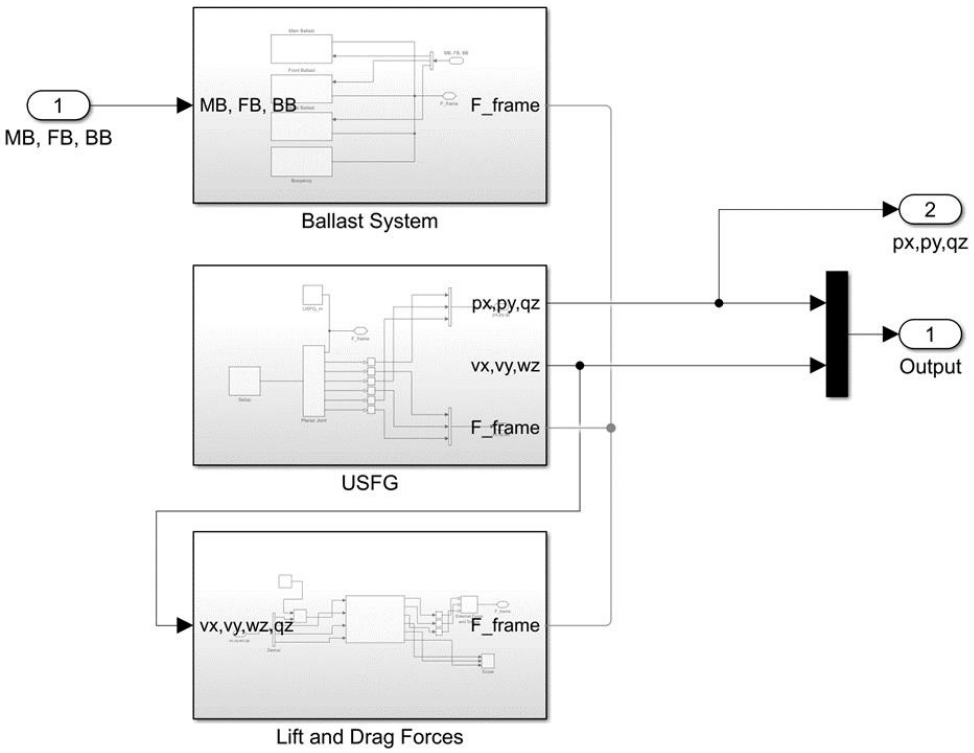

Figure 14 Simulink plant model - Lift and drag forces, ballast system, and USFG.

- *Ballast system:* this block model the dynamics of the actuating mechanism of the USFG. As described earlier, it serves input to the USFG block as a force by taking control of ballast inputs from the mass blocks. Finally, the buoyancy force of the glider is also simulated in this system.
- *Drag and lift force:* drag and lift force and the rotational torque are determined in this block. These are calculated based on the approach angle of the incoming flow. Velocities and the pitching angles of the USFG are utilized to calculate the forces. Equations (4) and (5) are used to calculate the drag and lift coefficients which are a function of approach angle (α) as depicted in Figure *10*. These are

the volumetric drag and lift coefficients used by Graver [30], as the shape of the USFG is similar to the glider proposed in his work.

$$C_L = 5\alpha^2 + 10\alpha \tag{4}$$

$$C_D = 0.4\alpha^2 + \alpha + 0.1 \tag{5}$$

3.3 LQR control and tuning

An LQR type control is utilized to optimize the performance of a closed-loop system by providing optimally tuned controller gains. LQR being a popular choice amongst AUVs, it has been employed for steering control by Bae et al. [31] and for controlling depth by Burlacu et al. [32]. The gain matrix (K) is derived for USFG by utilizing the dynamic state-space model. For USFG, the state space equations (6-9) for single input multiple outputs (SIMO) systems are:

$$\frac{ds_1}{dt} = As_1 + Bj_1 \tag{6}$$

$$\frac{ds_2}{dt} = As_2 + Bj_1 \tag{7}$$

$$z_1 = Cs_1 \tag{8}$$

$$z_2 = Cs_2 \tag{9}$$

A, *B* and *C* are the state, input, and output matrices, respectively. Whereas $z_{1,2}$, are scalar matrices of the system representing output, $s_{1,2}$ are the state variables, and j_1 is the input scalar matrix. State matrices of the system (*A*, *B,* and *C*) are calculated in *Section 3.3.1*.

The control law implemented here is given by equation (10), where *K* is the gain matrix.

$$j = -K\delta s \tag{10}$$

For an optimal gain matrix for LQR, *A* and *B* matrices are obtained from the linearization of the system. This is done to reduce the cost function formed based on the control law. It relies on the summation of the square of the input variables of the system. Equation (11) gives the cost function:

$$G = \int_0^\infty \delta s^T\, Q\delta s + \delta j^T\, R\delta j\, dt \tag{11}$$

Here *R* is the matrix for the penalty of control cost, and Q is the penalty for state cost. The aim is to adjust *Q* and *R* to find an optimal balance between actuator effort and the system's performance. Weights of these penalty matrices are adjusted to tune the LQR controller for the desired application. This is done in *Section 3.3.2.*

3.3.1 Linearization

The model used for linearization is from work presented by Ahmad and Xing [33]. Linearization for two case studies is performed in this section, i.e., *Case 1* and *Case 2*, as highlighted in *Section 3.4*. Previously Ahmad and Xing [34] investigated 30° and 40° glide angles for the linearization of the USFG model. As for *Case 2*, the model is linearized at a 38° gliding angle. Simulink model linearizer is used to linearize the mathematical model of the USFG at an established operational point. Open-loop inputs [ϑ; $\dot{x}$; $\dot{y}$; $\dot{\theta}$] and outputs [$\dot{\theta}$; $\ddot{x}$; $\ddot{y}$; $\ddot{\theta}$] are marked as shown in Figure *13*. This results in a 4x4 *A*, 4x1 *B,* and 2x4 *C* matrices as depicted in equation (12):

$$A = \begin{bmatrix} 0 & 0 & 0 & 1 \\ 0.4298 & -0.2032 & -0.2606 & 5.51 \times 10^{-12} \\ 0.6811 & -0.2941 & -0.4128 & 0 \\ -2.10 \times 10^{-08} & 1.12 \times 10^{-09} & 1.52 \times 10^{-09} & -3.15 \times 10^{-04} \end{bmatrix}$$

$$B = \begin{bmatrix} 0 \\ -1.58 \times 10^{-12} \\ -8.88 \times 10^{-13} \\ 2.64 \times 10^{-05} \end{bmatrix} \tag{12}$$

$$C = \begin{bmatrix} 0 & 0.7886 & -0.6149 & 0 \\ 0 & 0.4572 & -0.5863 & 0 \end{bmatrix}$$

3.3.2 Tuning of LQR

Based on the state matrices (*A*, *B,* and *C*) obtained from linearization, LQR is tuned to obtain the desired response of the glider. Tuning is done by adjusting the values (penalties) of the *Q* and *R* matrices. A complete and holistic understanding of the dynamics of the USFG is

essential to tune the controller. This involves studying the response time of the system for anticipated system performance. Additionally, Bryson's technique is employed to tune the values for the USFG model. This involves fine-tuning the Q and R matrices manually according to the final response of the glider (*Case 2: The 38° glide*). Penalty on the *R* matrix adjusts the controller effort. As for the *Q* matrix, it governs the acceptable error amongst the output variables/states. Detailed analysis for the controller tuning can be found in Ahmad and Xing [34], which also forms the basis of a good system response for this study. The Q and R matrices are presented in equation (13).

The 10^5 for the 41-coefficient represents that the acceleration in the pitch direction is penalized heavily, as the system is designed to attain a pitching angle of 38°. The gain matrix

$$Q = \begin{bmatrix} 0 \\ 0 \\ 0 \\ 10^5 \end{bmatrix} \qquad (13)$$

$$R = [0.01]$$

(*K*) is presented in equation (14).

$$K = [-5.31 \times 10^{-10} \quad 2.43 \times 10^{-10} \quad 3.21 \times 10^{-10} \quad 2.58] \qquad (14)$$

3.4 Controlled gliding of USFG

This section analyses two different glides of the USFG and the different characteristics of each controlled glide. The following cases are simulated.

- Case 1: Equilibrium glide
- Case 2: The 38° glide path

3.4.1 Equilibrium glide

The sawtooth path taken by the glider, as depicted in Figure *2*, is termed as an equilibrium glide or gliding path. The USFG follows this equilibrium path to extend its travel range as taking a pre-planned route may optimize the freight operations. Two equilibrium glide paths are simulated for this analysis and are presented in Figure 15. This plot represents the time series of the glider's pitch response.

For this study, the glider is programmed to follow an operating depth of 200 m while following a 38° glide angle by using two separate controllers: Proportional-integral-derivative (PID) and LQR type control. The objective of the investigation is to compare the heave response of the two different control systems against the planned path.

The tuning gains selected for this study are the most ideal for PID application, as other values increase the response time of the output. For this scenario, the glider changes the glide angle rapidly as it responds to changes in the commanded pitch. This leads to more glides/dives for a certain distance travelled, resulting in higher power consumption onboard. Overrun and overshoot can also be observed when PID is utilized to control the pitching motion of the glider. Moreover, these gains cannot be further optimized as doing so induces non-practical response times.

LQR type control enables the glider to respond to changes in operating conditions more efficiently and effectively by utilizing less actuator effort. An error of merely 3% is observed as compared to 11% for PID. With enhanced tuning, then this error can be further reduced for LQR. Furthermore, the deviations in the upper and lower bounds are also shortened due to reduced overrun.

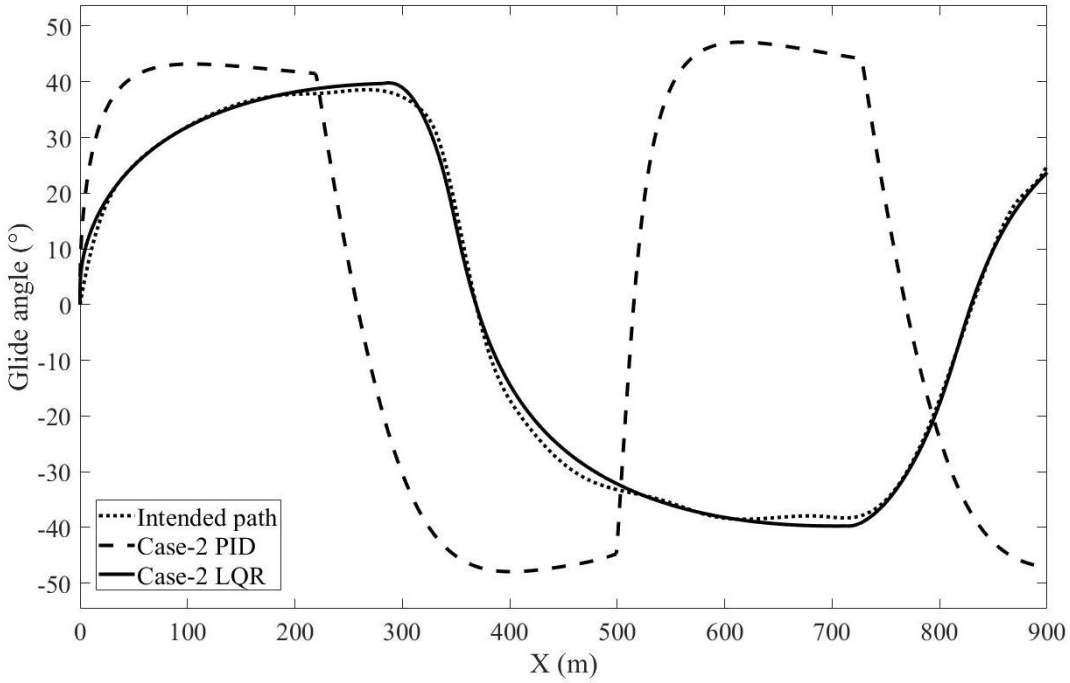

Figure 15 Equilibrium glide paths (PID vs LQR) in the vertical plane.

3.4.2 The 38° glide path

Figure *16* compares the pitch response of LQR and PID. This controlled glide of the USFG requires the glider to pitch at an angle of -38° while diving. The negative convention is to represent anti-clockwise rotation in a 2D vertical plane. Actuator effort is compared for both cases of the controller.

As illustrated in Figure 16, the PID controller fails to mitigate the noise from the output response. The oscillations in the pitch response increase the controller effort drastically. Consequently, the percentage overshoot and the signal's settling time increases significantly to 13.5 % and 15.4 seconds correspondingly. Moreover, higher overshoot/peaks affect the USFG's dynamics negatively. As the objective of the glider is to conserve energy while transporting cargo over larger distances, so excessive actuator effort spent on course correction is not ideal for this scenario. Finally, the PID controller employed for this controlled glide is tuned aggressively. This tuning does not add value to the overall system response. Subsequently leading to no room for improvement as far as the tunning of PID is concerned. Generally, a controller ideal for such applications is the one that causes fewer oscillations while reducing the settling time.

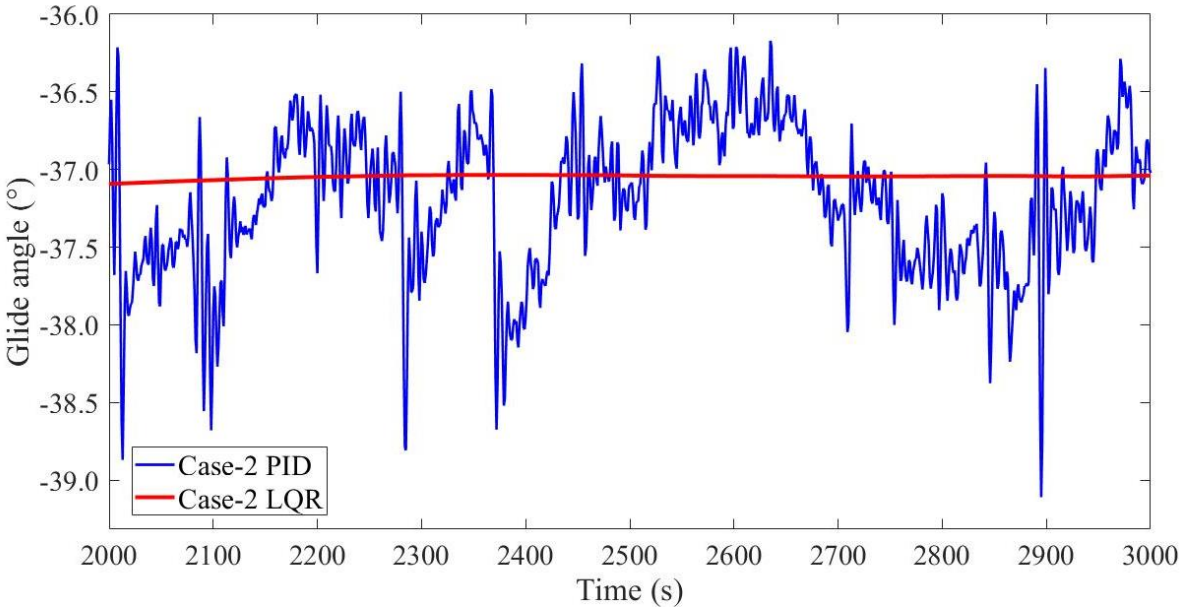

Figure 16 38° Glide path.

LQR is tuned according to the system's response to reduce the fluctuations. The controller effort is penalized lightly in the R matrix, as indicated in equation (13). This induces the controller to respond quickly following the desired steered command while decreasing the rise and settling time significantly. A downside of these gains is that the slope of the output signal increases slightly, but a comprise can be made for this application, as it is not of much concern for this analysis. The system becomes robust when an LQR-type control is utilized as the gains selected for this scenario are ideal compared to their counterparts. Moreover, in this case, the controller gains can be further optimized to get the desired characteristics, unlike for the PID controller.

4 CONCLUSIONS

In this paper, the baseline design of USFG is presented, consisting of a mechanical design and the control design. The final derived design is presented in Table 9. The control design consists of the manoeuvring model along with 2 case studies. The USFG aims to carry CO_2 for injection to the well sites, though reducing the overall carbon footprint of the freight industry. The baseline design of the USFG is developed to promote research in underwater cargo-carrying vessels while also serving as a potential replacement for conventional transport methods, i.e., pipelines and tankers. The main details of the design are presented in the first part of the work. The distinguishing feature of the USFG is its dual hull/shell design which utilizes an ACPS to reduce the overall structural weight. As for the second part, an extensive analysis is presented, which highlights the major differences between LQR and PID type controllers used for autonomous

naval applications. LQR is preferred for both cases of the controlled glides, as it reduces oscillations while enhancing the system's robustness. Finally, the tuning method of LQR is straightforward compared to the conventional PID control that requires unwarranted tunning and computational power for results to be converged.

Table 9 Design summary of USFG.

Vessel Features	**Value**
Length [m]	50.25
Beam [m]	5.5
Total power consumptions [kW]	8
Range [km]	400
Speed [knots]	2
Lightweight [ton]	495
Deadweight [ton]	531
Displacement [ton]	1026
Lightweight [m^3]	483
Deadweight [m^3]	518
Displacement [m^3]	1001

Appendix A. Calculation of reference wing area

The hydrofoils reference area of 5 m^2 is derived based on Graver's work [30]. Following parameters are used in the calculation of wing area.

- ***D_{ton}*:** described as DWT valued at 531 tons, is the amount of freight or cargo (CO_2 for this paper) that the USFG can transport.
- ***H*:** defined as nominal operating depth, which is estimated to be 200 m.
- ***BF*:** ballast fraction of 0.15% is preferred.
- ***ξ*:** the gliding angle of 30º is selected to conserve power while gliding at a constant speed.

The hydrofoil area can be calculated from these expressions:

$$BF = \frac{m_o}{D_{ton} \times 1000} \tag{15}$$

$$S = \sqrt[2]{\left(\frac{m_o \times g \times \sin\xi}{0.5 \times \rho_w \times C_{DVol} \times Vol^{\frac{2}{3}}}\right)} \tag{16}$$

$$S_x = S \times \cos\xi \tag{17}$$

$$D_{force} = S^2 \times 0.5 \times \rho_w \times C_{DVol} \times Vol^{\frac{2}{3}} \tag{18}$$

$$L_{force} = \frac{D_{force}}{\tan \xi} \tag{19}$$

$$A_{reference} = \frac{L}{S^2 \times 0.5 \times \rho_w \times C_L} \tag{20}$$

Where m_o is the mass of the USFG, S is the velocity of the glider, g is the gravitational constant, ρ_w is the density of water, C_{DVol} and C_L is the volumetric drag and lift coefficient of the USFG, Vol is the entire volume of the USFG, and L_{force} and D_{force} are the lift and drag forces, respectively.

The drag force is calculated to be 3907 Newtons, whereas the lift force comes out to be 6767 Newtons for this case. It must be noted that the USFG attains a total horizontal speed of 1 m/s for these conditions.

NOMENCLATURE

USFG	UiS subsea-freight glider
CCS	Carbon capture and storage
DWT	Dead-weight tonnage
SST	Subsea shuttle tanker
AUVs	Autonomous Underwater Vehicles
PID	Proportional-integral-derivative
ASME BPVC	American Society of Mechanical Engineers Boilers and Pressure Vessel Code
DNVGL-RU-NAVAL-Pt4Ch1	DNVGL Rules for Classification for Naval Vessels, Part 4 Sub-surface ships, Section 1 Submarine
GM	Metacentric height
G	Centre of gravity
B	Centre of buoyancy
LQR	Linear-quadratic regulator
K	Gain matrix
2D	Two-dimensional
M_e	External pitch moment
Z_e	Force in heave direction
X_e	Force in surge direction
SIMO	Single input multiple outputs
A, B, and C	State space matrices

5 REFERENCES

[1] R. FULLENBAUM, J. FALLON, and B. FLANAGAN, "Oil & Natural Gas Transportation & Storage Infrastructure: Status, Trends, & Economic Benefits," IHS Global Inc., 2013. [Online]. Available: https://www.circleofblue.org/wp-content/uploads/2014/12/API-Infrastructure-Investment-Study.pdf.

[2] A. C. Palmer and R. A. King, Subsea pipeline engineering, 2nd ed. Tulsa, Okla: PennWell, 2008.

[3] C. Vestereng. "Shuttle tankers in Brazil." DNV-Maritime Impact. https://www.dnv.com/expert-story/maritime-impact/shuttle-tankers-Brazil.html (accessed 30 January 2022).

[4] J. WILSON, "Shuttle tankers vs pipelines in the GOM frontier," World oil, vol. 229, no. 4, pp. 149-151, 2008.

[5] Y. Xing, "A conceptual large autonomous subsea freight-glider for liquid CO2 transportation," in International Conference on Offshore Mechanics and Arctic Engineering, 2021, vol. 85161: American Society of Mechanical Engineers, p. V006T06A052.

[6] Y. Xing, T. A. D. Santoso, and Y. Ma, "Technical–Economic Feasibility Analysis of Subsea Shuttle Tanker," Journal of Marine Science and Engineering, vol. 10, no. 1, p. 20, 2021.

[7] H. Stommel, "The Slocum mission," Oceanography, vol. 2, no. 1, pp. 22-25, 1989.

[8] Evo Logics. "Evo Logics BOSS - Manta Ray." https://evologics.de/projects/boss (accessed 31 January 2022).

[9] DOF Subsea. "Glider AUV." https://www.dofsubsea.com/rov/glider-auv/ (accessed 31 January 2022).

[10] P. Taylor and J. Montgomery, "Arctic submarine tanker system," in Offshore Technology Conference, 1977: OnePetro.

[11] L. R. Jacobsen, "Subsea Transport of Arctic Oil-A Technical and Economic Evaluation," in Offshore Technology Conference, 1971: OnePetro.

[12] L. Jacobsen, K. Lawrence, K. Hall, P. Canning, and E. Gardner, "Transportation of LNG from the Arctic by commercial submarine," Marine Technology and SNAME News, vol. 20, no. 04, pp. 377-384, 1983.

[13] G. Griffiths, Technology and applications of autonomous underwater vehicles. CRC Press, 2002.

[14] Equinor Energy AS. RD662093 Subsea Shuttle System, 2019.

[15] K.E. Ellingsen, O. Ravndal, L. Reinas, J.H. Hansen, F. Marra, E. Myhre and k. Sveberg, RD677082 Subsea Shuttle System, 2020.

[16] Y. Xing, M. C. Ong, T. Hemmingsen, K. E. Ellingsen, and L. Reinås, "Design considerations of a subsea shuttle tanker system for liquid carbon dioxide transportation," Journal of Offshore Mechanics and Arctic Engineering, vol. 143, no. 4, 2021.

[17] Y. Ma, Y. Xing, M. C. Ong, and T. H. Hemmingsen, "Baseline design of a subsea shuttle tanker system for liquid carbon dioxide transportation," Ocean Engineering, vol. 240, p. 109891, 2021.

[18] J. W. Bahlman, S. M. Swartz, D. K. Riskin, and K. S. Breuer, "Glide performance and aerodynamics of non-equilibrium glides in northern flying squirrels (Glaucomys

sabrinus)," (in eng), J R Soc Interface, vol. 10, no. 80, pp. 20120794-20120794, 2012, DOI: 10.1098/rsif.2012.0794.

[19] Norwegian Petroleum Directorate (NPD). "Carbon Capture and Storage." http://www.norskpetroleum.no/en/environment-and-technology/carbon-capture-and-storage (accessed 1 February 2022).

[20] Equinor. "Northern Lights CC." https://www.equinor.com/en/what-we-do/northern-lights.html (accessed 1 February 2022).

[21] P. Taylor, "Energy Technology Perspectives," International Energy Agency, 2010.

[22] A. Papanikolaou, Ship design: methodologies of preliminary design. Springer, 2014.

[23] Carbon Capture Storage, and Association. "What Is CCS?" http://www.ccsassociation.org/what-is-ccs/ (accessed 2 February 2022).

[24] ASME. Boiler and Pressure Vessel Code, Section VIII, Division 2; The American Society of Mechanical Engineers: New York, NY, USA, 2015.

[25] DNV-GL Rules for Classification, Naval Vessels, Part 4 Sub-Surface Ships. Available online: https://rules.dnv.com/docs/pdf/DNV/RU-NAVAL/2018-01/DNVGL-RU-NAVAL-Pt4Ch1.pdf (accessed on 4 February 2022).

[26] National Centers for Environmental, and Information (NCEI). "Greenland, Iceland, and Norwegian Seas Regional Climatology." https://www.ncei.noaa.gov/products/greenland-iceland-and-norwegian-seas-regional-climatology (accessed 7 February 2022).

[27] A. Mariano, E. Ryan, B. Perkins, and S. Smithers, "The Mariano Global Surface Velocity Analysis 1.0," p. 61, 07/01 1995.

[28] G. Ersdal, "An overview of ocean currents with emphasis on currents on the Norwegian continental shelf," 2001.

[29] R. Sætre, The Norwegian coastal current: oceanography and climate. Akademika Pub, 2007.

[30] J. G. Graver, "Underwater gliders: Dynamics, control and design," 2005.

[31] Bae, S. B. Shin, D. H. Kwon, S. T. Joo, and M. G, "An LQR controller for autonomous underwater vehicle," Journal of Institute of Control, Robotics and Systems, vol. 20, no. 2, pp. 132-137, 2014.

[32] P. Burlacu, V. Dobref, N. Badara, and O. Tarabuta, "A LQR controller for an AUV depth control," Annals of DAAAM & Proceedings, pp. 125-127, 2007.

[33] U. Ahmad and Y. Xing, "A 2D model for the study of equilibrium glide paths of UiS Subsea Freight-Glider," in IOP Conference Series: Materials Science and Engineering, 2021, vol. 1201, no. 1: IOP Publishing, p. 012022.

[34] U. Ahmad and Y. Xing, "UIS Subsea Freight Glider: controller design and analysis," in International Conference on Offshore Mechanics and Arctic Engineering, 2022, American Society of Mechanical Engineers.

Figure Captions List

Table Caption List

Determination of extreme responses of USFG's equilibrium glide path hovering in ocean current

Usman Nawaz Ahmad[1], Yihan Xing[1, *], Shuaishuai Wang[2]

1) University of Stavanger, Norway
2) Norwegian University of Science and Technology, Trondheim, Norway

*Corresponding author: yihan.xing@uis.no

Abstract

The UiS subsea-freight glider (USFG) is a state-of-the-art autonomous vessel designed to be an alternative to existing transportation technologies and serve the demands of small-scale fields for CO_2 transportation. Generally, these smaller fields cannot economically justify the costs of large tanker or cargo ships or underwater pipelines on the seabed, as the transport volume is nominal compared to larger fields. The USFG can travel underwater at an operational depth of 200 m, allowing the glider to carry freight operations without considering ideal weather windows. It can manoeuvre itself underwater by monitoring the flow between the ballast tanks aboard. During the entire mission of the USFG, from capturing to injection locations, it follows a pre-laid saw-tooth path while experiencing transient loads from the ocean current. The extreme surge and heave responses of the USFG are vital for its design. Extreme motion along the surge direction affects the range of the glider (vital for battery design) and the dynamic controller parameters concerning manoeuvrability. For this paper, the averaged conditional exceedance rate (ACER) is employed to scrutinize the extreme motion (surge direction) of the USFG while gliding to a defined depth. This is done when the glider is exposed to an average current velocity of 0.5 m/s and 1.0 m/s. The data used for analysis in this study is obtained from the time-domain simulations carried out on a two-dimensional mathematical model developed in Simulink. The presented ACER method efficiently uses the available data points and accurately predicts the extreme surge responses precisely and accurately. This study can effectively promote the design improvement of the USFG; thus, the safety and economic benefits can be essentially enhanced.

1. Introduction

The UiS subsea-freight glider (USFG), depicted in **Figure 1**, is a state-of-the-art sizeable underwater cargo-carrying vessel proposed by Xing [1]. Subsequently, work by Ahmad and Xing [2] studied the critical controller parameters to design an optimal and robust control for the autonomous gliding capabilities of the USFG. This formed the basis for choosing an ideal controller for the USFG for its gliding capabilities, as highlighted by Ahmad and Xing [3]. Xing et al. [4] contended that for an autonomous freight carrying vessel to be economically feasible, the assigned payload should be a minimum of 50 % of its volumetric displacement. Xing et al. [4] also proposed numerous optimization techniques and innovative design features to reduce the overall weight of the vessel significantly. Founded on these considerations, Ahmad et al. [5] developed the baseline design of the USFG.

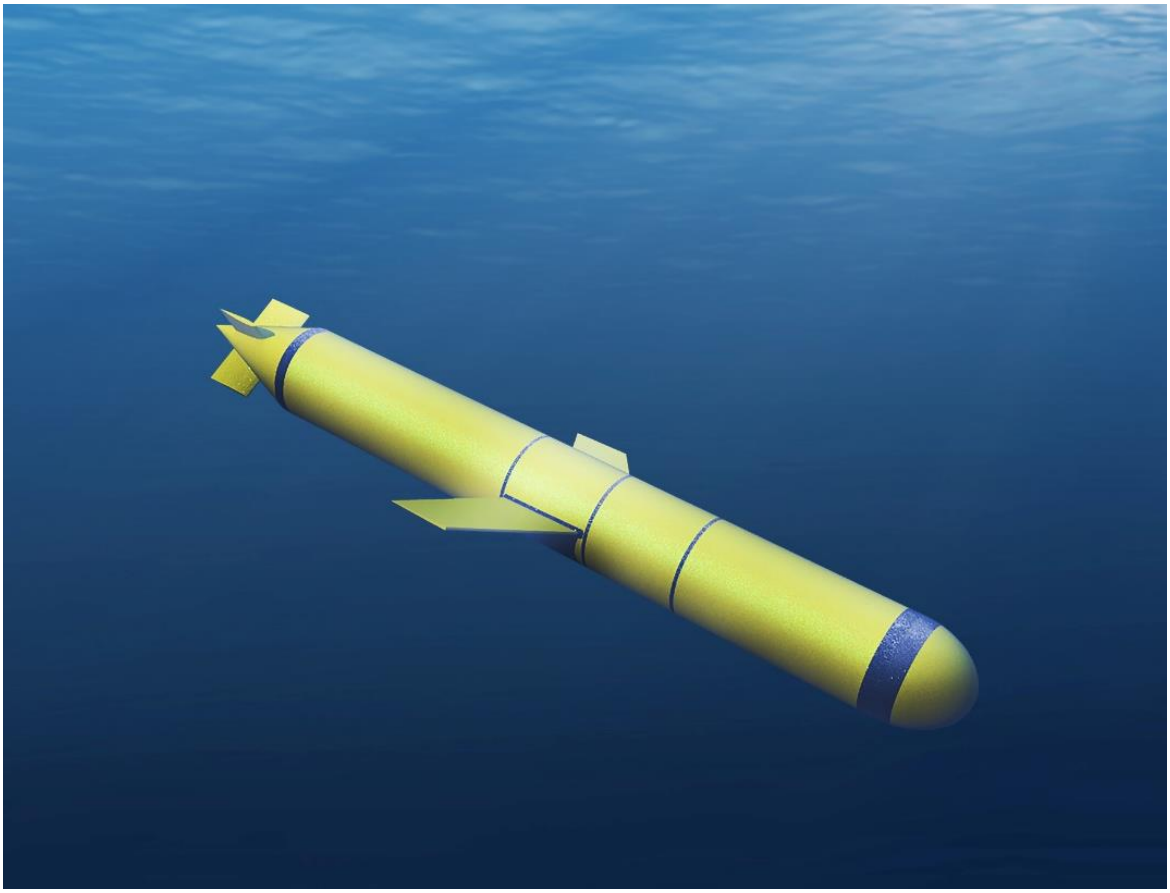

Figure 1 The UiS subsea-freight glider (USFG).

The baseline design of the USFG is a 531-deadweight tonnage (DWT) subsea glider. It is planned to play a pivotal role in the transportation operations for carbon capture and storage (CCS). The glider aims to carry the CO_2 from the capturing facilities to the storage facilities offshore, injecting the CO_2 into the seabed with the aid of wells located at the seabed, as shown in **Figure 2**. The USFG travels at an operating depth of 200 m, where waves and wind loads do not affect the critical freight operations. Consequently, the USFG is not weather restricted; owing to its autonomous and submarine capabilities, it can transport CO_2 even in extreme sea conditions compared to conventional tankers.

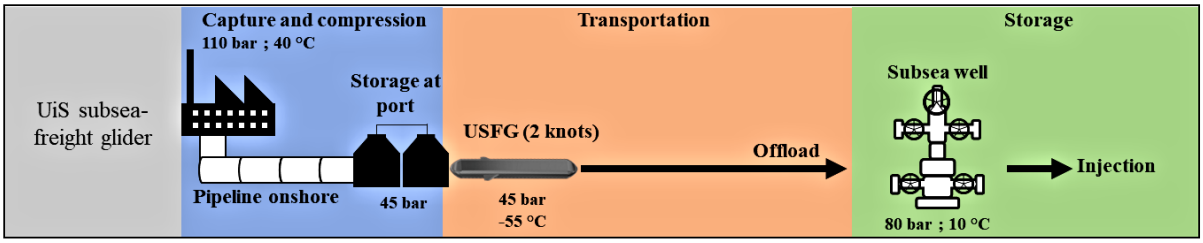

Figure 2 USFG in CCS.

The USFG can be fully incorporated into the ongoing CCS projects on the Norwegian Continental Shaft (NCS), namely, Snøhvit, Sleipner, and Utgard fields, as shown in **Figure 3**. It aims to assist as an auxiliary solution to the conventional transport methods such as pipelines and tankers. As for small fields with lower storage volume, the costs of tanker ships and subsea pipelines cannot be commercially justified. Additionally, as considered in Xing et al. [6], the cost/ton of carrying CO_2 is anticipated to be more cost-effective than pipelines and tankers. Moreover, the transportation cost is projected to be equivalent to the innovative subsea shuttle tanker (SST) presented by Ma et al. [7]. With design optimizations such as argued by Jamissen et al. [8], the USFG can be an increasingly attractive underwater vessel fiscally. The baseline USFG is used for the study in this work; **Table 1** highlights the key design features of the USFG.

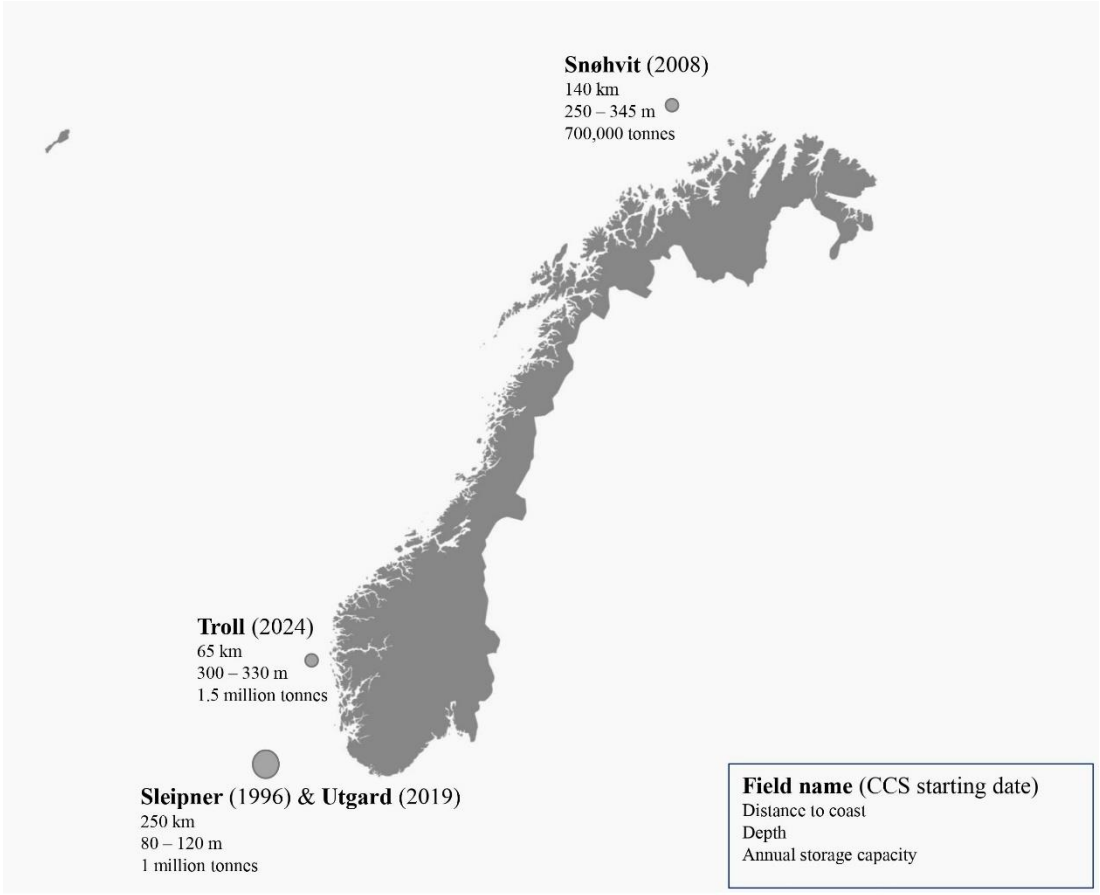

Figure 3 Sites on NCS for CCS to integrate USFG.

Table 1 USFG's design characteristics.

Parameter	Value	Unit
Length	50.25	m
Operating depth	200	m
Center of gravity (CoG) $[x_{cg}, y_{cg}, z_{cg}]$	[-0.78, 0.00, 0.40]	m
Weight	1379	tons
CO_2 cargo capacity	518	m^3
Beam	5.5	m
Range	400	km
Center of buoyancy (CoB) $[x_{cb}, y_{cb}, z_{cb}]$	[-1.48, 0.00, 0.00]	m
Wing area	5	m^2

The USFG can manoeuvre itself freely by operating the ballast tanks aboard. As depicted in Figure 4, the pre-planned path or route of the USFG is also known as the equilibrium gliding path [9]. Positive net buoyancy and negative pitch angle are generated by pumping out the ballast water primarily. This allows the vessel to rise with an angle of attack (bow heading up). Consequently, a lift force is produced due to the relative velocity acting between the incoming seawater and the glider, which allows the glider to move in the required direction. Correspondingly, the glider can return to its primary depth by pumping in the ballast, which generates a negative net buoyant force and positive pitch angle (bow heading down). While moving forward in this saw-tooth pattern, the large hydrofoils are responsible for generating propulsion. This cyclic process is repeated throughout the entire mission of the USFG until it reaches its targeted destination though being exposed to the environmental loads as highlighted in **Figure 4**. The Linear Quadratic Regulator (LQR) is responsible for controlling the motion of the USFG, which is fine-tuned and modelled by Ahmad et al. [5].

Extreme surge responses are vital considering the design of the USFG. When CO_2 is transported from offshore to an onshore field during the mission, following a pre-planned path is vital. This must be done to maximize the travel or operational range of the glider. The path is also dependent on the extreme surge motion (which can also influence motion in the heave direction). The glider's ability to manoeuvre accurately underwater is of utmost importance for controller design. The controller must cater to the undershoot or overshoot in the surge direction, as depicted in **Figure *4***. The goal is to utilize not more than one-fourth of the battery power by following a defined path, which can likely reduce power consumption, as argued by Langebrake [10]. It is of great importance to follow the route, as this can remedy the problem of limited position tracking of AUVs, as emphasized by Griffiths et al. [11]. Any deviation from the route must be avoided as it can lead to severe consequences, i.e., loss of vessel control.

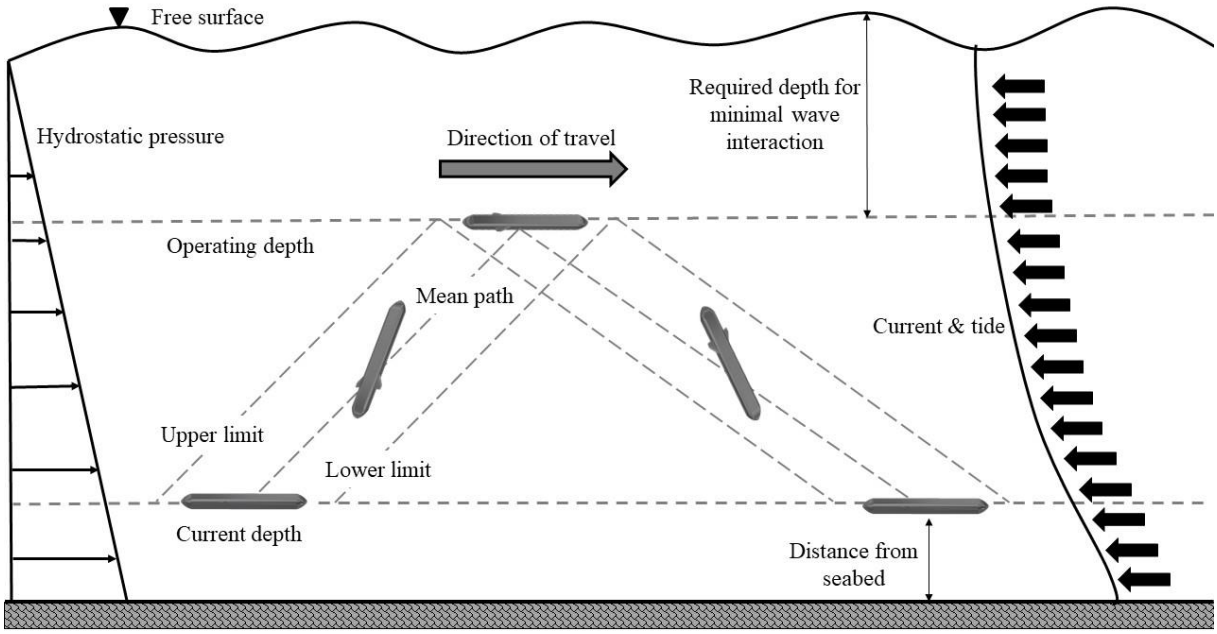

Figure 4 USFG subjected to environmental loads during equilibrium glides.

In this work, the averaged conditional exceedance rate (ACER) is utilized to study the extreme motion (surge direction) of the USFG during gliding. This is done when the vessel is exposed to an average current velocity of 0.5 m/s and 1.0 m/s. The ACER method is defined by a combination of two methods: an extrapolation method utilizing tail behaviour and a numerical method that evaluates the extreme value distribution intrinsic to the acquired data. Compared to other extreme value prediction methods, the ACER method is accurate, convenient to use, and robust at the same time. Previously, the ACER design method has been effectively utilized for various applications in the field of marine engineering to evaluate extreme sea states involving current profiles [12], waves and wind profiles [13-15], and wave heights [14,16]. Also, for structural applications such as [17-23]. The glide problem under consideration is highly non-linear. Consequently, ACER is utilized for this study, as it studies the non-linearities of the system beyond making any generalizations or simplifications with an added advantage of it being Monte Carlo-based. All the data in this study is obtained from the time-domain simulations carried out on a two-dimensional mathematical model design in Simulink, ref Section 2. The ACER method is presented in Section 3. Detailed findings of this work and conclusions are presented in Sections 4 and 5, respectively.

2. Two-dimensional mathematical model

MATLAB has been used to capture the dynamics of the USFG by modeling it as blocks or modules which represent the various components of the vessel. The USFG is represented by a planar multibody model which has been developed in the Simulink environment. The model is presented in this section.

2.1 Coordinate system

A body-bounded and an earth frame are defined to capture the system dynamics of the USFG fully. The body-bounded frame (O_{bb}, X_{bb}, Y_{bb}, Z_{bb}) is accurately positioned at USFG's centre of gravity (G). The axis movement includes a local north, east, and down coordinate system (O_{EB},

X_{EB}, Y_{EB}, Z_{EB}). The buoyancy centre (B) falls directly above the geometric centre to ensure the vessel's stability. The vessel's motion and its vector direction and axis system is presented in figure 5 below.

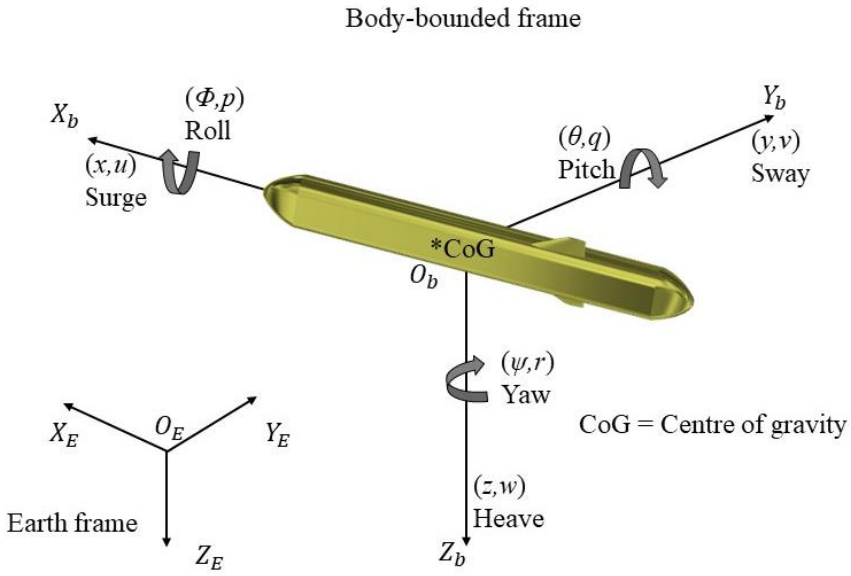

Figure 5 USFG's axis system.

2.2 Simulink layout

The control loop and mathematical model of the USFG designed in Simulink are shown in **Figure 6** and **Figure 7**, respectively.

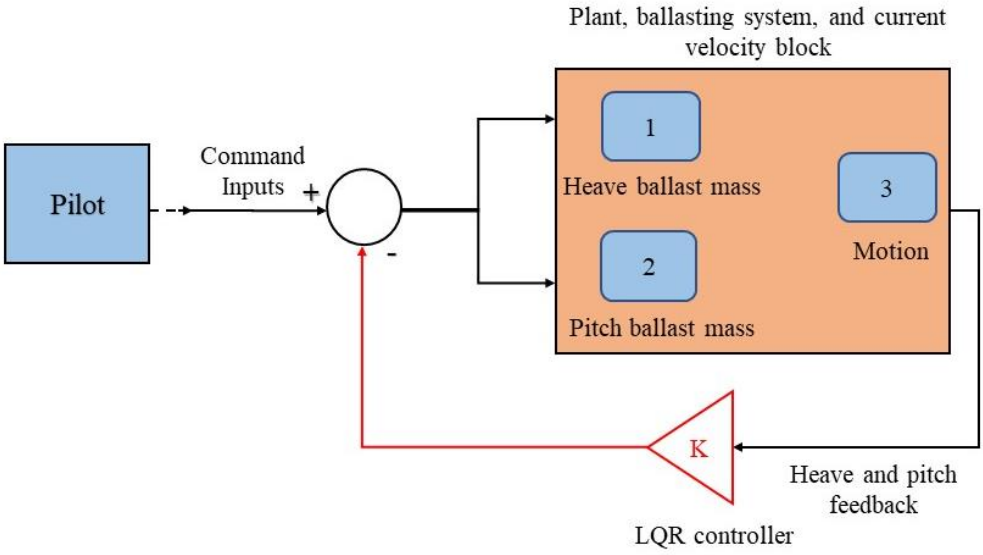

Figure 6 Control loop for USFG's mathematical model.

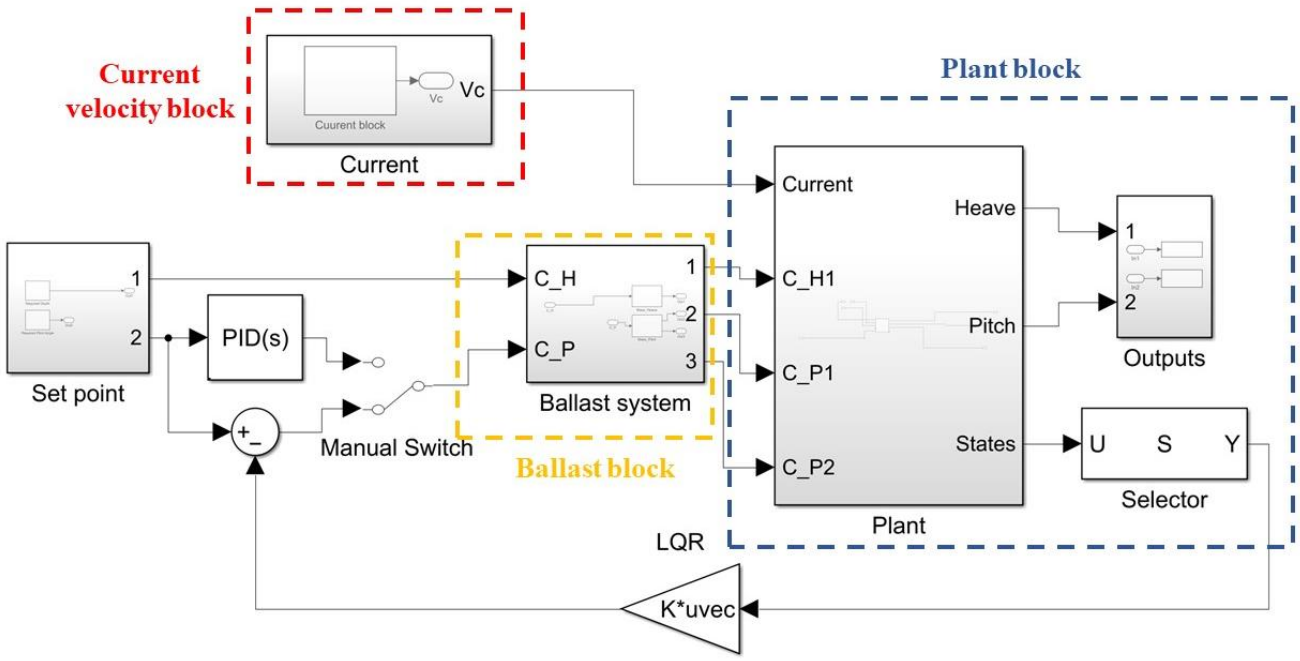

Figure 7 Simulink design - ballast, current velocity, and plant block

This model was initially developed by Ahmad and Xing [2] to capture the system dynamics of the USFG during equilibrium gliding while following a pre-planned path. Later, Ahmad and Xing [3] extended their work to include an LQR-based control for depth and pitch control using a hydrofoil while undergoing loads from the current.

The main modules of the USFG are the following:

- *Plant module/block:* this block represents the USFG in the Simulink environment. It is responsible for executing and solving the equation of motions for the USFG. This is done by considering the effect of hydrofoil and the body's lift and drag forces, hydrostatics of the vessel, and hydrodynamic derivatives.
- *Ballast system module/block:* it is responsible for regulating the mass of the ballast between the tanks aboard the vessel. This block provides actuation to the glider that allows it to manoeuvre in the heave direction with the aid of its hydrofoils, which are responsible for producing the drag and lift forces. Also, the pitching motion of the glider is controlled by this block by varying the ballast water; this allows the glider to pitch forward (bow heading downwards) and vice versa. Further, to limit the volumetric flow rate of the ballast between the tanks, a rate-limiter is also applied in this block. Similarly, the amount of ballast regulated amongst the tanks is also limited by a saturation unit.
- *Current block:* to simulate the response of the USFG in ocean currents, this block is added to generate the current velocities.
- *Control system block:* termed LQR in **Figure 6**, this module represents the entire control system for the USFG.
- More details of this model can be found in work by Ahmad and Xing [5].

2.2.1 Plant module/block

This section fully defines the plant module highlighted in **Figure 7**. A two-dimensional rigid body is defined to represent the vessel. The body can move freely in three directions or degrees of freedom (*x, z, and q*), representing surge, heave, and pitch, as depicted in **Figure 5**.

The equations of motion are stated below:

$$M(\dot{u} + wq - xq^2 + z\dot{q}) = \sum X_e \tag{1}$$

$$M(\dot{w} + uq - zq^2 + x\dot{q}) = \sum Z_e \tag{2}$$

$$I_{zz}\dot{q} + M\lfloor z(\dot{u} + wq) - x(\dot{w} - uq)\rfloor = \sum Q_e \tag{3}$$

where M is the mass of the USFG, Q_e, is the external pitching moment, and Z_e and X_e are damping and added forces in the heave and surge direction, respectively. Velocities are represented by u (velocity in surge direction), w (velocity in heave direction), and q (pitching velocity). Similarly, acceleration in the respective direction is given by $\dot{u}$, $\dot{q}$, and $\dot{w}$, and I_{zz} is the moment of inertia of the vessel in the pitch direction. Moreover, the external forces acting on the USFG are presented as a summation on the right-hand side of equations (1-3), whereas inertial terms are shown on the left-hand side.

The external forces such as lift (L_f) and drag (D_f), along with the rotational torque (M_T) acting on the body of the USFG are also calculated in this module, which is given by equation (4).

$$\begin{aligned} L_f &= \frac{1}{2} \times L_c \times \delta \times V_s \times V^2 \\ D_f &= \frac{1}{2} \times D_c \times \delta \times V_s \times V^2 \\ M_T &= -\frac{1}{2} \times C_M \times \delta \times V_s \times q^2 \end{aligned} \tag{4}$$

where δ is the seawater density, V_s is the total submerged volume of the USFG, and V is the total velocity with which the USFG manoeuvres. L_c and D_c are the lift and drag coefficients given by equations (5) and (6), respectively, whereas C_M is the damping moment coefficient whose value is defined as 1000.

$$L_c = 5\alpha^2 + 10\alpha \tag{5}$$

$$D_c = 0.4\alpha^2 + \alpha + 0.1 \tag{6}$$

These volumetric constants are dependent on the approach angle or the angle of attack (α) of the external flow. Further, the coefficients are determined based on the work by Graver [24], which is applied for this study because the proposed glider by Graver is comparable to USFG's outer hull.

Similarly, the drag and lift generated by the large hydrofoils are also applied and modelled in this plant model. Ahmad et al. [5] calculated the reference wing area for the hydrofoils that are incorporated into this module. NACA 4412 airfoil [25] geometry is used to model the dynamics of the USFG's wings. External forces and the rotational moment/torque remain the same as equation (4), except for volumetric coefficients. H_L and H_D are the lift and drag forces generated by the hydrofoils, while M_H is the moment. The modified equations for the hydrofoils are given below:

$$\begin{aligned} H_L &= \frac{1}{2} \times L_{ch} \times \delta \times V_s \times V^2 \\ H_D &= \frac{1}{2} \times D_{ch} \times \delta \times V_s \times V^2 \\ M_H &= -\frac{1}{2} \times C_{Mh} \times \delta \times V_s \times q^2 \end{aligned} \tag{7}$$

whereas L_{ch}, D_{ch}, and C_{Mh} are the modified volumetric coefficients given below.

$$\begin{aligned} L_{ch} &= a\alpha^3 + b\alpha^2 + c\alpha + d \\ a &= -10 \times 10^{-5}; b = -9 \times 10^{-4}; c = 0.114; d = 0.4942 \end{aligned} \tag{8}$$

$$\begin{aligned} D_{ch} &= Ae^{(B\alpha)} + Ce^{(D\alpha)} \\ A &= 2 \times 10^{-3}; B = -0.2093; C = 2.5 \times 10^{-3}; D = 0.1892 \end{aligned} \tag{9}$$

$$\begin{aligned} C_{Mh} &= q + w\cos(\alpha u) + r\sin(\alpha u) + t\cos(2\alpha u) + y\sin(2\alpha u) \\ q &= -0.085; w = -0.026; r = 0.014; t = 0.0076; y = -0.0076 \\ u &= 0.1595 \end{aligned} \tag{10}$$

2.2.2 Ballast module/block

The dynamics of the actuating system of the USFG ballast tanks are modelled in this block. It is noted that the model by Ahmad and Xing [3] utilizes only ballast tanks for propulsion, where the actuator mechanism does not encompass any secondary sources such as thrusters, propellers, or skegs for manoeuvring of USFG. The overall arrangement and placement of all the tanks aboard the USFG are illustrated in **Figure 8**.

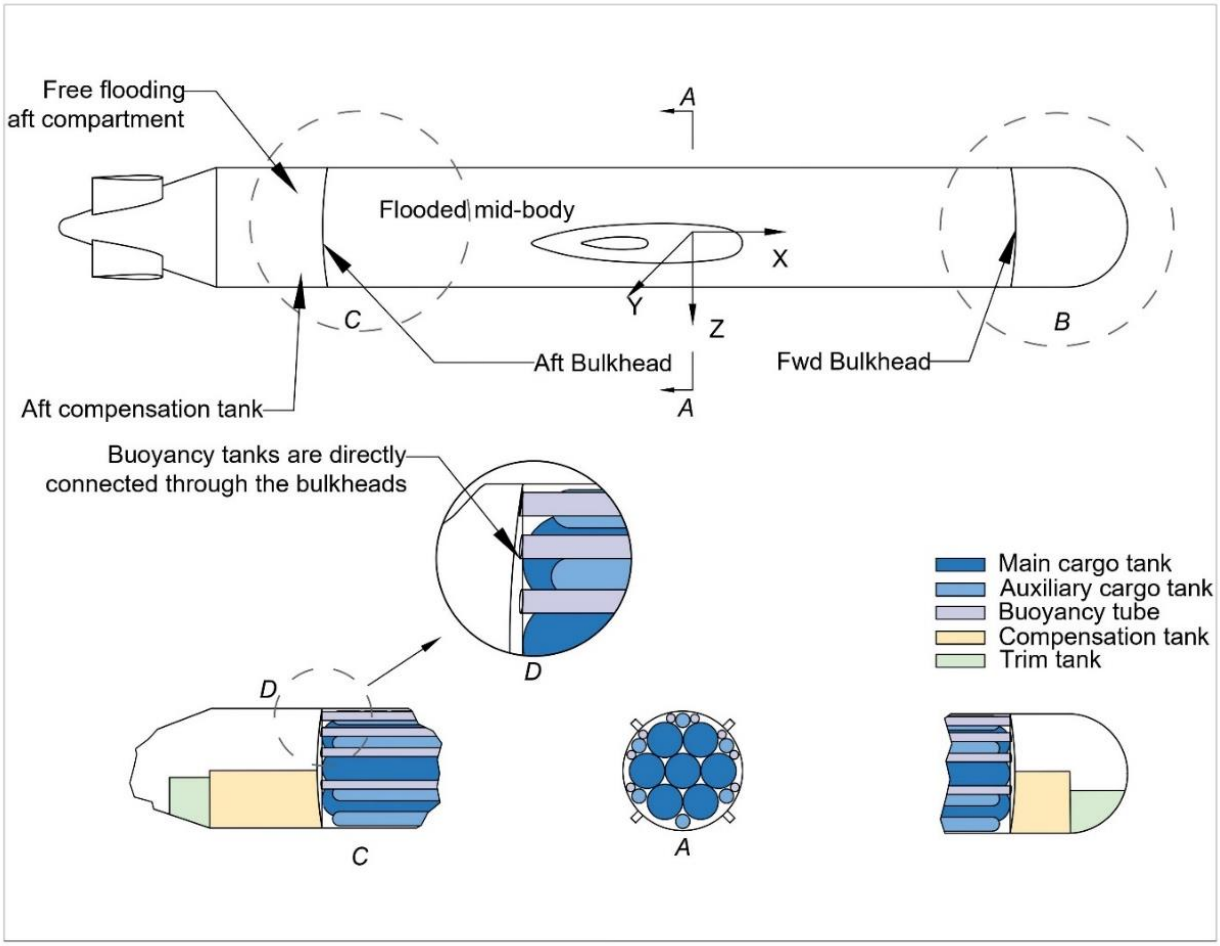

Figure 8 Tank arrangement of USFG [5].

The ballast tanks on the USFG are divided into trim and compensation, responsible for the vessel's stability as they induce neutrally trim and floating conditions. The compensation tanks at the stern and bow provide the vessel with the required trimming moment and ballast mass to attain neutral buoyancy. Moreover, a pair of smaller trim tanks (in volume) located at the same position ensures that the G of the vessel always remains below the B, providing finer alterations. Doing this allows the vessel to maintain a neutral or zero trim state. Also, apart from the ballast tanks, the buoyancy tanks onboard the USFG can enhance the overall stability of the vessel by increasing the ballasting capacity.

2.2.3 Current module/block

The first-order Gauss-Markov process [26] is used to simulate the ocean current. Current velocity U_c, and the incoming current flow angle φ_c is given by equations (11) and (12).

$$\dot{U}_c + \nu_1 U_c = \lambda_1 \tag{11}$$

$$\dot{\varphi}_c + \nu_2 \varphi_c = \lambda_2 \tag{12}$$

To determine the time constants of the Gauss-Markov process, constants ν_1 and ν_2 are used and adhering to Fossen [26], their magnitude should be a positive value. λ_1 and λ_2 are expressed as Additive White Gaussian Noises (AWGN). To generate a steady current, smaller values of ν_1 and ν_2 are utilized in this analysis, i.e., 1. For producing a fluctuating effect in the current direction and velocity, the noise power is limited to 1/10. The maximum current velocity experienced at the NCS is 1 m/s [27], but the design current speed for USFG is reduced to 0.5 m/s; for this analysis.

Current velocities in heave and surge directions, as expressed in USFG's body frame, are given as:

$$u_{wc} = U_c \cos \varphi_c \tag{13}$$

$$w_{wc} = U_c \sin \varphi_c \tag{14}$$

The velocity of the water in vertical (z) and horizontal (x) directions is given by w_{wc} and u_{wc}, respectively. The incoming relative velocity encountered by the USFG in heave and surge is given below.

$$w = w_{USFG} - w_{wc} \tag{15}$$

$$u = u_{USFG} - u_{wc} \tag{16}$$

where u_{USFG} and w_{USFG} are USFG's velocities in surge and heave.

2.2.4 Control system module/block

Linear quadratic regulator (LQR) type control is applied in this analysis, which controls the vessel's motion in heave and pitch directions. Previously, LQR has been applied to numerous autonomous marine vehicles due to its robust and stable performance. Burlacu et al. [28] and Bae et al. [29] used LQR for depth and steering control of marine vehicles, respectively. The LQR-type control utilizes full state feedback to stabilize the system's step responses. For LQR's control strategy, adaptive and optimum gains are fed into the close-loop; this enhances the

system's overall response. Gains can be derived from the USFG's state-space equations. For a single input and multiple output system, state-space equations are given in equations (17) and (18) for equations.

$$\frac{dx_{1,2}}{dt} = Jx_{1,2} + Ku_{1,2} \tag{17}$$

$$y_{1,2} = Lx_{1,2} \tag{18}$$

Here $y_{1,2}$ represents the output vector of the system, $u_{1,2}$ and $x_{1,2}$ are the input and state vectors, respectively. While L signifies output matrix, $K$and J are expressed as input and state matrices correspondingly. These matrices L, K, and J are calculated in the *System linearization* section below.

Actuator effort and system performance are compared and balanced to achieve the ideal and robust controller gain matrix for LQR-type control. The control law implemented in this study is represented by $S = -Gx$; here, G is the optimum gain matrix. The control law aims to decrease the infinite sum of variations from the principal quantities, also known as the quadratic cost function:

$$C = \int_0^\infty \delta x^T N \delta x + \delta u^T M \delta u \, dt \tag{19}$$

Here N and M are weight matrices for the state and energy (actuator effort), respectively; the idea is to adjust the weights of both matrices to obtain a robust system performance efficiently by applying little actuator effort. LQR controller can be tuned by varying the weights (values) of N and M matrices; this is highlighted in section *Controller tunning* below.

System linearization

For a front-to-front inflow of ocean current, Ahmad and Xing [2] investigated that the 38° equilibrium glide path is suitable, which is the targeted analysis for this study. Earlier, Ahmad and Xing [3] linearized the mathematical model of the USFG at two different glide angles, 30° and 40°. For this work, the model is linearized at a gliding angle of 38° by using the model linearizer in the Simulink environment. The outputs $[\dot{\theta}; \ddot{x}; \ddot{y}; \ddot{\theta}]$ and inputs $[\theta; \dot{x}; \dot{y}; \dot{\theta}]$ into the system are designed as open-loop and are linearized at a functioning point for a stable current speed of 0.5 m/s. As a result, a 4 by 4 state, 2 by 4 output, and 4 by 1 input matrix are given by equations (20-22).

$$J = \begin{bmatrix} 0 & 0 & 0 & 1 \\ 0.43 & -0.20 & -0.26 & 6 \times 10^{-12} \\ 0.68 & -0.29 & -0.41 & 0 \\ -2 \times 10^{-08} & 1 \times 10^{-09} & 2 \times 10^{-09} & -3 \times 10^{-04} \end{bmatrix} \tag{20}$$

$$K = \begin{bmatrix} 0 \\ -1.58 \times 10^{-12} \\ -8.88 \times 10^{-13} \\ 2.64 \times 10^{-05} \end{bmatrix} \tag{21}$$

$$L = \begin{bmatrix} 0 & 0.79 & -0.61 & 0 \\ 0 & 0.46 & -0.59 & 0 \end{bmatrix} \tag{22}$$

Controller tunning

To obtain an optimal response of the USFG during equilibrium gliding, the LQR-type controller is tuned by utilizing the state-space matrices (J and K). The system's dynamics should be entirely explicit to the user to tune the controller efficiently. This can be done by varying the weights or values of the N and M matrices while observing the transient response of the system in retort to the output or performance. Adjusting the weights of the N matrix varies the steady-state error of the output. At the same time, M matrix is utilized to regulate the amount of energy spent on the actuators. N and M matrices are highlighted in equation (23).

$$N = \begin{bmatrix} 0 \\ 0 \\ 0 \\ 10^3 \end{bmatrix} \qquad M = [10^{-2}] \tag{23}$$

To have an enhanced response for pitch motion, the acceleration coefficient, i.e., 10^3 is weighted heavily. This yields a gain matrix G given below.

$$G = [-5.3 \times 10^{-10} \quad 2.4 \times 10^{-10} \quad 3.2 \times 10^{-10} \quad 2.6] \tag{24}$$

3. The average conditional exceedance rate (ACER) design method

$H(t)$ represents the long-drawn-out global or total response of the USFG during gliding, measured for a timespan $(0, S)$. The process $H(t)$ measurements are given by $H_1, \dots, H_N$, which are measured at a distinct timespan $s_1, \dots, s_N$ in $(0, S)$. This aids in approximating the distribution function of the extreme responses or values $E_N = \max\{X_j ; j = 1, \dots, N\}$. Later this can be used to acquire the cumulative density function (CDF), $P(\zeta) = \text{Prob}(E_N \leq \zeta)$. This is done to have an approximate CDF for large-scale output ζ values. Hence, the following functions are introduced for this study, having random nature.

$$Q_{kj}(\zeta) = \mathbf{1}\{H_j > \zeta, H_{j-1} \leq \zeta, \dots, H_{j-k+1} \leq \zeta\}, \qquad j = k, \dots, N, k = 2, 3, \dots \tag{25}$$

in addition

$$R_{kj}(\zeta) = \mathbf{1}\{H_j > \zeta, H_{j-1} \leq \zeta, \dots, S_{j-k+1} \leq \zeta\}, \qquad j = k, \dots, N, k = 2, 3, \dots \tag{26}$$

Here $\mathbf{1}\{\mathcal{K}\} = 1$ if $\mathcal{K}$ is correct or true, whereas it is 0 otherwise. As highlighted in Naess et al. [18][20][21][23]:

$$P_k(\zeta) \approx \exp\left(-\sum_{j=k}^{N} \frac{\mathbb{E}[Q_{kj}(\zeta)]}{\mathbb{E}[R_{kj}(\zeta)]}\right) \approx \exp\left(-\sum_{j=k}^{N} \mathbb{E}\left[Q_{kj}(\zeta)\right]\right), \qquad \zeta \to \infty \tag{1}$$

To render $\mathbb{E}[Q_{kj}(\zeta)]$ to a constant term, the logged time series is separated into *K* successive (transient) blocks or modules. So that for adequately huge values of ζ, $\sum_{j\in B_i}\mathbb{E}\left[Q_{kj}(\zeta)\right] \approx \sum_{j\in B_i} q_{kj}\left(\zeta\right)$. Consequently, resulting in $\sum_{j=k}^{N}\mathbb{E}\left[Q_{kj}(\zeta)\right] \approx \sum_{j=k}^{N} q_{kj}\left(\zeta\right)$. For the recorded time series, $q_{kj}(\zeta)$ represents the realized values of $Q_{kj}(\zeta)$, while B_i depicts the group of indices for the module with the number i; through $i = 1, \dots, K$. Subsequently, we have the following relation for the given stationary process:

$$P_k(\zeta) \approx \exp\left(-(N-k+1)\hat{\xi}_k(\zeta)\right) \tag{2}$$

where,

$$\hat{\xi}_k(\zeta) = \frac{1}{N-k+1}\sum_{j=k}^{N} q_{kj}\left(\zeta\right) \tag{3}$$

To approximate the short-term or transient values by utilizing the detected values of $q_{kj}(\zeta)$ functions, an assumption of ergodicity is employed for every transient part of the logged time series. By examining the empirical probability distribution of $l = 1,..,L$ sea current states have probabilities p_l, so that $\sum_{l=1}^{L} p_l = 1$, an alternate method of expressing the non-transient extreme value distribution, equation (28), can be attained.

Accordingly, the long-term/non-transient ACER function having an order of magnitude *k* is given by:

$$\mathrm{ACER_k}(\zeta) \equiv \sum_{l=1}^{L} \hat{\xi}_k(\zeta, l)\, p_l \tag{4}$$

whereas $\hat{\xi}_k(\zeta, l)$ is limited to an exact sea-state having a number *L*, which is the same as in equation (29). Founded on the ACER function having an order *k*, the non-transient extreme value distribution of $E(S)$ can be expressed as:

$$P(\zeta) \approx \exp\left(-D\times\mathrm{ACER_k}(\zeta)\right) \tag{5}$$

This can also be seen in Naess et al. [18][20][21][23]. $\mathrm{ACER_k}(\zeta)$ represents the long-term/non-transient observed ACER function having an order of magnitude *k* with $k \ll D$. where *D* specifies the overall size of data points from the observed frequency distribution that is utilized to estimate the ACER functions. These are the extreme or output values from the gauged time record.

$\mathrm{ACER_k}(\zeta)$ is observed to converge quickly with increasing values of *k*; this also enhances the accuracy of equation (31), also argued in [18][20][21][23]. By increasing the processing level *k*, the data clustering effects (narrow-banded components of the output) can be catered to in the analysis. This enhances the accuracy of the projected extreme values, thus avoiding the unstable or impractical design values.

For higher output/response values of ζ, the behaviour in the tail is relatively consistent or steady for the $\mathrm{ACER_k}$ represented as functions. Moreover, for $\zeta \geq \zeta_0$, the tail performs intimately like $\exp\{-q(\zeta + r)^u + v\}$ with q, r, u, v representing the appropriate constant values.

Log-level optimization can be performed by minimizing the error function W by considering q_k, r_k, u_k, v_k as the input arguments.

$$F(q_k, r_k, u_k, v_k) = \int_{\zeta_0}^{\zeta_1} \alpha(\zeta) \left\{ \ln\left(\mathrm{ACER_k}(\zeta)\right) - v_k + (q_k\zeta + r_k)^{u_k} \right\}^2 d\zeta, \qquad \zeta \geq \zeta_0 \tag{6}$$

The highest output value that permits the calculation of the confidence interval is represented by ζ_1, it is also known as the designed limit for cut-off. Where α is the weight function represented as $\alpha(\zeta)=\{\ln C^+(\zeta) - \ln C^-(\zeta)\}^{-2}$with $\left(C^-(\zeta),\ C^+(\zeta)\right)$ depicting the 95% confidence interval (CI), analytically approximated from the recorded data. The comprehensive optimization process for the parameters q_k, r_k, u_k, v_k is highlighted and discussed in Naess et al. [18][20][21][23].

4. Results and discussions

Current velocities of 0.5 m/s and 1 m/s are utilized for this analysis. The average current velocity of 0.5 m/s is used as a targeted base-case for USFG, which forms the basis of USFG manoeuvrability in a head-on current of 1 m/s. A total of 60, 750-seconds cases are collectively simulated for this study.

A tuning study is done for various cases of LQR gains. This is done to enhance the overall step-performance of the control system. The tunning cases are highlighted in **Table 2**.

Table 2 Gains for tuning sensitivity study.

Cases	**Gains**		
Case-1 LQR	$N =$ diag (0,0,0,10^3)	$M =$ diag (10^{-2})	
Case-2 LQR	$N =$ diag (0,0,0,10^1)	$M =$ diag (10^{-2})	
Case-3 LQR	$N =$ diag (0,0,0,10^3)	$M =$ diag (10^{-4})	
Case-4 PID	$P = 102$	$I = 0.18$	$D = 12881$

Case-4 PD depicts the proportional-derivative (PD) type control used for the collation analysis for the rise time analysis. Depth sensitivity analysis is also presented as a case study in this paper, highlighting the changes in USFG's response in heave for varying operational depth.

This work extends the method for predicting the extreme surge responses of the USFG during its single cycle of equilibrium glide. These responses are estimated while the USFG targets to attain a pre-defined pitch angle and operating depth while manoeuvring in the ocean current. This paper's numeric data is obtained from explicit mathematical simulations based on the Simulink model discussed in Section 2. Section 3 presents the novel ACER method. The presented ACER method utilizes the available data efficiently and predicts the extreme surge responses precisely and accurately. It is established that the ACER method efficiently integrates the disturbances from the environment while providing robust and accurate response values, given the numerical data is exact.

To minimize the power consumption and any accidental damages during the mission, this well-defined approach can serve as an input to the design and analysis stage of USFG. This can assist in providing optimal and robust control parameters for the glider during operation.

4.1 Performance analysis of the control system

A systematic tuning study is performed in this section. Here, the minus sign indicates that the glider is descending (bow heading down). The desired response is to attain a pitch angle of -38°.

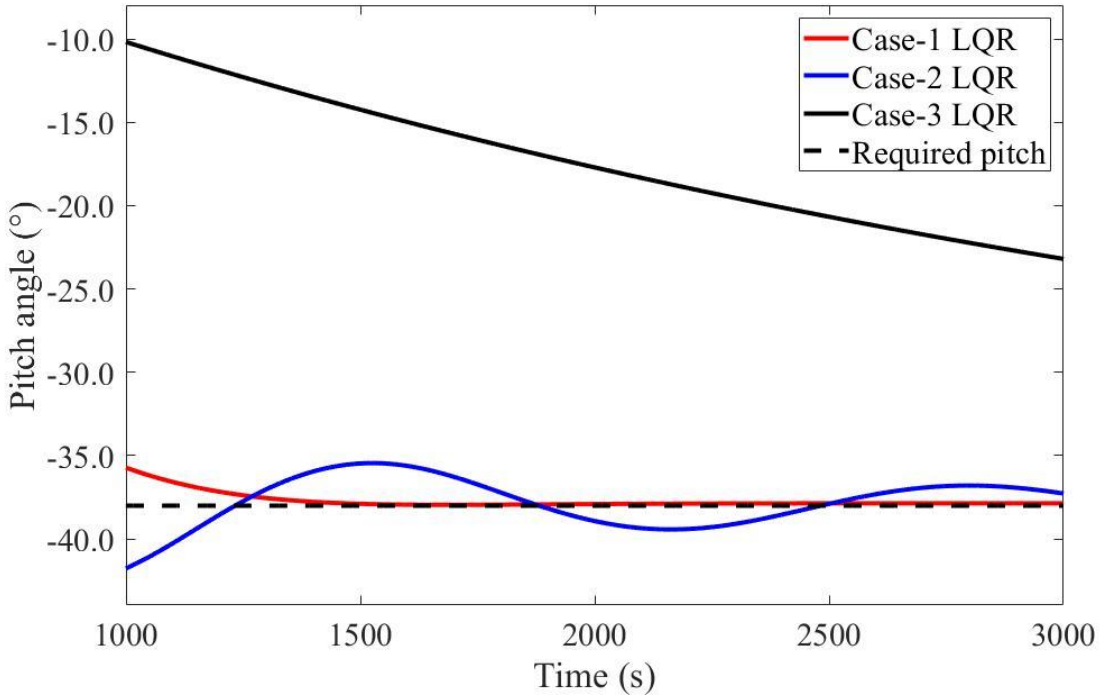

Figure 9 Pitch responses for LQR tuning.

USFG is tuned with different controller gains to study the dynamic response of the glider. Various tuning cases are highlighted in Table 2. The system's response time, stability, and robustness are studied and discussed here.

Figure 9 depicts the three-pitch responses of the USFG simulated for different cases of the LQR controller. For Case-1 LQR, the steady-state error is the minimum, as shown in **Figure 9**. Here the *N* matrix is penalized heavily in this case which cuts down the system's response time (1700 seconds) drastically, compelling it to maintain the commanded pitch angle. Moreover, the system is most stable for these gains, as it doesn't experience any oscillations in the output response.

Case-2 LQR depicts an oscillating response as the system minimizes the steady-state error. This increases the response time of the glider (>10000 seconds). This does not represent the ideal controller gains because the system's stability is compromised due to the large variations in the output values. Moreover, the controller spends excessive effort and energy compensating for over-shoot, and under-shoot in each successive cycle: as the cost of *N* matrix is reduced.

As for the last scenario, Case-3 LQR, the *M* matrix cost is reduced to 10^{-4}. Doing this allows the controller to overcompensate the output pitch response, which increases the response time (>17000 seconds). Therefore, these LQR gains are not robust and practical for USFG's surge control application as they increase the settling time of the output response.

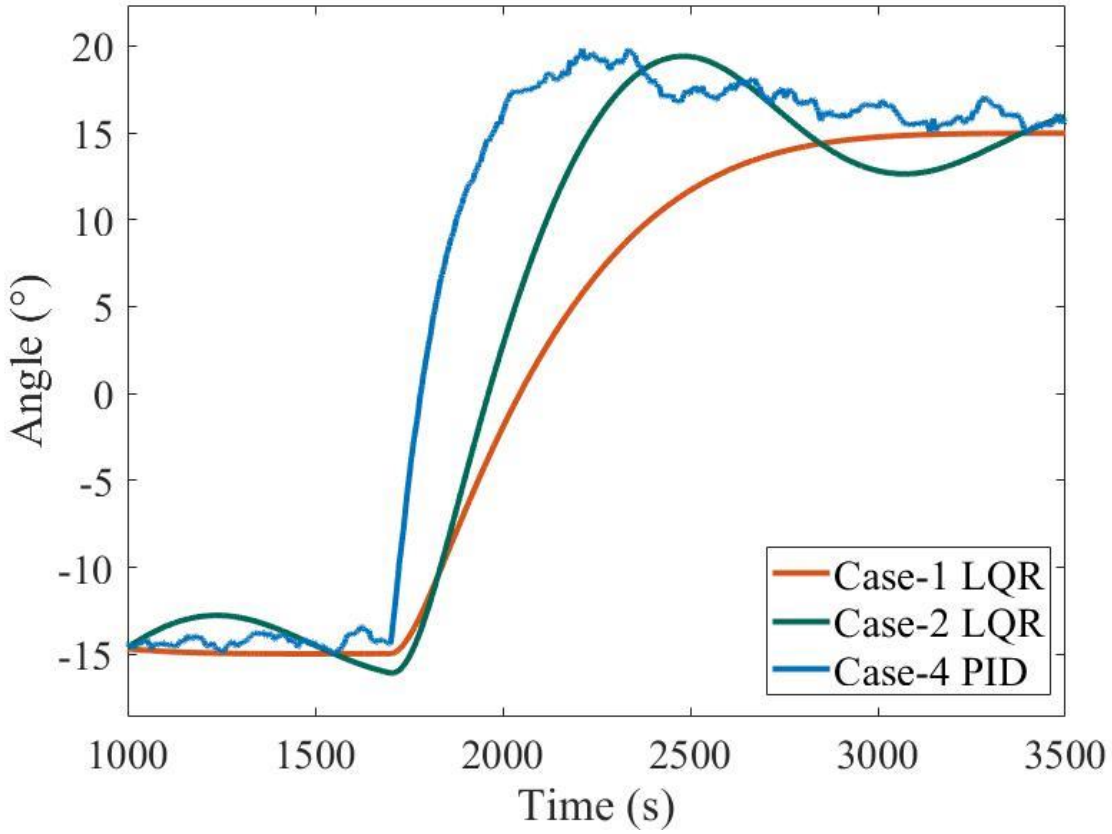

Figure 10 Settling times for various tuning gains.

To measure the robustness of the controller, a settling-time study is framed for different controllers used in this analysis. As depicted in **Figure 10**, the glider is allowed initially to attain a diving angle of -15° (bow heading down); afterwards, it is commanded to achieve a +15° (bow heading up). This analysis is designed to tackle the unexpected changes in operating conditions of the USFG during its mission. It must be noted that the Case-3 gains for the LQR-type control are not utilized in this study owing to the sluggish response.

As highlighted in **Figure 10**, the PID controller has the minimum settling time among the controllers. This changes from 250 seconds for Case-4-PID to 500 seconds and 800 seconds for Case-2 LQR and Case-1 LQR, respectively. Consequently, Case-2 LQR and Case-4 PID experience oscillations in their final output response as they are not robust enough to mitigate the noise induced by the ocean current. On the contrary, Case-1 LQR results in a stable and noise-free response at the expense of significant settling times.

Overall, tuning gains for Case-1 LQR are preferred for this analysis as they yield a minimum error in the output without inducing any fluctuations in the system. Further, these weights are also preferred for their minimum expense of actuator effort. They are also utilized for depth sensitivity analysis and univariate extreme response analysis.

4.2 Depth sensitivity analysis

A depth sensitivity study is performed for the USFG to observe the system's responsiveness to changes in operating depths. The USFG is designed for an operating depth of 200 meters, as defined by Ahmad et al. [5] while travelling at an optimal gliding angle of 38°, as argued by

Graver [24]. While doing so, the glider covers a total distance of 256 meters in the surge direction.

This section studies the changes in surge motion for the variable functional depth of the glider. For each functional depth, 200, 300, and 400 meters, the distance covered by the glider is measured and compared against the actual distance. The study aims to observe and mitigate the steady-state error if any in the surge motion.

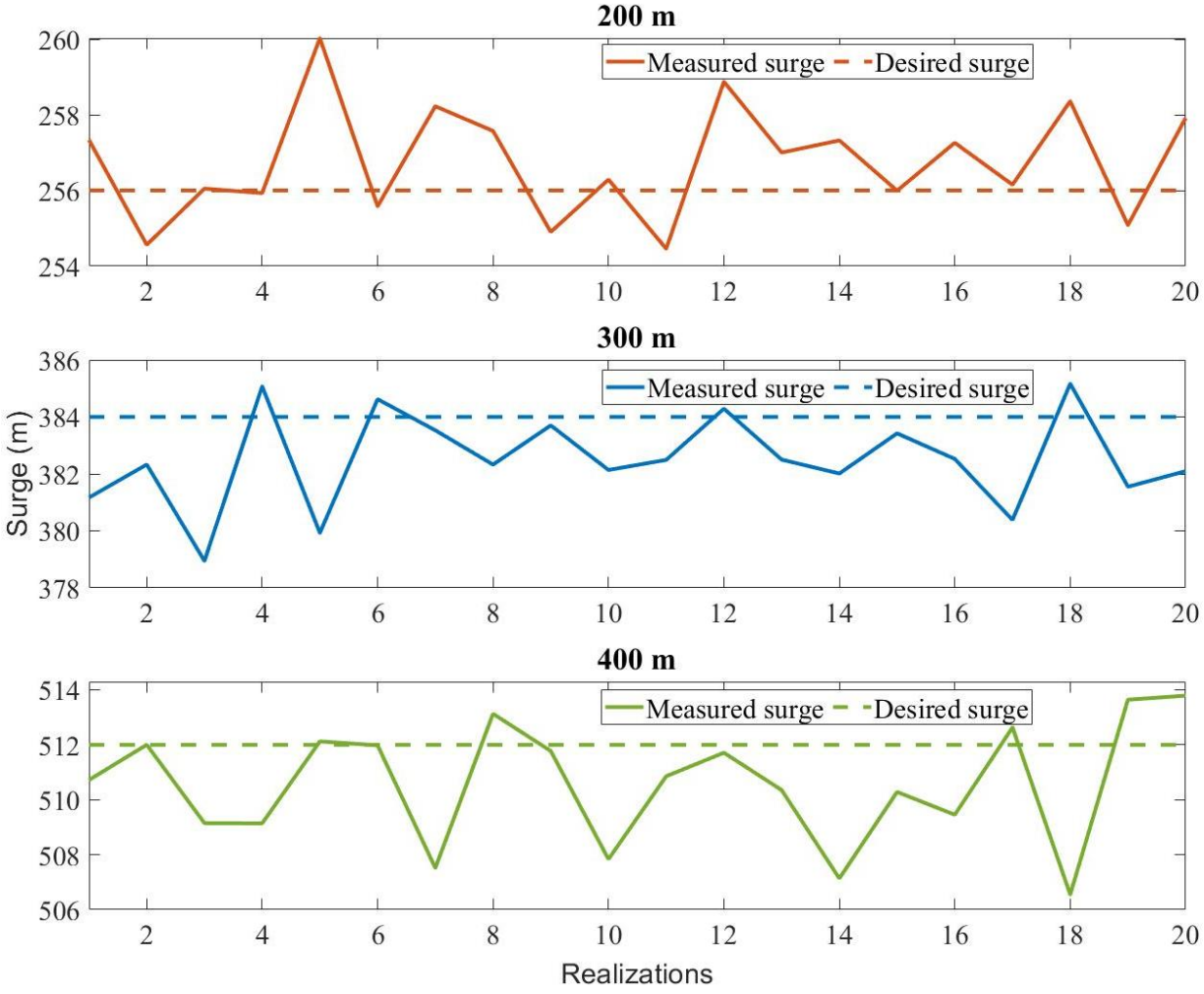

Figure 11 Simulated responses for 20 surge realizations.

The 750-second responses for 20 realizations of this study are depicted in **Figure 11**. For each case, the distances covered by the USFG are different, which are highlighted in **Table 3**, along with respective errors.

As depicted in **Table 3**, the percentage error between the required surge motion values and the desired values is less than 0.4 % for all the cases. So, the surge response for variable depths is acceptable within the defined error. This means that additional measures, i.e., increasing ballast fraction or propeller, are not needed in this case. The controller specifications presented in this work can tackle changes in operating conditions while catering to any depth changes throughout the entire mission of the USFG.

Table 3 Average errors for depth sensitivity analysis.

Cases	Desired distance (m)	Average measured distance (m)	Percentage error (%)
200 m	256	257	0.391
300 m	384	383	0.260
400 m	512	511	0.195

4.3 Extreme response prediction: univariate surge analysis

This section highlights the arithmetic results produced by univariate analysis, i.e. ACER1D, for the surge responses for the USFG [18][20][21][23]. For a safe, robust, and reliable design of the USFG, accurate estimation of extreme surge responses is vital.

depicts the univariate response for surge and a 95% confidence interval indicated by the dotted lines. Results for several return periods are shown in **Table *4***; the preferred return periods serve as an example. The Gumbel plot for the surge output is shown in **Figure 13**. The fitted curve is extrapolated to represent higher return periods, i.e., 5-year and 10-year. The estimated values given in **Figure 13** can be collated with the ones in

(Lower). While both methods estimate a 3-month return period surge of about 290 meters ($1.0\ m/s$ case), it is observed that the Gumbel data points from the 20 simulations do not accurately fit a straight curve. Comparable behaviour is observed for all the return periods presented in **Table *4***. This indicates that the studied data points have not established the asymptotic generalized extreme value (GEV) condition. Additionally, the ACER 95% CI is noticeably narrower than the 95% CI projected by the Gumbel plot. This is a distinct benefit of utilizing the advanced ACER method for extreme value prediction.

For all the return periods, the extreme surge responses are, in general, more significant than the desired distance (256 meters). For instance, for a return period of 5-Year, the extreme values are 1.1 to 1.2 times higher than the anticipated distance. To compensate for this overshoot, an observer can be employed to the Simulink model that can ensure that the glider follows the path accurately. The difference in the predicted extreme surge values for all the return periods is minimal while moving from left to right in **Table *4***. For $0.5\ m/s$ current velocity, an alteration of 3 meters is observed between 3-Months and 5-Year return periods for both ACER and Gumbel methods. Similar behaviour is also detected for $1.0\ m/s$ current velocity, where a variation of 6 meters is realized for both methods.

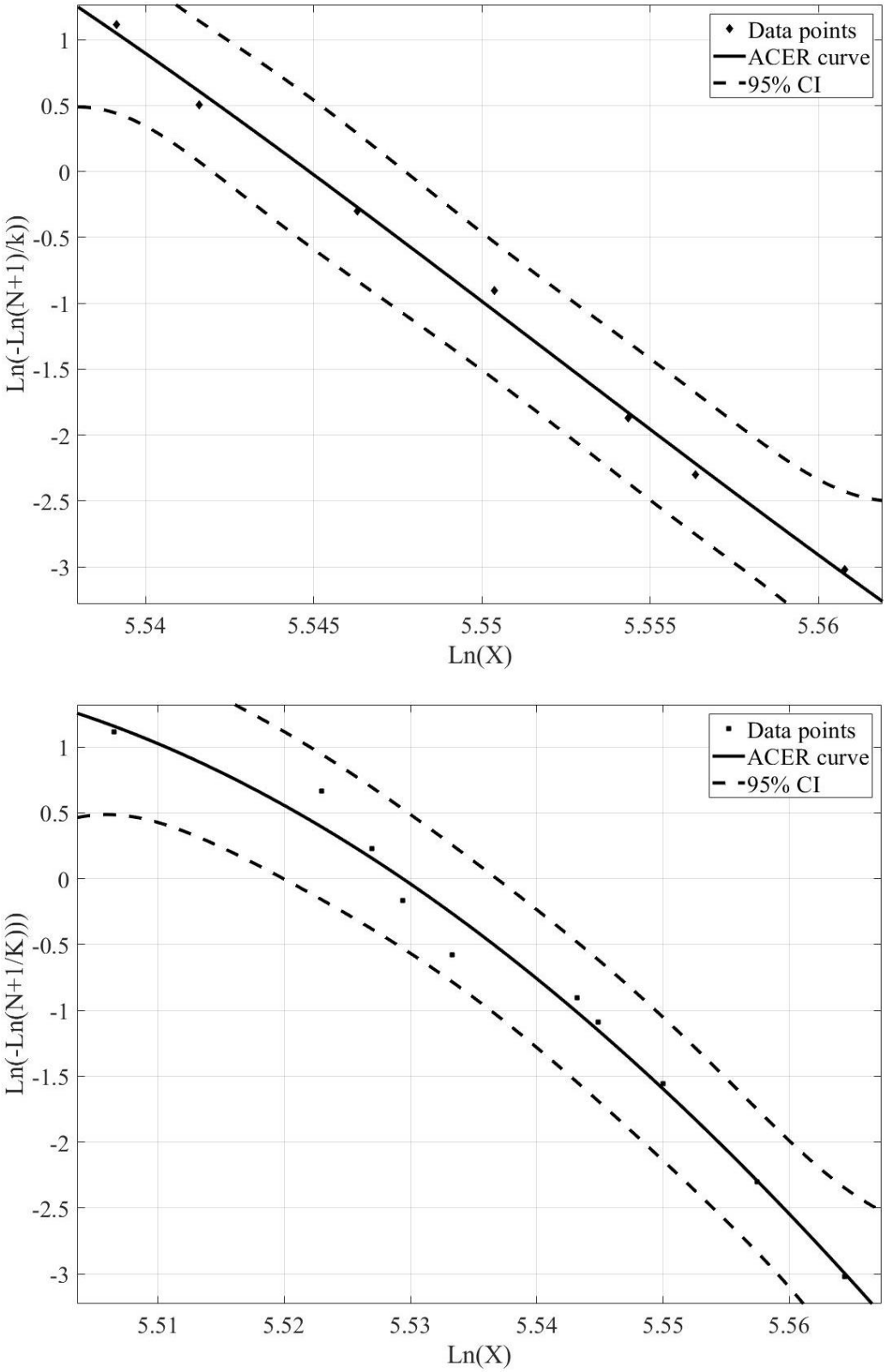

Figure 12 ACER 1D extreme surge responses in log-scale. Upper: with a current velocity of 0.5 m/s; Lower: with a current velocity of 1.0 m/s.

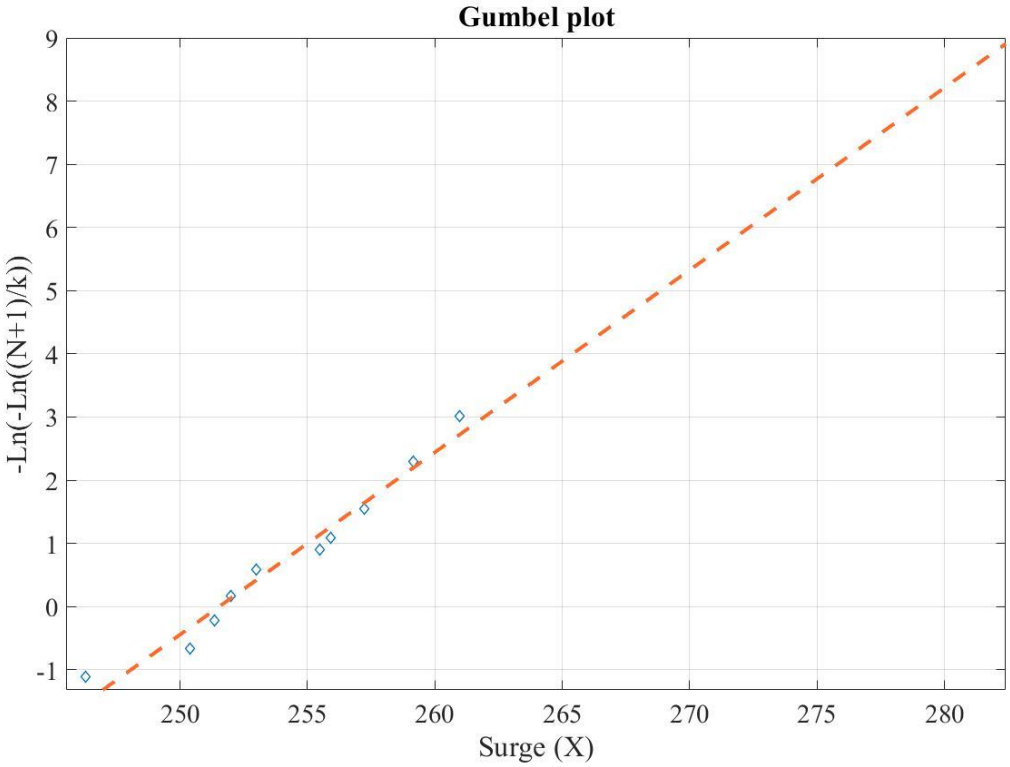

Figure 13 Gumbel plot for surge, dashed line specifies extrapolation toward a return period of 10-year. 20 750-seconds simulated responses. Current velocity of 1.0 m/s.

Table 4 presents the surge output response of the USFG in meters for 5 return periods, i.e., 3-months, 6-months 1-year, 2-year, and 5-year. The Gumbel fit fails to provide accurate and precise estimations in contrast to the 95% CI band predicted by the ACER method.

Table 4 Surge response (meters) predictions for several return periods.

Current velocity	Method	3-Months	6-Months	1-Year	2-Year	5-Year
0.5 m/s	**ACER 95% CI**	270.62 (245.01,307.87)	270.80 (245.18,308.07)	271.25 (245.58,308.58)	271.93 (246.20,309.36)	273.04 (247.20,310.62)
	Gumbel 95% CI	270.29 (203.77,317.27)	270.46 (203.90,317.47)	270.89 (204.23,317.98)	271.54 (204.72,318.74)	272.58 (205.50,319.96)
1.0 m/s	**ACER 95% CI**	290.99 (231.29,348.60)	291.49 (231.69,349.20)	292.76 (232.70,350.72)	294.68 (234.22,353.02)	297.82 (236.72,356.79)
	Gumbel 95% CI	288.49 (218.32,432.51)	288.93 (218.65,433.17)	290.03 (219.48,434.81)	291.69 (220.74,437.30)	294.37 (222.77,441.32)

5. Conclusions

The USFG is a pioneering subsea-freight transportation vessel in its initial design and development phases. The vessel presents numerous exciting development and research challenges to be resolved. The ability of the glider to conserve energy and travel larger distances during the mission is exceptionally vital for the battery design and the economic feasibility of the USFG. The Simulink model for the USFG is presented in the first part of the work. Numerical modelling is utilized to capture the dynamics of the vessel. The main blocks of the USFG (Plant, Ballast system, Current, and Control system modules) are presented briefly. This paper proposed utilizing the state-of-the-art average conditional exceedance rate (ACER) design method to study the extreme surge responses (offset from the pre-planned surge motion also influences the heave motion of the vessel) while manoeuvring in ocean current during the mission. The surge responses are studied in only the half cycle of the glide, as indicated in **Figure 4**. Knowledge of extreme responses of the USFG is vital as it gives the maximum range and depth, which governs the controller gains for motion control and hydrostatic pressure loads, respectively.

Settling and response times are significant for Case-2 LQR and Case-3 LQR, making them impractical for controlling pitching motion. Whereas for Case-1, it was observed that these gains are quite efficient and robust as studied performance analysis of the control system. Furthermore, the PID controller utilized in this study yields a rapid response with fluctuations. This is not suitable as it renders the system unstable. Finally, the tunning gains of Case-1 LQR were preferred owing to small steady-state errors in the response.

From the depth sensitivity analysis, it was concluded that no secondary source of propulsion is needed for USFG. For various operating depths, the maximum error in the output response was about 0.4%, highlighting LQR's tremendous ability in path following.

It is observed that the extreme surge responses for all the return periods are higher, around 1.1 to 1.2 times than the mathematical 750-second response. This specifies that an observer, commonly Luenberger Observer [30], can be integrated into the mathematical model of the USFG to ensure path-following even for extreme surge responses, such as depicted in **Table *4***.

The method proposed in this work enables the USFG design to be matured further. It also contributes to optimizing dynamic vessel parameters and minimizing probable damage to the glider. Finally, for future work, the proposed approach can also be applied to the complete equilibrium gliding path (1 complete cycle with turning motion) of the USFG, as presented by Ahmad and Xing [2].

References

1. Xing, Y. (2021). A conceptual large autonomous subsea freight-glider for liquid CO2 transportation. International Conference on Offshore Mechanics and Arctic Engineering,
2. Ahmad, U., & Xing, Y. (2021). A 2D model for the study of equilibrium glide paths of UiS Subsea Freight-Glider. IOP Conference Series: Materials Science and Engineering,
3. Ahmad, U., & Xing, Y. (2022). UiS Subsea Freight Glider: controller design and analysis. International Conference on Offshore Mechanics and Arctic Engineering,

4. Xing, Y., Ong, M. C., Hemmingsen, T., Ellingsen, K. E., & Reinås, L. (2021). Design considerations of a subsea shuttle tanker system for liquid carbon dioxide transportation. *Journal of Offshore Mechanics and Arctic Engineering*, *143*(4).
5. Ahmad, U., Xing, Y., & Ma, Y. (2022). UiS Subsea-Freight Glider: A Large Buoyancy-Driven Autonomous Cargo Glider. *Journal of Offshore Mechanics and Arctic Engineering, Under Review*.
6. Xing, Y., Santoso, T. A. D., & Ma, Y. (2021). Technical–Economic Feasibility Analysis of Subsea Shuttle Tanker. *Journal of Marine Science and Engineering*, *10*(1), 20.
7. Ma, Y.; Xing, Y.; Ong, M.C.; Hemmingsen, T. Baseline design of a subsea shuttle tanker system for liquid carbon dioxide transportation. *Journal of Ocean Engineering* **2021**, 240, 109891.
8. Jamissen, P.L.; Ma, Y.; Xing, Y.H. 2022. Probabilistic design of ring-stiffened cylindrical hull structures applied on large cargo submarines, under review in International Conference on Ocean, Offshore and Arctic Engineering.
9. Bahlman, J. W., Swartz, S. M., Riskin, D. K., & Breuer, K. S. (2012). Glide performance and aerodynamics of non-equilibrium glides in northern flying squirrels (Glaucomys sabrinus). *Journal of the Royal Society, Interface*, *10*(80), 20120794-20120794. https://doi.org/10.1098/rsif.2012.0794.
10. Langebrake, L. C. (2003). AUV sensors for marine research. *Technology and Applications of Autonomous Underwater Vehicles*, 245-277.
11. Griffiths, G. (2002). *Technology and applications of autonomous underwater vehicles* (Vol. 2). CRC Press.
12. Yu, S., Wu, W., Xie, B., Wang, S., & Naess, A. (2020). Extreme value prediction of current profiles in the South China Sea based on EOFs and the ACER method. *Applied Ocean Research*, *105*, 102408.
13. Naess, A., & Karpa, O. (2015). Statistics of extreme wind speeds and wave heights by the bivariate ACER method. *Journal of Offshore Mechanics and Arctic Engineering*, *137*(2).
14. Gaidai, O., Naess, A., Xu, X., & Cheng, Y. (2019). Improving extreme wind speed prediction based on a short data sample, using a highly correlated long data sample. *Journal of Wind Engineering and Industrial Aerodynamics*, *188*, 102-109.
15. Gaidai, O., Naess, A., Karpa, O., Xu, X., Cheng, Y., & Ye, R. (2019). Improving extreme wind speed prediction for North Sea offshore oil and gas fields. *Applied Ocean Research*, *88*, 63-70.
16. Gaidai, O., Xu, X., Wang, J., Ye, R., Cheng, Y., & Karpa, O. (2020). SEM-REV offshore energy site wind-wave bivariate statistics by hindcast. *Renewable Energy*, *156*, 689-695.
17. Xu, X., Gaidai, O., Naess, A., & Sahoo, P. (2019). Improving the prediction of extreme FPSO hawser tension, using another highly correlated hawser tension with a longer time record. *Applied Ocean Research*, *88*, 89-98.
18. Naess, A., & Moan, T. (2013). *Stochastic dynamics of marine structures*. Cambridge University Press.
19. Gaidai, O., Xu, X., Naess, A., Cheng, Y., Ye, R., & Wang, J. (2021). Bivariate statistics of wind farm support vessel motions while docking. *Ships and Offshore Structures*, *16(2)*, 135-143.
20. Naess, A., & Gaidai, O. (2008). Monte Carlo methods for estimating the extreme response of dynamical systems. *Journal of engineering mechanics*, *134(8)*, 628-636.

21. Naess, A., Gaidai, O., & Batsevych, O. (2010). Prediction of extreme response statistics of narrow-band random vibrations. *Journal of engineering mechanics, 136(3),* 290-298.
22. Hui, G., Gaidai, O., Naess, A., Storhaug, G., & Xu, X. (2019). Improving container ship panel stress prediction, based on another highly correlated panel stress measurement. *Marine Structures, 64,* 138-145.
23. Naess, A., Stansberg, C., Gaidai, O., & Baarholm, R. (2008). Statistics of extreme events in airgap measurements. International Conference on Offshore Mechanics and Arctic Engineering,
24. Graver, J. G. (2005). Underwater gliders: Dynamics, control and design.
25. Tools, A. *NACA 4412 (naca4412-il).* http://airfoiltools.com/airfoil/details?airfoil=naca4412-il
26. Fossen, T. I. (2011). *Handbook of marine craft hydrodynamics and motion control*. John Wiley & Sons.
27. G. Ersdal (2001). An overview of ocean currents with emphasis on currents on the Norwegian continental shelf. Norwegian Petroleum Directorate.
28. Burlacu, P., Dobref, V., Badara, N., & Tarabuta, O. (2007). A LQR controller for an AUV depth control. *Annals of DAAAM & Proceedings*, 125-127.
29. Bae, Shin, S. B., Kwon, D. H., Joo, S. T., & G, M. (2014). An LQR controller for autonomous underwater vehicle. Journal of Institute of Control, Robotics and Systems, 20(2), 132-137.
30. Luenberger, D. (1971). An introduction to observers. IEEE Transactions on automatic control, 16(6), 596-602.